Active Site Identification and Mathematical Modeling of Polypropylene Made with Ziegler-Natta Catalysts

by

Ahmad Alshaiban

A thesis

presented to the University of Waterloo

in fulfillment of the

thesis requirement for the degree of

Master of Applied Science

in

Chemical Engineering

Waterloo, Ontario, Canada, 2008

AUTHOR'S DECLARATION

I hereby declare that I am the sole author of this thesis. This is a true copy of the thesis, including any required final revisions, as accepted by my examiners.

I understand that my thesis may be made electronically available to the public.

Abstract

Heterogeneous Ziegler-Natta catalysts are responsible for most of the industrial production of polyethylene and polypropylene. A unique feature of these catalysts is the presence of more than one active site type, leading to the production of polyolefins with broad distributions of molecular weight (MWD), chemical composition (CCD) and stereoregularity. These distributions influence strongly the mechanical and rheological properties of polyolefins and are ultimately responsible for their performance and final applications. The inherent complexity of multiple-site-type heterogeneous Ziegler-Natta catalysts, where mass and heat transfer limitations are combined with a rather complex chemistry of site activation in the presence of internal and external donors, plus other phenomena such as comonomer rate enhancement, hydrogen effects, and poisoning, makes the fundamental study of these systems a very challenging proposition.

In this research project, new mathematical models for the steady-state and dynamic simulation of propylene polymerization with Ziegler-Natta heterogeneous catalysts have been developed. Two different modeling techniques were compared (population balances/method of moments and Monte Carlo simulation) and a new mechanistic step (site transformation by electron donors) were simulated for the first time. Finally, polypropylene tacticity sequence length distributions were also simulated.

The model techniques showed a good agreement in terms of polymer properties such as molecular weights and tacticity distribution. Furthermore, the Monte Carlo simulation technique allowed us to have the full molecular weight and tacticity distributions. As a result, the ^{13}C NMR analytical technique was simulated and predicted.

Acknowledgements

My most grateful unqualified gratitude is to Allah, the Almighty who guided me in every facet of this work in his infinite wisdom and bounties.

In this thesis, I would like to express my deeply indebted to my supervisor Professor. João Soares. This thesis would never have been accomplished without his kind support, continuous encouragement, and valuable advice throughout this academic period. From this work we were able to visualize and state directions of possible future research and further improvements.

I would like also to appreciate the valuable comments from Professor Leonardo Simon and Professor Costas Tzoganakis. They spent considerable time and effort in reviewing my thesis and showed extreme care in our discussions.

I would also like to acknowledge the financial and technical support from Saudi Basic Industries Corporation (SABIC).

Finally, my deep and grateful thanks go to my parents and my wife for their love, support and encouragement, help and motivation.

Table of Contents

List of Figures

List of Tables

Nomenclature

Al	Alkylaluminum concentration ($mol \cdot L^{-1}$)
B^j_r	Polymer segment with chain length r at state $j = I$ or II
C_d	Deactivated catalyst site
C_j	Inactive catalyst site concentration at state $j = I$ or II ($mol \cdot L^{-1}$)
$D^j_{r,i}$	Dead chain with chain length r and i stereoblocks terminated at state $j = I$ or II
Do	Electron donor concentration ($mol \cdot L^{-1}$)
H	Hydrogen concentration ($mol \cdot L^{-1}$)
I	Catalyst poison
$k_{p,j}$	Rate constant for monomer propagation at state $j = I$ or II ($L \cdot mol^{-1} s^{-1}$)
k^+_{Do}	Forward rate constant for transformation by donor ($L \cdot mol^{-1} s^{-1}$)
k^-_{Do}	Backward rate constant for transformation by donor (s^{-1})
k_{a1}	Rate constant for activation (subscript "1" or "2" stands for the state I and II respectively) ($L \cdot mol^{-1} s^{-1}$)
$k_{Al \cdot I}$	Rate constant for the scavenging or passivation by alkylaluminum ($L \cdot mol^{-1} s^{-1}$)
k_{Al1}	Rate constant for transfer to alkylaluminum (subscript "1" or "2" stands for the state I and II respectively) ($L \cdot mol^{-1} s^{-1}$)
k_d	Rate constant for deactivation (s^{-1})
k_{dI}	Rate constant for deactivation by poison I ($L \cdot mol^{-1} s^{-1}$)
k_{H1}	Rate constant for transfer to hydrogen (subscript "1" or "2" stands for the state I and II respectively) ($L \cdot mol^{-1} s^{-1}$)
k_{i1}	Rate constant for initiation of the free active site P_0 (subscript "1" or "2" stands for the state I and II respectively) ($L \cdot mol^{-1} s^{-1}$)

k_{iH1} Rate constant for the reinitiation of the metal hydride active site P_H (subscript "1" or "2" stands for the state *I* and *II* respectively) ($L \cdot mol^{-1} s^{-1}$)

k_{iR1} Rate constant for the reinitiation of P_{Et} (subscript "1" or "2" stands for the state *I* and *II* respectively) ($L \cdot mol^{-1} s^{-1}$)

k_{M1} Rate constant for transfer to monomer (subscript "1" or "2" stands for the state *I* and *II* respectively) ($L \cdot mol^{-1} s^{-1}$)

$k_{\beta 1}$ Rate constant for transfer by β-hydride elimination (subscript "1" or "2" stands for the state *I* and *II* respectively) (s^{-1})

L Ligand

M Monomer (propylene) concentration ($mol \cdot L^{-1}$)

M_n Number average molecular weight (g/mol)

M_w Weight average molecular weight (g/mol)

P Probability

P_0 Monomer-free active site

PDI Polydispersity index

P_{Et} Active site coordinated with an ethyl group

P_H Active site coordinated with hydrogen (metal hydride)

$P^j_{r,i}$ Living chain with chain length *r* and *i* stereoblocks at state $j = I$ or *II*

P_r Living chain with chain length *r*

R Reaction rate

r_n Number average chain length

r_w Weight average chain length

t Time (s)

$X^m_{j,i}$ Moment ($m = 0^{th}$, 1^{st} , or 2^{nd}) of dead chains terminated at state $j = I$ or *II* and with *i* stereoblocks

$Y^{m}_{j,i}$ Moment (m = 0^{th} , 1^{st} , or 2^{nd}) of living chains terminated at state $j = I$ or II and with i stereoblocks

Superscripts

I (Super or subscript *I*) stands for stereospecific site type (isotactic)

II (Super or subscript *II*) stands for non-stereospecific site type (atactic)

Subscripts

r Chain length

i Number of stereoblocks in a chain

Chapter 1

Introduction

Ziegler-Natta catalysts are the most important catalysts for the industrial production of polyolefins. They can be homogeneous or heterogeneous; homogeneous catalysts are mostly used for the synthesis of polyolefin elastomers, while heterogeneous catalysts are used for making plastics such as polyethylene and polypropylene. Polypropylene consumption in the world is growing continuously due to its excellent properties and versatility, as well as several improvements on polypropylene manufacturing technology.

Polypropylene chains have three main configurations, depending on how the methyl groups are positioned along the polymer backbone: if all of methyl groups are on the same side of the plane of the main backbone, the polymer is called *isotactic*; if the methyl groups are on alternating sides, the polymer is called *syndiotactic*; finally, if the methyl groups are randomly distributed on either side, the polymer is called *atactic*. Commercially, polypropylene is produced mainly as its isotactic isomer, with a small amount (around 2-5%) of atactic polypropylene. The fraction of isotactic chains in commercial polypropylene is quantified with the *isotacticity index*, generally measured as the mass fraction of polypropylene insoluble in boiling heptane.

Several developments have been carried out over the last fifty years to increase the isotacticity index of polypropylene. Different Ziegler-Natta catalyst generations and several *internal* and *external donor* types were used to maximize the fraction of isotactic polypropylene in commercial resins. Internal donors are used during catalyst manufacturing to maximize the

fraction of stereospecific sites that produces isotactic polymer while external donors are added to the reactor during the polymerization to replace the internal donor molecules lost during catalyst activation (Barino and Scordamaglia, 1998). Several polymerization kinetics and mathematical modeling investigations have also been used to quantify how different catalyst types and polymerization conditions affect polypropylene properties.

In Chapter 2, we reviewed the most relevant publications on propylene polymerization using multiple-site heterogeneous Ziegler-Natta catalysts. The review focuses on the effect of hydrogen concentration, and donor type and concentration, on propylene polymerization kinetics and final polymer properties.

In Chapter 3, a mechanism for propylene polymerization with single and multiple-site catalysts is proposed. The model includes a donor-assisted, site transformation step that has never been modeled before. The model describes several average properties for the isotactic, atactic and stereoblock chains made with these catalysts. Population balances based on this mechanism were developed and the method of moments applied to obtain equations to predict the molecular weight averages of the polymer.

In Chapter 4, we applied the moments equations developed in Chapter 3 to simulate the polymerization of propylene in steady-state and dynamic CSTRs. The effect of changing the concentrations of donor, hydrogen and propylene on the microstructures of the several polymer populations was investigated in details.

In Chapter 5, we developed a Monte Carlo model based on the polymerization kinetics mechanism introduced in Chapter 3. Monte Carlo simulation allows us to predict the complete distributions molecular weight and tacticity sequences in the polymer, providing the maximum amount of information on the polymer microstructure.

Finally, Chapter 6 presents our concluding remarks and suggest some future research topics associated with this thesis.

Chapter 2

Literature Review and Theoretical Background

2.1 Background

Ziegler-Natta catalysts for propylene polymerization have passed through many improvements since their discovery in the fifties. These improvements encompassed changes in catalyst precursors, cocatalysts, and internal and external electron donors. Internal donors are used during catalyst manufacturing to maximize the fraction of stereospecific sites that produces isotactic polymer; external donors are used during the polymerization to replace internal donors lost due to alkylation and reduction reactions with the cocatalyst. In addition to its use for passivation (poison scavenging), the cocatalyst is used to activate the catalyst by the reduction and alkylation of the transition metal (Busico *et al.*, 1985; Barino and Scordamaglia, 1998; Chadwick *et al*., 2001).

The 1st and 2nd commercial generations of Ziegler-Natta catalysts were composed of crystalline $TiCl_3$ in four different geometries (α = hexagonal, β = fiber or chain shape, γ = cubic, and δ = alternating between hexagonal and cubic). Three of these geometries (α, γ and δ) have high steroselectivity and can be activated with a diethylaluminum cocatalyst. The δ-$TiCl_3$ complex, in particular, has the highest activity towards propylene polymerization. δ-$TiCl_3$ is obtained as porous particles with relatively small diameters (20-40 μm); the controlled fragmentation of the

catalyst particles during polymerization was one of the major challenges to the development of heterogeneous Ziegler-Natta catalysts.

The use of electron donors (Lewis bases) during polymerization increases the steroselectivity and productivity of this type of catalyst, leading to the 2nd generation Ziegler-Natta catalysts. Due to the structural arrangement of these two first catalyst generations (most of the potential active sites were located inside the catalyst crystals where they could not promote polymerization), they had poor productivity per mole of titanium and required post-reactor steps for deashing (removal of catalyst residuals). Their lower stereoselectivity also demanded a post-reactor step for atactic polypropylene extraction. The elimination of these two shortcomings was among the main driving forces behind the development of new types of heterogeneous Ziegler-Natta catalysts.

A new catalyst generation came about when $TiCl_4$ was supported on porous $MgCl_2$ particles. These 3rd generation ($TiCl_4/MgCl_2$) Ziegler-Natta catalysts had very high activity and steroselectivity. Shell (1960) was able to produce the first 3rd generation catalyst using $TiCl_4$ supported on $MgCl_2$ with very high activity and controlled stereoselectivity using several types of electron donors. The activity of 3rd generation catalysts can be as high as 27 kg-polypropylene per gram of catalyst, which is almost six times higher than that of 2nd generation catalysts. Their isotacticity index (*II*) is 92-97% compared to 88-93% for 2nd generation catalysts. (The isotacticity index measures the fraction isotactic polypropylene – or, more correctly, the fraction of propylene insoluble in boiling heptane – in the resin.) Therefore, one of the biggest

advantages of the 3rd generation catalysts is the elimination of the post-reactor steps for atactic polypropylene removal and catalyst residue deashing.

In the early eighties, a new class of catalyst appeared in the form of metallocene complexes. Metallocenes produce polyolefins with much better control over molecular weight and chemical composition distributions than those made with Ziegler-Natta catalysts and have been used particularly for the production of differentiated commodity polyethylene and polypropylene resins.

A typical $TiCl_4/MgCl_2$ catalyst is prepared in four main temperature-controlled steps: digestion, activation, washing, and drying. The digestion step includes the reaction of an organo-magnesium (MgOR) compound, $TiCl_4$, and an internal electron donor in a chlorinated organic solvent. In this step, the active $TiCl_4$ will be dispersed in the precursor porous surface, forming the $MgCl_2$ crystal and $TiCl_3$.OR. The latter is removed by further addition of $TiCl_4$ and solvent in the activation step. Then, the formed catalyst is washed using a volatile organic compound in the washing step. Finally, the catalyst is obtained as a free-flowing powder after the volatile organic compound is evaporated using hot nitrogen in the drying step.

Table 2-1 lists the main steps in the development of electron donors for Ziegler-Natta catalysts. Initially, aromatic monoesters, such as ethyl benzoate (EB), were used as internal donors to increase the *II* from 40% to 60%. Later on, in addition to their use as internal donors, aromatic monoesters were also used as external donors, increasing the *II* to 95%. Furthermore, the *II* was

increased to 97 – 99% with the use of aromatic diesters as internal donors (di-iso-butylphthalate, DIBP), and silanes as external donors (n-propyl,tri-methoxysilane, NPTMS). Later studies showed that very high *II* values (97 – 99%) could be obtained in the absence of external donors when using diethers as internal donors (Morini *et al.*, 1996).

Some hypotheses have been proposed to explain the effect of electron donors on propylene polymerization. Electron donors may block or poison most of the less stereospecific active sites on the catalyst (Busico *et al.*, 1985), or convert aspecific sites to stereospecific sites (Arlman *et al.*, 1964).

Table 2-1: Summary of electron donor development

Internal Donor	External Donor	Isotactic Index (*II*)
Aromatic Monoesters (EB)	--	60 %
Aromatic Monoesters (EB)	Aromatic Monoesters (methyl *p*-toluate)	95 %
Aromatic Diesters (DIBP)	Silanes (NPTMS)	97 – 99 %
Diethers (1,3-diether)	--	97 – 99 %

Electron donors are supposed to control the $TiCl_4$ distribution on the (100) and (110) faces of the $MgCl_2$ surface as illustrated in Figure 2-1 (Busico *et al.*, 1985; Chadwick *et al*., 2001). Ti_2Cl_8 species coordinate with the (100) faces through dinuclear bonds to form the isospecific polymerization sites, while the electron donor molecules tend to coordinate with the non-

stereospecific (more acidic) sites on the (110) faces. When aromatic monoesters and diesters are used as internal donors, the addition of alkylaluminiums (alkylation) will result in the partial removal of the internal donors; therefore, the use of external donors is essential to maintain the high steroselectivity level of these catalysts. During catalyst preparation there is still a chance of the internal donor to coordinate with the (100) face; but it has been reported that, in the case of ethyl benzoate, $TiCl_4$ is able to remove the donor from that stereospecific face (100) during the titanation step (addition of $TiCl_4$ during the activation step). However, when 1,3-diethers are used as internal donors, they coordinate strongly with the (110) faces and cannot be removed by alkylaluminiums (Barino and Scordamaglia, 1998). As a consequence, Ziegler-Natta catalysts with excellent isospecificity are obtained with diether internal donors in the absence of external donors.

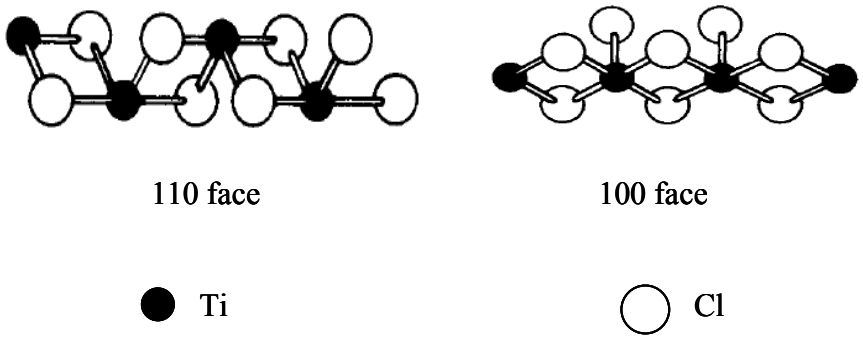

Figure 2-1: Lateral faces of a $TiCl_4/MgCl_2$ Ziegler-Natta catalyst (Busico *et al.*, 1985).

The microstructure of polypropylene chains can be classified (Chadwick *et al.*, 1996) from a regioregularity point of view as regioregular (regular 1,2 insertions) and regioirregular (random 1,2 and 2,1 insertions). These chains can also be classified as isotactic (with methyl groups aligned selectively at one side of the plane) as shown in Figure 2-2, or atactic (with a random

placement of methyl groups on either side of the plane), as illustrated in Figure 2-3. Isotactic regioregular chains are also called stereoregular chains, and atactic chains are called stereoirregular chains. Other arrangements for isotactic and atactic regioirregular chains are illustrated in Figure 2-4 and Figure 2-5.

In the following sections, we will discuss the effects of hydrogen and electron donor on the stereo- and regioregularity of polypropylene chains.

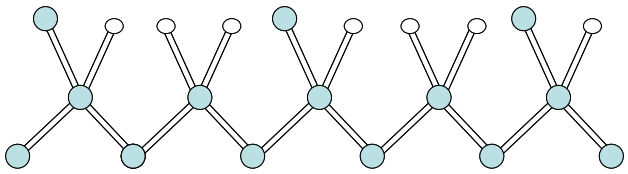

Figure 2-2: Isotactic regioregular chain (stereospecific).

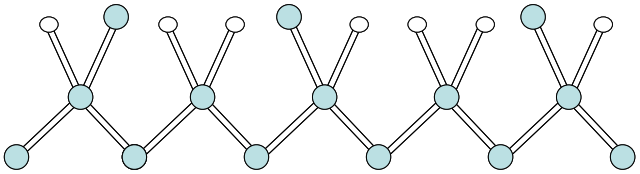

Figure 2-3: Atactic regioregular chain (stereoirregular).

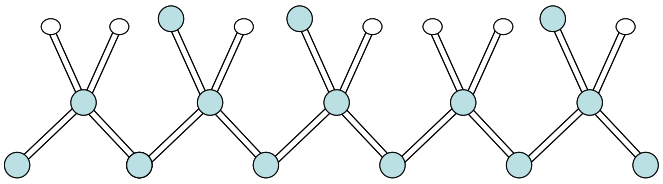

Figure 2-4: Isotactic regioirregular chain.

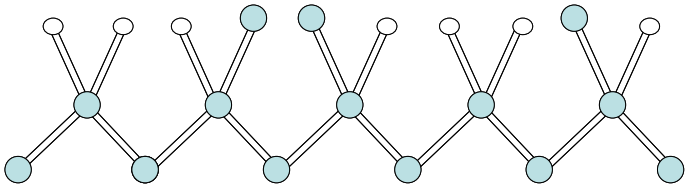

Figure 2-5: Atactic regioirregular chain.

2.2 Hydrogen Effect

Hydrogen always acts as a chain transfer agent during olefin polymerization: when the hydrogen concentration increases, the molecular weight of the polyolefin decreases. On the other hand, the effect of hydrogen on catalyst activity during olefin polymerization is less predictable and varies depending on the type of catalyst, monomer, and donor systems. For instance, hydrogen generally reduces the polymerization rate of ethylene and increases the polymerization rate of propylene when high-activity $TiCl_4/MgCl_2$ catalysts are used (Shaffer and Ray, 1996).

The initial rate of propylene polymerization increases when the partial pressure of hydrogen is increased, which seems to indicate that the hydrogen activation process is very fast. Some researchers have proposed that this polymerization rate increase was due to the ease access of monomer to the catalyst active site since, in the presence of hydrogen, the molecular weight of the polymer decreases and the monomer diffusion rate would be higher (Boucheron, 1975). This is not true, however, in the case of ethylene, where the polymerization rate generally decreases

when hydrogen is introduced into the reactor. Other investigators have assumed that the decrease in the overall polymerization rate is due to the decrease in the rate of reinitiation of metal-hydride sites (Ti-H) formed after transfer to hydrogen (Natta, 1959; Soga and Sino, 1982).

It has also been reported (Chadwick *et al*., 1996) that the ratio of propagation rate to chain transfer rate depends on the stereo- and regioregularity of the last monomer unit added to the polymer chain in the order: stereoregular > stereoirregular > regioirregular.

Due to detection limitations of ^{13}C NMR spectroscopy on regio-defects of highly isotactic polypropylene, Busico *et al*. (1992) studied polypropylene samples of very small molecular weight averages (propylene oligomers) by using excess hydrogen as the chain transfer agent. The oligomers were characterized by chromatography/mass spectrometry (GC-MS). Monomer insertions were classified as primary 1,2 (k_{pp} = head-to-tail or k_{sp} = head-to-head) or secondary 2,1 (k_{ps} = tail-to-tail or k_{ss} = tail-to-head), as shown in Schemes 2-1 and 2-2. Their experimental results showed that the ratio of 1,2 to 2,1 insertions increased as the degree of polymerization decreased, that is, shorter chains made at higher hydrogen concentrations had fewer 2,1 regioirregularities.

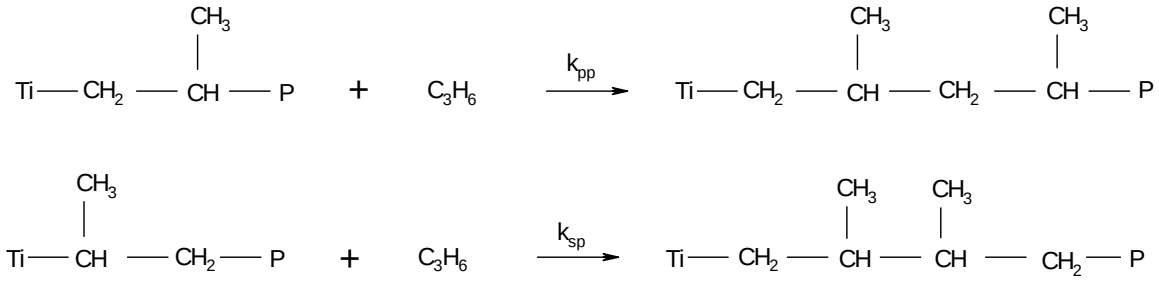

Scheme 2-1: 1,2 propylene insertion.

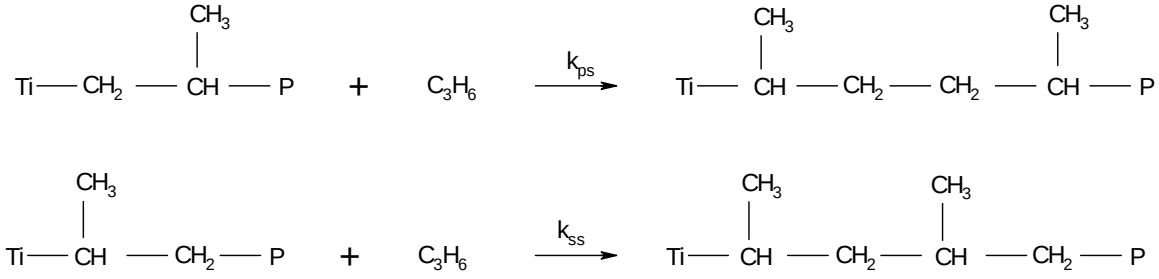

Scheme 2-2: 2,1 propylene insertion.

The increase in propylene polymerization rate by addition of hydrogen is well known. In the absence of hydrogen, regioirregular-terminated chains will be formed on some of the catalyst sites. These sites are considered “dormant” because the regioirregular insertions at the chain end slow down the next monomer insertion, thus reducing the overall propylene polymerization rate (Rishina *el al*., 1994). When hydrogen is added to the reactor, it reacts with the “dormant” 2,1-terminated chains, freeing up the sites for polymerization (Kissin and Rishina, 2002; Kissin *et al.*, 1999; Kissin *et al.*, 2002). Busico *et al*. (1992) showed that the ratio of 1,2 to 2,1 insertions increased (the chains became more regioregular) as the molecular weight decreased because hydrogen will more likely terminate chains after a 2,1 insertion due to their lower rate of chain

growth. These conclusions have been supported by the analyses of Chadwick *et al*. (1994) for chain-end determination. They showed that donors with a lower hydrogen activation effect produced polypropylene with the lowest fraction of chain-ends formed by chain transfer after 2,1-insertion.

Guastalla and Giannini (1983) carried out some experiments measuring the effect of the initial concentration of hydrogen on the polymerization rate measured after one minute of polymerization. They showed that the propylene polymerization rate increased dramatically by increasing the hydrogen concentration up to a certain maximum hydrogen partial pressure of about 0.6 kg/cm^2, after which no more rate effects were detected. They suggested that this behaviour was caused by the adsorption of hydrogen on the catalyst surface, but did not provide any further evidence to support their explanation.

Kissin and Rishina (2002) studied the effect of hydrogen concentration on propylene and ethylene polymerization. They concluded that the existence of dormant or stable Ti-$CH(R)CH_3$ sites (R is CH_3 for propylene and H for ethylene polymerization) is the reason for the different effect that hydrogen has on the polymerization rate of propylene and ethylene. Their explanation for the effect of hydrogen on propylene polymerization coincides with the one proposed by Busico *et al* (1992) discussed above. For the rate decrease effect of hydrogen on ethylene polymerization, they proposed the formation of a dormant site with the general structure Ti-CH_2CH_3. One of the hydrogen atoms bonded to the β carbon interacts with the vacancy on the titanium atom (β-agostic interaction), slowing down monomer propagation. They argue that the

Ti-CH_2CH_3 is formed after ethylene insertion on a Ti-H site produced by transfer to hydrogen. Consequently, as hydrogen concentration increases, the fraction of Ti-H sites and "dormant" Ti-CH_2CH_3 species will also increase. One must be aware, however, that β-hydride elimination also produces Ti-H sites and that transfer to ethylene will form Ti-CH_2CH_3 sites and, therefore, this explanation is only strictly valid if the main transfer mechanism in the absence of hydrogen is transfer to cocatalyst.

2.3 Stereoregularity

Understanding the geometry of Ziegler-Natta catalysts helps simplify the complexity of the electron donor roles and explain the behavior of different active site types. As discussed above (Busico *et al.*, 1985; Barino and Scordamaglia, 1998; Chadwick *et al*., 2001), internal donors are used to block non-stereoselective (110) catalyst faces on the catalyst. These internal donors (aromatic monoesters or aromatic diesters) are partially lost during the alkylation process; therefore, the use of external donors during the polymerization reaction is essential to maintain high stereoselectivity of the catalysts to make highly isotactic polypropylene. Figure 2-6 shows a molecular model for a $TiCl_4/MgCl_2$ catalyst used for propylene polymerization (Kakugo *et al.,* 1988). Three different site structures have been proposed: a highly isotactic, a low isotactic, and an atactic site. The highly isotactic site has only one coordination vacancy and all its chlorine atoms are bonded to magnesium atoms on the surface of the support. Despite of also having only

one coordination vacancy, two chlorine atoms of the low isotactic site are not bonded to a magnesium atom, accounting for its lower isotacticity. Finally, the two coordination vacancies of the atactic site allow for coordination of propylene in a random orientation, forming atactic polypropylene chains.

The addition of electron donors is explained in Figure 2-7 and Figure 2-8. When the electron donor complexes with the low isotactic site, it blocks the coordination vacancy, rendering the site inactive for polymerization. On the other hand, when the electron donor complexes with one of the coordination vacancies of the atactic site, the site becomes isotactic, since only one coordination vacancy (and, therefore, only one mode of monomer orientation) is left for propylene polymerization. It is interesting to notice that some donors may completely kill the catalyst when used in excess. This phenomenon is utilized in some commercial processes to kill the polymerization (self extinction) during plant shutdowns. This procedure avoids contaminating the reaction system with undesired poisons such as carbon monoxide. In this case, the excess donor will block not only the coordination vacancies on the atactic and low isotactic site, but also on the isotactic sites. However, not all donors act as catalyst poisons, even if an excess is added to the polymerization reactor.

Busico *et al.* (1999) prefer to classify the catalyst sites as highly isotactic, poorly isotactic (isotactoid), and syndiotactic. Atactic polypropylene is assumed to be produced in the poorly isotactic and syndiotactic sites, due to the transformation of one site into the other. Figure 2-9 shows the three types of sites proposed by Busico. The highly isotactic site (a) has either two

ligands (a chlorine or a donor atom) or one ligand with a strong steric hindrance to prevent a wrong insertion of monomer at position S2. The isotactoid site (b) has only one ligand. The syndiotactic site (c) has two vacancies and no stereoselective control. Busico *et al.* have proposed that the loss of steric hindrance may lead to the transformation of highly isotactic sites to isotactoid and then to syndiotactic sites.

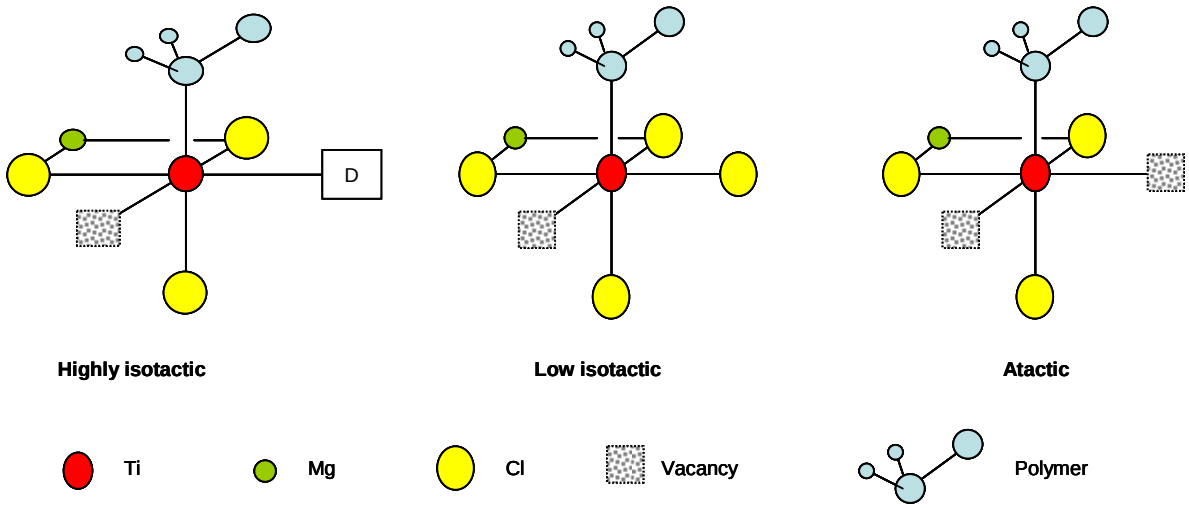

Figure 2-6: Catalyst site geometric models. *D* stands for the donor (Kakugo *et al.,* 1988).

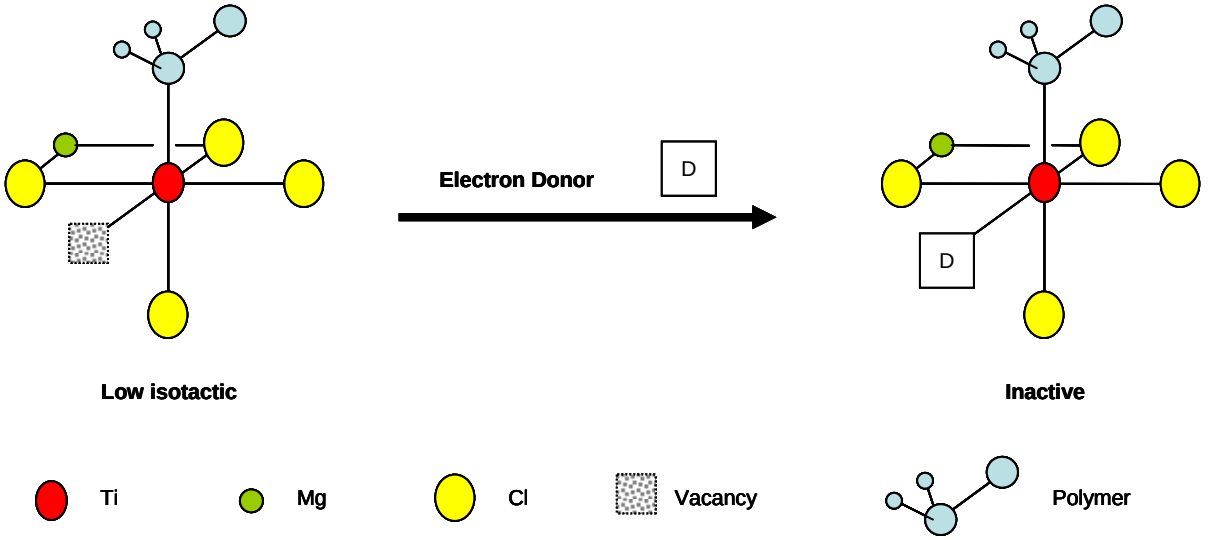

Figure 2-7: Donor addition to low isotactic site (Kakugo *et al.,* 1988).

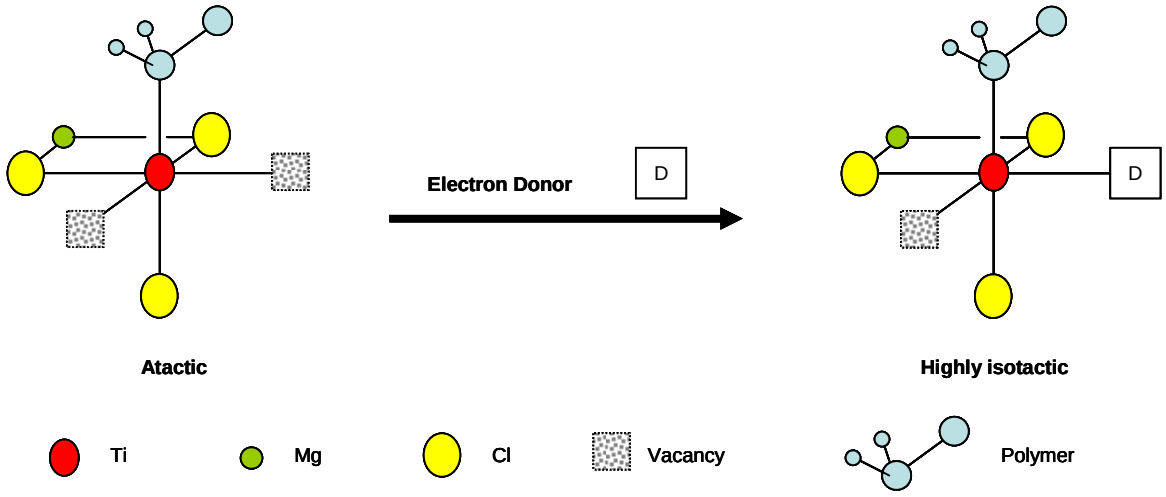

Figure 2-8: Donor addition to atactic site (Kakugo *et al.,* 1988).

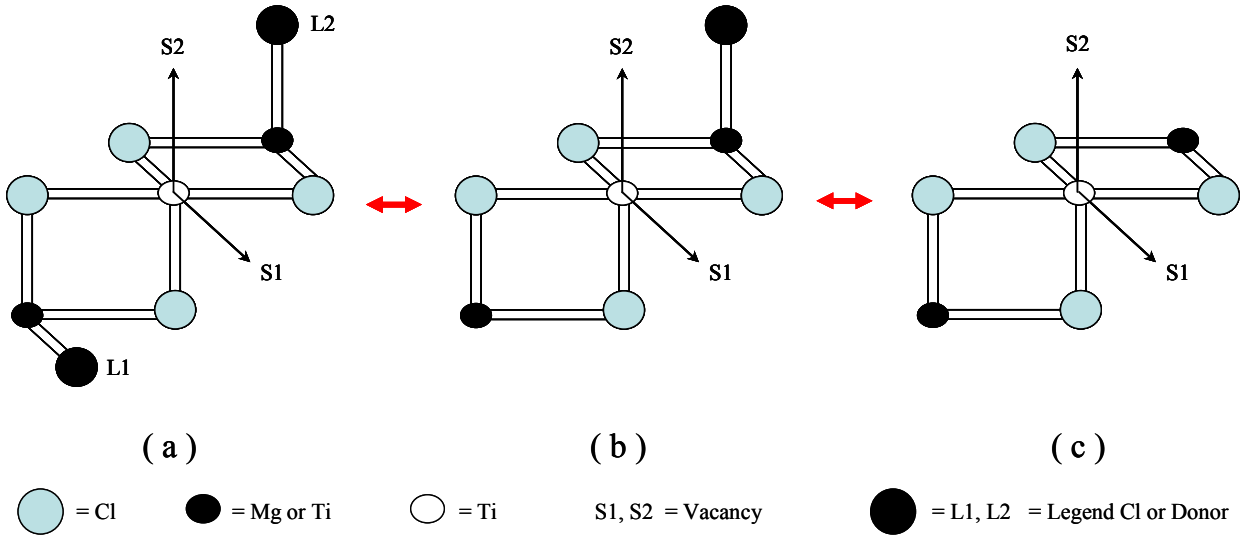

Figure 2-9: Active species models: (a) highly isotactic (b) isotactoid (c) syndiotactic (Busico *et al*., 1999).

2.4 Regioregularity

Chain regioregularity has a significant effect on the properties of polypropylene. There are two possible modes of propylene insertion: 1-2 or 2-1. Regioregular chains are composed of many 1-2 or 2-1 insertions, without any insertion defects. For the coordination polymerization of propylene, the most common insertion type is 1-2, since the methyl group "prefers" to be positioned away from the active site due to steric hindrances. A 2-1 insertion after a 1-2 insertion will cause a regioirregular sequence in the polymer chain. This irregularity will decrease the melting temperature and crystallinity of the polymer.

For propylene made with $MgCl_2/TiCl_4$/diether system, there is a relation between chain transfer by hydrogen and the type of insertion (Chadwick *et al*., 1996). Polypropylene chains terminated with normal-butyl or iso-butyl groups result from transfer to hydrogen following 2-1 or 1-2 insertions, respectively. These chain transfer reactions depend on the components of the reaction system (catalyst, cocatalyst, donor, and monomer) and on the hydrogen concentration (Chadwick *et al*., 1995; Chadwick *et al*., 1996). Table 2-2 shows that polypropylene tacticity (as measured by the fraction of polymer insoluble in boiling xylene, XS) depends on electron donor type and hydrogen concentration. In their work, three different external donors were used with $MgCl_2/TiCl_4$/DIBP catalyst: phenyltriethoxysilane (PTES), cyclohexylmethyldimethoxysilane (CHMDMS), and dicyclopentyldimethoxysilane (DCPDMS). These three donors were chosen because they produced catalyst systems with different hydrogen sensitivities on polymer molecular weight. PTES shows the lowest and DCPDMS shows the highest hydrogen response. Chadwick *et al*. (1995) reported that for CHMDMS and DCPDMS donors, propagation after 2-1 insertion could happen due the presence of regioirregular (head-to-head) sequences in the xylene soluble fraction. However, no regioregularity was detected in the isotactic fraction. The chain-end distribution of the isotactic fraction made with the three donors is shown in Table 2-3. The three possible chain-end types are illustrated in Scheme 2-3. The fraction of *n-Bu* terminated chains decreases when hydrogen concentration increases.

Table 2-2: Properties of polypropylene samples made with different donor types and hydrogen concentrations (Chadwick *et al*., 1995)

External Donor	**H_2**	**PP yield**	**XS**	**[η]**
	vol. %	**Kg/g.cat**	**Wt %**	**dL/g**
PTES	0	10	3.6	7.09
	6	22	3.7	1.16
	16	27	7.1	0.89
CHMDMS	0	8	3.8	6.73
	6	30	2.9	1.41
	16	32	3.0	1.05
DCPDMS	0	9	2.8	10.42
	6	29	1.6	2.32
	16	35	2.3	1.35

PTES: phenyltriethoxysilane, CHMDMS: cyclohexylmethyldimethoxysilane, DCPDMS: dicyclopentyldimethoxysilane

$$Ti - CH_2 - CH(CH_3) - CH_2 - CH(CH_3) \sim ..... + H_2 \rightarrow Ti - H + i.Bu - CH(CH_3) \sim ....$$

$$Ti - H + propylene \rightarrow Ti - CH_2 - CH_2 - CH_3 \Rightarrow Ti - [CH_2 - CH(CH_3)]_n - n.propyl$$

$$Ti - [CH_2 - CH_2(CH_3)]_n - n.propyl + CH_2 - CH_2 - CH_3$$

$$\rightarrow Ti - CH(CH_3) - CH_2 - [CH_2 - CH(CH_3)]_n - n.propyl$$

$$Ti - CH(CH_3) - CH_2 - [CH_2 - CH(CH_3)]_n - n.propyl + propylene + H_2$$

$$\rightarrow Ti - H + n.Butyl - CH(CH_3) - [CH_2 - CH(CH_3)]_n - n.propyl$$

Scheme 2-3: Polypropylene chain-end types (Chadwick *et al*., 1995)

Table 2-3: Chain-end distribution in isotactic sample (Chadwick *et al*., 1995)

External donor	H_2 vol. %	Chain-end distribution in %		
		n- propyl	*i- butyl*	*n-butyl*
PTES	6	50	31	19
	16	50	41.5	8.5
CHMDMS	6	50	27	23
	16	50	38	12
DCPDMS	16	50	33	17

However, it has been also reported by Chadwick *et al*. (1996) that for highly isotactic polypropylene made with $MgCl_2/TiCl_4$/diether at low H_2 concentration, the fraction of chains with *n*-Bu chain ends was high. Therefore, they concluded that for the $MgCl_2/TiCl_4$/diether system, highly stereospecific sites were not totally regiospecific, contrarily to their previous investigation (Chadwick *et al.*, 1995). This shows the danger of postulating general rules for these complex catalyst/donor systems.

Chapter 3

Reaction Mechanism and Mathematical Modeling

3.1 Introduction

Mathematical models for olefin polymerization are useful to predict polymer microstructure and properties in laboratory and industrial reactor scales. There are several methods for modeling olefin polymerization reactors (Soares, 2001). Most of them start by defining the polymerization mechanism and then setting up population balances for all the chemical species involved in the polymerization. The dynamic solution of the complete population balances, to generate the molecular weight distribution (MWD) of polyolefins, requires sophisticated ordinary differential equation (ODE) solvers, since the set of population balance ODEs may involve thousands of equations. A more common alternative is to use the method of moments to reduce the size of the ODE system to just a few equations for the leading moments. These systems are much easier to solve, but only some of the molecular weight averages can be predicted, not the complete MWD. Finally, the method of instantaneous distributions uses closed analytical solutions for the instantaneous MWD that can be integrated over time. This method requires the lowest computation time and generates complete microstructural distributions but, unfortunately, instantaneous distributions are not available for all polymerization mechanisms.

Monte Carlo simulation is also a very powerful modeling approach. It also starts by defining the polymerization mechanism but, contrarily to the methods discussed in the previous paragraph, there is no need to formulate population balances. The polymerization mechanism is used to create an algorithm where polymer chains are generated one by one using a set of reaction probabilities based on the polymerization kinetic constants. Monte Carlo simulation gives the maximum amount of information on polymer microstructure but it is generally the most time consuming technique of all discussed above.

The tacticity distribution of polypropylene resins is one of their most important properties. However, no detailed mathematical model has been developed to date to describe the tacticity distribution of polypropylene chains made with multiple-site catalysts. We may postulate the existence of at least three types of active sites on Ziegler-Natta catalysts used for propylene polymerization: sites that make only atactic chains, sites that only make isotactic chains, and sites that may alternate between stereoselective and aspecific states. Based on the mechanistic studies of Kakugo *et al*. (1988) and Busico *et al*. (1995, 1999) (See Figure 2-7 and Figure 2-8), atactic sites can be reversibly converted to isotactic sites by complexation with an electron donor molecule. Therefore, these sites could have two states: one atactic and one isotactic state. If this conversion takes place during the lifetime of a polypropylene chain, stereoblock chains (atactic-isotactic-atactic-isotactic-…) may be formed.

The active site type that can alternate between stereospecific and aspecific states can produce three types of dead polymer chains: 1) purely isotactic chains are formed when they grow during the stereospecific state and terminate before transformation to the atactic state, 2) purely atactic chains are formed when they grow during the aspecific state and terminate before transformation to the stereospecific state, and 3) stereoblock chains are formed when the site state changes from stereospecific to aspecific and/or vice-versa during the life time of the chain. Stereoblock chains can be further subdivided into diblock, triblock, tetrablock, and higher multiblock chains as presented in Figure 3-1. On the other hand and in order to overview the entire population of the polymer chains, they were classified based on the segment type as illustrated in Figure 3-2.

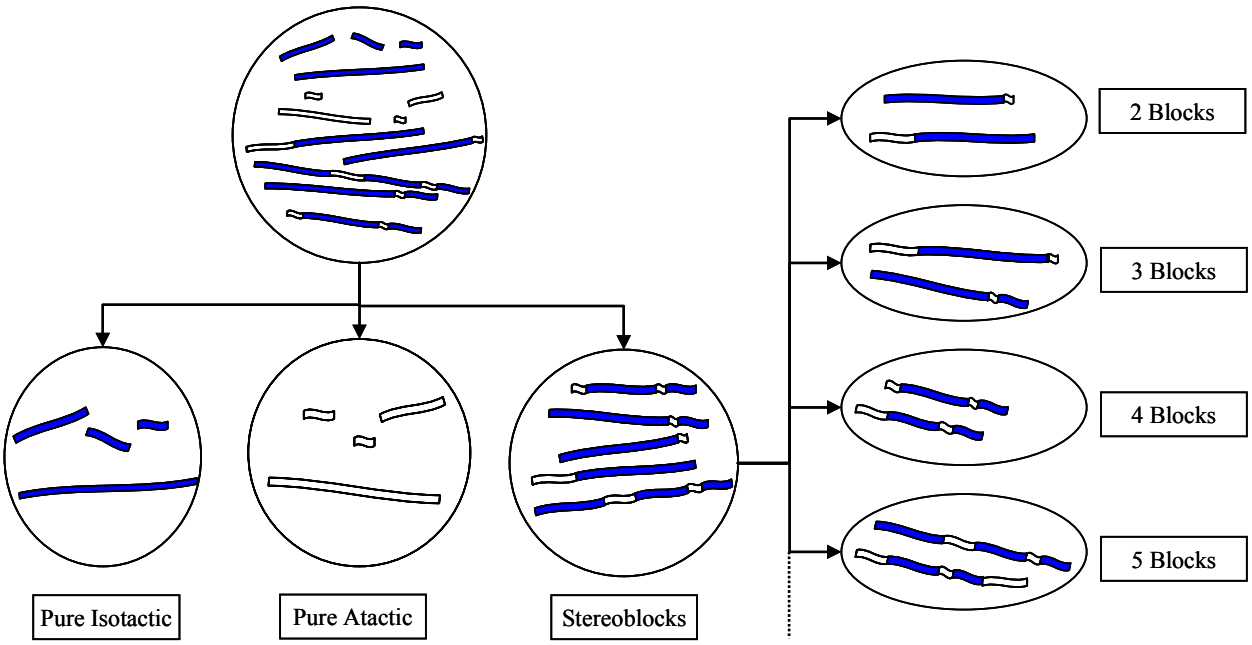

Figure 3-1: Chain populations with different number of stereoblocks. (Whole chains.)

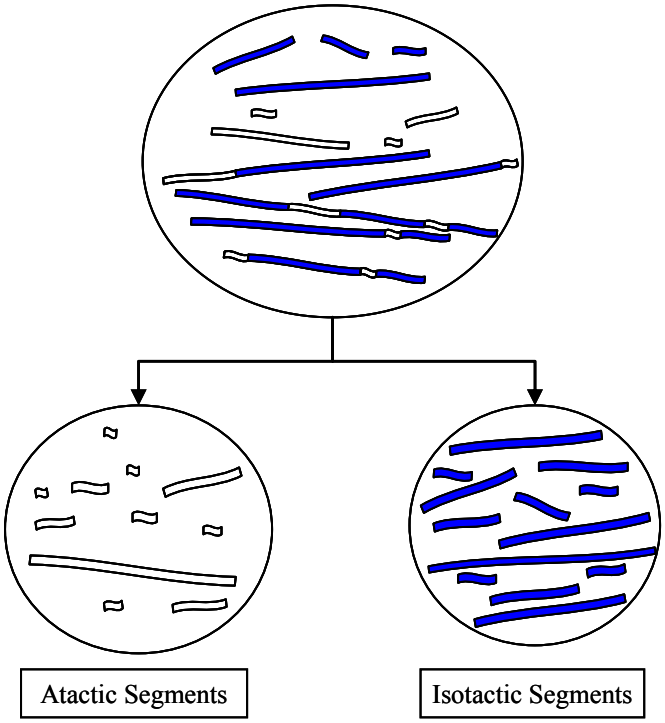

Figure 3-2: Chain length distributions for chain segments.

3.2 Reaction Mechanism

It has been reported by Busico *et al.* (1995) that the reversible transformation from stereospecific to aspecific state by reaction with electron donor molecules may happen during chain growth. Based on this mechanism, we proposed the following polymerization kinetic steps for active sites that can assume stereospecific (state *I*) and aspecific (state *II*) states.

Activation

Catalyst (C_I and C_{II}) at state *I* or *II* is activated (alkylated and reduced) by reaction with alkylaluminum cocatalysts (*Al*) according to Equations (3-1) and (3-2), forming monomer-free active sites, P_0^I and P_0^{II}, where the subscript "0" indicates that there are no monomer units attached to the active site:

$$C_I + Al \xrightarrow{k_{a1}} P_0^I \tag{3-1}$$

$$C_{II} + Al \xrightarrow{k_{a2}} P_0^{II} \tag{3-2}$$

Passivation

Alkylaluminum molecules (such as triethylaluminum TEA) can also act as scavengers by reacting with polar molecules such as water or oxygen (*I*) present in the system in trace amounts, according to the reaction:

$$Al + I \xrightarrow{k_{Al \cdot I}} Al \cdot I \tag{3-3}$$

Initiation

Monomer-free sites, either resulting from catalyst activation (P_0^I , P_0^{II}) or chain transfer reactions (P_H^I , P_H^{II} , P_{Et}^I , P_{Et}^{II}), are initiated by insertion of the first monomeric unit (*M*) according to the following elementary steps:

$$P_0^I + M \xrightarrow{k_{i1}} P_{1,1}^I \tag{3-4}$$

$$P_0^{II} + M \xrightarrow{k_{i2}} P_{1,1}^{II} \tag{3-5}$$

$$P_H^I + M \xrightarrow{k_{iH1}} P_{1,1}^I \tag{3-6}$$

$$P_H^{II} + M \xrightarrow{k_{iH2}} P_{1,1}^{II} \tag{3-7}$$

$$P_{Et}^I + M \xrightarrow{k_{iR1}} P_{1,1}^I \tag{3-8}$$

$$P_{Et}^{II} + M \xrightarrow{k_{iR2}} P_{1,1}^{II} \tag{3-9}$$

Notice that we adopted the following convention to keep track of polymer chain length, number of blocks per chain, and catalyst state: $P^{state}_{chain\,length,\ number\ of\ blocks}$

Site Transformation by Electron Donor

The most important innovation in the mathematical model proposed in this thesis is modeling of the reversible site transformation from the stereospecific state *I* to the aspecific state *II* in the presence of the electron donor (*Do*). As the site state changes from *II* to *I* (by coordination with

an electron donor molecule) or from *I* to *II* (by release of an electron donor molecule), the polymer chain length is not altered (*r* remains the same), but the number of stereoblocks increases by 1 (*i*+1), as shown in the equations below:

$$P_0^{II} + Do \xrightarrow{k_{Do}^+} P_0^I \tag{3-10}$$

$$P_0^I \xrightarrow{k_{Do}^-} P_0^{II} + Do \tag{3-11}$$

$$P_H^{II} + Do \xrightarrow{k_{Do}^+} P_H^I \tag{3-12}$$

$$P_H^I \xrightarrow{k_{Do}^-} P_H^{II} + Do \tag{3-13}$$

$$P_{Et}^{II} + Do \xrightarrow{k_{Do}^+} P_{Et}^I \tag{3-14}$$

$$P_{Et}^I \xrightarrow{k_{Do}^-} P_{Et}^{II} + Do \tag{3-15}$$

$$P_{r,i}^{II} + Do \xrightarrow{k_{Do}^+} P_{r,i+1}^I \tag{3-16}$$

$$P_{r,i}^I \xrightarrow{k_{Do}^-} P_{r,i+1}^{II} + Do \tag{3-17}$$

Equations (3-16) and (3-17) keep track of the number of blocks and chain length of the whole polymer chain. However, it is also useful to find out the distribution of sizes of isotactic (*I*) and atactic (*II*) blocks. For this distribution, we have to reformulate our equations so that we describe the concentration of blocks of length *r* (B_r^I and B_r^{II}), according to the equations:

$$P_{r,i}^{II} + Do \xrightarrow{k_{Do}^+} B_r^{II} + P_{0,i+1}^I \tag{3-18}$$

$$P_{r,i}^{I} \xrightarrow{k_{Do}} B_{r}^{I} + P_{0,i+1}^{II} + Do \tag{3-19}$$

Notice that, after a site transformation step, the length of the living polymer is reset to zero, since a new block starts forming at this moment. With these expressions, we are able to follow the length of all isotactic and atactic segments in the reactor without considering the particular chain (isotactic, atactic, stereoblock) they belong to.

Propagation

Propagation is the most common step during polymerization. The addition of monomer to sites in state *I* or *II* increases the length of the chain by one unit (*r*+1), as indicated below:

$$P_{r,i}^{I} + M \xrightarrow{k_{p1}} P_{r+1,i}^{I} \tag{3-20}$$

$$P_{r,i}^{II} + M \xrightarrow{k_{p2}} P_{r+1,i}^{II} \tag{3-21}$$

Although there could be four different types of regio insertions (head-to-head, head-to-tail, tail-to-head, and tail-to-tail) leading to four different propagation constants, we will not distinguish between them in this model.

Chain Transfer

The five most common chain transfer steps in coordination polymerization are β-hydride-elimination, β-methyl-elimination, transfer to hydrogen, transfer to monomer, and transfer to cocatalyst. These chain transfer steps are described in more details below.

β-hydride elimination: During β-hydride elimination, one of the hydrogen atoms attached to the β carbon atom is transferred to the titanium active site, forming a metal hydride Ti-H site (P_H^I or P_H^{II}) and a dead chain with a terminal unsaturated ($D_{r,i}^I$ or $D_{r,i}^{II}$).

$$P_{r,i}^I \xrightarrow{k_{\beta 1}} P_H^I + D_{r,i}^I \tag{3-22}$$

$$P_{r,i}^{II} \xrightarrow{k_{\beta 2}} P_H^{II} + D_{r,i}^{II} \tag{3-23}$$

β-methyl elimination: During β-methyl elimination, the methyl group attached to the β carbon atom is transferred to the titanium active site, forming a metal methyl Ti-CH_3 site and a dead polypropylene with terminal vinyl group. This transfer step may be important for some metallocene catalyst but happens rarely with Ziegler Natta catalyst and will not be included in this model.

Transfer to hydrogen: The main transfer step in industrial-scale propylene polymerization is transfer to hydrogen. This transfer step will also generate a metal hydride Ti-H site, as for β-hydride elimination, but the dead chain will have a saturated chain end. Varying hydrogen

concentration in the reactor is the main technique to control molecular weight averages of industrial polypropylene resins.

$$P_{r,i}^{I} + H_2 \xrightarrow{k_{H1}} P_H^I + D_{r,i}^I \tag{3-24}$$

$$P_{r,i}^{II} + H_2 \xrightarrow{k_{H2}} P_H^{II} + D_{r,i}^{II} \tag{3-25}$$

Transfer to monomer: Transfer to monomer takes place when a monomer molecule coordinated to the active site "fails" to insert in the growing polymer chains but, instead, terminates chain growth, forming a living polymer chain of unity length and a dead chain with a terminal unsaturation.

$$P_{r,i}^{I} + M \xrightarrow{k_{M1}} P_{1,1}^I + D_{r,i}^I \tag{3-26}$$

$$P_{r,i}^{II} + M \xrightarrow{k_{M2}} P_{1,1}^{II} + D_{r,i}^{II} \tag{3-27}$$

Transfer to cocatalyst: In some reactor operation conditions, especially at elevated polymerization temperatures, transfer to cocatalyst may be considerable. It is, however, generally negligible at normal polymerization temperatures with $TiCl_4/MgCl_2$ Ziegler-Natta catalysts. When this transfer step occurs, an active site bonded to the alkyl group of the alkylaluminum compound (an ethyl group in the case of triethylaluminum) and a dead polymer chain with saturated chain end (bonded to the aluminum compound) will be formed, as illustrated in the equations below.

$$P_{r,i}^{I} + Al \xrightarrow{k_{Al1}} P_{Et}^{I} + D_{r,i}^{I} \tag{3-28}$$

$$P_{r,i}^{II} + Al \xrightarrow{k_{Al2}} P_{Et}^{II} + D_{r,i}^{II} \tag{3-29}$$

Site Deactivation

Most Ziegler-Natta catalysts deactivate according to first or second order kinetics, generating a dead polymer chain and a deactivated site (C_d) that is unable to catalyze polymerization. We have adopted the first order deactivation kinetics for simplicity in this model.

$$P_{r,i}^{I} \xrightarrow{k_{d1}} C_d + D_{r,i}^{I} \tag{3-30}$$

$$P_{r,i}^{II} \xrightarrow{k_{d2}} C_d + D_{r,i}^{II} \tag{3-31}$$

Catalyst Poisoning

The existence of catalyst poisons in the polymerization system is considered one of the worst conditions in industrial polymerization processes. One of the functions of alkylaluminum catalysts is to passivate the system by removing most of the polar poisons in the reactor prior to catalyst injection and polymerization. Catalyst poisoning will result in an inactive catalyst and a dead polymer chain. Even though the kinetics of catalyst poisoning is not well understood, we have adopted the simple bimolecular mechanism shown below to describe a generic poisoning step with a polar impurity (I):

$$P_{r,i}^{I} + I \xrightarrow{k_{dI1}} C_d + D_{r,i}^{I} \tag{3-32}$$

$$P_{r,i}^{II} + I \xrightarrow{k_{dI2}} C_d + D_{r,i}^{II} \tag{3-33}$$

3.3 Mathematical Modeling of Olefin Polymerization in Continuous Stirred Tank Reactors

The proposed model can describe the MWD and molecular weight averages of purely isotactic, purely atactic, and stereoblock chains, as illustrated in Figure 3-1. The model can also describe the MWD and molecular weight averages of isotactic and atactic segments, as shown in Figure 3-2. These two approaches permit a very detailed description of the polymer microstructure, as will be demonstrated below.

We formulated three types of population balances, to monitor different aspects of the polypropylene chain microstructures:

1) Balances for the whole chains, without monitoring the number or type of stereoblocks per chain (Section 3.3.1)
2) Balances for purely isotactic, purely atactic, and stereoblock chains (Section 3.3.2)
3) Balances for chain segments (Section 3.3.3)

Since these population balances are difficult to solve, we will also formulate the moment equations for each population balance (Sections 3.3.4 to 3.3.6).

The balances derived in this chapter describe only the polymerization taking place in active sites that can undergo the stereospecific-aspecific transition discussed above. Active sites that produce only isotactic or atactic chains are much easier to model, since their behavior is a particular solution (when no site transition takes place) of the general model derived herein.

The following lumped kinetic constants will be used in our derivation to reduce the size of the resulting population balance and moment equations:

$$K_{T1} = k_{\beta 1} + k_{M1}M + k_{H1}H_2 + k_{Al1}Al \tag{3-34}$$

$$K'_{T1} = k_{\beta 1} + k_{H1}H_2 + k_{Al1}Al \tag{3-35}$$

$$K_{D1} = k_{d1} + k_{dI1}I \tag{3-36}$$

$$K_{T2} = k_{\beta 2} + k_{M2}M + k_{H2}H_2 + k_{Al2}Al \tag{3-37}$$

$$K'_{T2} = k_{\beta 2} + k_{H2}H_2 + k_{Al2}Al \tag{3-38}$$

$$K_{D2} = k_{d2} + k_{dI2}I \tag{3-39}$$

By inspection of the polymerization mechanism shown in Equations (3-1) to (3-33), the following molar balances can be written for monomer-free active sites in a continuous stirred-tank reactor (CSTR)

$$\frac{\mathrm{d}C_I}{\mathrm{d}t} = \hat{C}_I - (k_{a1}Al + s)C_I \tag{3-40}$$

$$\frac{\mathrm{d}C_{II}}{\mathrm{d}t} = \hat{C}_{II} - (k_{a2}Al + s)C_{II} \tag{3-41}$$

where $\hat{C}_I$ and $\hat{C}_{II}$ are the molar flow rates of catalyst in state *I* and *II* to the reactor and *s* is the reciprocal of the average residence time in the CSTR. The molar balances for the other active species are given by the equations

$$\frac{\mathrm{d}P_0^I}{\mathrm{d}t} = k_{a1}C_I Al + k_{Do}^+ DoP_0^{II} - (k_{i1}M + k_{Do}^- + K_{D1} + s)P_0^I \tag{3-42}$$

$$\frac{\mathrm{d}P_0^{II}}{\mathrm{d}t} = k_{a2}C_{II} Al + k_{Do}^- P_0^I - (k_{t2}M + k_{Do}^+ Do + K_{D2} + s)P_0^{II} \tag{3-43}$$

$$\frac{\mathrm{d}P_H^I}{\mathrm{d}t} = (k_{\beta 1} + k_{H1}H)\sum_{i=1}^{\infty}\sum_{r=1}^{\infty} P_{r,i}^I + k_{Do}^+ DoP_H^{II} - (k_{iH1}M + k_{Do}^- + K_{D1} + s)P_H^I \tag{3-44}$$

$$\frac{\mathrm{d}P_H^{II}}{\mathrm{d}t} = (k_{t\beta 2} + k_{tH2}H)\sum_{i=1}^{\infty}\sum_{r=1}^{\infty} P_{r,i}^{II} + k_{Do}^- P_H^I - (k_{iH2}M + k_{Do}^+ Do + K_{D2} + s)P_H^{II} \tag{3-45}$$

$$\frac{\mathrm{d}P_{Et}^I}{\mathrm{d}t} = k_{Al1}Al\sum_{i=1}^{\infty}\sum_{r=1}^{\infty} P_{r,i}^I + k_{Do}^+ DoP_{Et}^{II} - (k_{iR1}M + k_{Do}^- + K_{D1} + s)P_{Et}^I \tag{3-46}$$

$$\frac{\mathrm{d}P_{Et}^{II}}{\mathrm{d}t} = k_{Al2}Al\sum_{i=1}^{\infty}\sum_{r=1}^{\infty} P_{r,i}^{II} + k_{Do}^- P_{Et}^I - (k_{iR2}M + k_{Do}^+ Do + K_{D2} + s)P_{Et}^{II} \tag{3-47}$$

3.3.1 Population Balances for Whole Chains

The population balance for living chains with length $r = 1$ growing on a site at state *I* is given by

$$\begin{aligned}\frac{dP_1^I}{dt} &= (k_{i1}P_0^I + k_{iH1}P_H^I + k_{iR1}P_{Et}^I)M \\ &+ k_{M1}M\sum_{r=1}^{\infty}P_r^I + k_{Do}^+ DoP_1^{II} - k_{p1}MP_1^I - (k_{Do}^- + K_{T1} + K_{D1} + s)P_1^I\end{aligned} \tag{3-48}$$

Notice that the subscript *i*, used to count the number of blocks in the chain ($P_{r,i}^I$), is not required in this balance and was removed to simplify the notation.

For living chains with lengths greater than 1, $r \geq 2$, the equivalent population balance is

$$\frac{dP_r^I}{dt} = k_{p1}MP_{r-1}^I + k_{Do}^+ DoP_r^{II} - k_{p1}MP_r^I - (k_{Do}^- + K_{T1} + K_{D1} + s)P_r^I \tag{3-49}$$

Similarly, the population balance for living chains with length $r = 1$ at state *II* is

$$\begin{aligned}\frac{dP_1^{II}}{dt} &= (k_{i2}P_0^{II} + k_{iH2}P_H^{II} + k_{iR2}P_{Et}^{II})M + k_{M2}M\sum_{r=1}^{\infty}P_r^{II} \\ &+ k_{Do}^- P_1^I - k_{p2}MP_1^{II} - (k_{Do}^+ Do + K_{T2} + K_{D2} + s)P_1^{II}\end{aligned} \tag{3-50}$$

and, for living chains with $r \geq 2$ at state *II*

$$\frac{dP_r^{II}}{dt} = k_{p2} M P_{r-1}^{II} + k_{Do}^{-} P_r^{I} - k_{p2} M P_r^{II} - (k_{Do}^{+} Do + K_{T2} + K_{D2} + s) P_r^{II} \tag{3-51}$$

Population balances for dead chains are also easily formulated as follow

$$\frac{dD_r^{I}}{dt} = (K_{T1} + K_{D1}) P_r^{I} - s D_r^{I} \tag{3-52}$$

$$\frac{dD_r^{II}}{dt} = (K_{T2} + K_{D2}) P_r^{II} - s D_r^{II} \tag{3-53}$$

3.3.2 Population Balances for Isotactic, Atactic and Stereoblock Chains

Isotactic Chains

Purely isotactic living chains are those growing on sites at state *I* with only one block (i=1). If the site state changes to *II*, the chain is reclassified as stereoblock, as described below. The population balances for these chains are given by the expressions

$$\frac{dP_{1,1}^{I}}{dt} = (k_{i1}P_0^I + k_{iH1}P_H^I + k_{iR1}P_{Et}^I)M + k_{M1}M\sum_{r=1}^{\infty}P_r^I - k_{p1}MP_{1,1}^I - (k_{Do}^- + K_{T1} + K_{D1} + s)P_{1,1}^I \quad (3\text{-}54)$$

$$\frac{dP_{r,1}^{I}}{dt} = k_{p1}M(P_{r-1,1}^I - P_{r,1}^I) - (k_{Do}^- + K_{T1} + K_{D1} + s)P_{r,1}^I \quad (3\text{-}55)$$

Atactic Chains

Similarly, purely atactic living chains are those growing on a site at state *II* with only one block (i=1). Their population balances are expressed as follows:

$$\frac{dP_{1,1}^{II}}{dt} = (k_{i2}P_0^{II} + k_{iH2}P_H^{II} + k_{iR2}P_{Et}^{II})M + k_{M2}M\sum_{r=1}^{\infty}P_r^{II} - k_{p2}MP_{1,1}^{II} - (k_{Do}^+Do + K_{T2} + K_{D2} + s)P_{1,1}^{II} \quad (3\text{-}56)$$

$$\frac{dP_{r,1}^{II}}{dt} = k_{p2}M(P_{r-1,1}^{II} - P_{r,1}^{II}) - (k_{Do}^+Do + K_{T2} + K_{D2} + s)P_{r,1}^{II} \quad (3\text{-}57)$$

Stereoblock Chains

Stereoblock chains have two or more blocks, $i \geq 2$, and are formed when the site state changes from aspecific to stereospecific or vice-versa. Their population balances are also easily derived from the polymerization mechanism adopted in the model:

$$\frac{dP_{r,i}^{I}}{dt} = k_{p1}M(P_{r-1,i}^I - P_{r,i}^I) + k_{Do}^+DoP_{r,i-1}^{II} - (k_{Do}^- + K_{T1} + K_{D1} + s)P_{r,i}^I \quad (3\text{-}58)$$

$$\frac{\mathrm{d}P_{r,i}^{II}}{\mathrm{d}t} = k_{p2}M(P_{r-1,i}^{II} - P_{r,i}^{II}) + k_{Do}^{-}P_{r,i-1}^{I} - (k_{Do}^{+}Do + K_{T2} + K_{D2} + s)P_{r,i}^{II} \tag{3-59}$$

Population balances for the equivalent dead polymer chains are

$$\frac{\mathrm{dD}_{r,1}^{I}}{\mathrm{d}t} = (K_{T1} + K_{D1})P_{r,1}^{I} - sD_{r,1}^{I} \tag{3-60}$$

$$\frac{\mathrm{d}D_{r,1}^{II}}{\mathrm{d}t} = (K_{T1} + K_{D1})P_{r,1}^{II} - sD_{r,1}^{II} \tag{3-61}$$

$$\frac{\mathrm{dD}_{r,i}^{I}}{\mathrm{d}t} = (K_{T1} + K_{D1})P_{r,i}^{I} - sD_{r,i}^{I} \tag{3-62}$$

$$\frac{\mathrm{d}D_{r,i}^{II}}{\mathrm{d}t} = (K_{T1} + K_{D1})P_{r,i}^{II} - sD_{r,i}^{II} \tag{3-63}$$

3.3.3 Population Balances for Chain Segments

Chain segments are denoted as B_r^I or B_r^{II}. Purely isotactic or atactic chains are counted as one segment. Population balances for chains segments are listed below. The only difference between these moment equations and the ones derived in the previous section for isotactic, atactic, and stereoblock chains is that the state transformation reaction is treated as a pseudo-transfer reaction, zeroing the length of the chain and starting a new segment of different stereoregularity.

Isotactic Segments

$$\frac{dB_r^I}{dt} = k_{p1}M(B_{r-1}^I - B_r^I) - (k_{Do}^- + K_{T1} + K_{D1} + s)B_r^I \tag{3-64}$$

$$\frac{dB_1^I}{dt} = k_{i1}MB_0^I - k_{p1}MB_1^I - (k_{Do}^- + K_{T1}^{'} + K_{D1} + s)B_1^I \tag{3-65}$$

$$\frac{dB_0^I}{dt} = k_{a1}AlC_I + k_{Do}^+ DoB_0^{II} + k_{Do}^+ Do\sum_{r=1}^{\infty} B_r^{II} + K_{T1}^{'}\sum_{r=1}^{\infty} B_r^I - k_{i1}MB_0^I - (k_{Do}^- + K_{D1} + s)B_0^I \tag{3-66}$$

Atactic Segments

$$\frac{dB_r^{II}}{dt} = k_{p2}M(B_{r-1}^{II} - B_r^{II}) - (k_{Do}^+ Do + K_{T1} + K_{D1} + s)B_r^{II} \tag{3-67}$$

$$\frac{dB_1^{II}}{dt} = k_{i2}MB_0^{II} + k_{p2}MB_1^{II} - (k_{Do}^+ Do + K_{T1}^{'} + K_{D1} + s)B_1^{II} \tag{3-68}$$

$$\frac{dB_0^{II}}{dt} = k_{a2}AlC_{II} + k_{Do}^- B_0^I + k_{Do}^-\sum_{r=1}^{\infty} B_r^I + K_{T2}^{'}\sum_{r=1}^{\infty} B_r^{II} - k_{i2}MB_0^{II} - (k_{Do}^+ Do + K_{D2} + s)B_0^{II} \tag{3-69}$$

3.3.4 Moments Equations for Whole Chains

The population balances developed in Sections 3.3.1 and 3.3.3 encompass thousands of equations, one for each polymer of a given chain length *r*. Even though mathematical methods exist to solve these very large systems of differential equations, it is much easier to apply the

method of moments to reduce the number of equations required in the simulation. The moments of the living and dead chains for the whole chains are defined by Equations (3-70) and (3-71), respectively, where $j = I$ or II (site state), and m is the moment order:

$$Y_j^m = \sum_{r=1}^{\infty} r^m P_r^j \tag{3-70}$$

$$X_j^m = \sum_{r=1}^{\infty} r^m D_r^j \tag{3-71}$$

The zeroth moment, defined when $m = 0$, measures the total number of polymer moles in a given population. The first moment, $m = 1$, is the total mass of the polymer population. Finally, the second moment, $m = 2$, does not have physical meaning but is required to calculate the weight average molecular weight.

The method of moments can be used to estimate the number (M_n) and weight (M_w) average molecular weights of the polymer populations with the following equations:

$$M_n = mw. \frac{\sum_{r=1}^{\infty} rN_r}{\sum_{r=1}^{\infty} N_r} = mw. \frac{X_I^1 + Y_I^1 + X_{II}^1 + Y_{II}^1}{X_I^0 + Y_I^0 + X_{II}^0 + Y_{II}^0} \tag{3-72}$$

$$M_w = mw. \frac{\sum_{r=1}^{\infty} r^2 N_r}{\sum_{r=1}^{\infty} rN_r} = mw. \frac{X_I^2 + Y_I^2 + X_{II}^2 + Y_{II}^2}{X_I^1 + Y_I^1 + X_{II}^1 + Y_{II}^1} \tag{3-73}$$

where *mw* is the molar mass of the repeating unit (*mw* = 42 g/mol for propylene).

Finally, the polydispersity index is easily calculated as

$$PDI = \frac{M_w}{M_n} \tag{3-74}$$

Using the definition for the zeroth moment of living polymer, and also ignoring the number of blocks per chain for the whole chains equations, Equations (3-44) and (3-46) can be rewritten as

$$\frac{\mathrm{d}P_H^I}{\mathrm{d}t} = (k_{\beta 1} + k_{H1}H)Y_I^0 + k_{Do}^+ DoP_H^{II} - (k_{iH1}M + k_{Do}^- + K_{D1} + s)P_H^I \tag{3-75}$$

$$\frac{\mathrm{d}P_{Et}^I}{\mathrm{d}t} = k_{Al1}AlY_1^0 + k_{Do}^+ DoP_{Et}^{II} - (k_{iR1}M + k_{Do}^- + K_{D1} + s)P_{Et}^I \tag{3-76}$$

By substituting Equations (3-48) and (3-49) into Equation (3-70) and summing over all *r* values, we obtain the moments of the living chains at state *I* for the whole chains:

$$\frac{dY_I^0}{dt} = (k_{i1}P_0^I + k_{iH1}P_H^I + k_{iR1}P_{Et}^I)M + k_{Do}^+ DoY_{II}^0 - (k_{Do}^- + K_{T1}^{'} + K_{D1} + s)Y_I^0 \quad (3\text{-}77)$$

$$\frac{dY_I^1}{dt} = (k_{i1}P_0^I + k_{iH1}P_H^I + k_{iR1}P_{Et}^I)M + k_{p1}MY_I^0 + k_{Do}^+ DoY_{II}^1 - (k_{Do}^- + K_{T1}^{'} + K_{D1} + s)Y_I^1 \quad (3\text{-}78)$$

$$\frac{dY_I^2}{dt} = (k_{i1}P_0^I + k_{iH1}P_H^I + k_{iR1}P_{Et}^I)M + k_{p1}M(2Y_I^1 + Y_I^0) + k_{Do}^+ DoY_{II}^2 - (k_{Do}^- + K_{T1}^{'} + K_{D1} + s)Y_I^2 \quad (3\text{-}79)$$

Similarly, moment equations for dead polymers are derived by substituting Equations (3-52) and (3-70) into Equation (3-71) and summing over all *r* values:

$$\frac{dX_I^0}{dt} = (K_{T1} + K_{D1})Y_I^0 - sX_I^0 \quad (3\text{-}80)$$

$$\frac{dX_I^1}{dt} = (K_{T1} + K_{D1})Y_I^1 - sX_I^1 \quad (3\text{-}81)$$

$$\frac{dX_I^2}{dt} = (K_{T1} + K_{D1})Y_I^2 - sX_I^2 \quad (3\text{-}82)$$

Moment equations for chains growing on sites at state *II* are derived in an analogous way and are listed below:

$$\frac{dY_{II}^0}{dt} = (k_{i2}P_0^{II} + k_{iH2}P_H^{II} + k_{iR2}P_{Et}^{II})M + k_{Do}^- Y_I^0 - (k_{Do}^+ Do + K_{T2}^{'} + K_{D2} + s)Y_I^0 \quad (3\text{-}83)$$

$$\frac{dY_{II}^{1}}{dt} = (k_{i2}P_{0}^{II} + k_{iH2}P_{H}^{II} + k_{iR2}P_{Et}^{II})M + k_{p2}MY_{II}^{0} + k_{Do}^{-}Y_{I}^{1} - (k_{Do}^{+}Do + K_{T2}^{'} + K_{D2} + s)Y_{II}^{1} \quad (3\text{-}84)$$

$$\frac{dY_{II}^{2}}{dt} = (k_{i2}P_{0}^{II} + k_{iH2}P_{H}^{II} + k_{iR2}P_{Et}^{II})M + k_{p1}M(2Y_{II}^{1} + Y_{II}^{0}) + k_{Do}^{-}Y_{I}^{2} - (k_{Do}^{+}Do + K_{T2}^{'} + K_{D2} + s)Y_{II}^{2} \quad (3\text{-}85)$$

$$\frac{dX_{II}^{0}}{dt} = (K_{T2} + K_{D2})Y_{II}^{0} - sX_{II}^{0} \quad (3\text{-}86)$$

$$\frac{dX_{II}^{1}}{dt} = (K_{T2} + K_{D2})Y_{II}^{1} - sX_{II}^{1} \quad (3\text{-}87)$$

$$\frac{dX_{II}^{2}}{dt} = (K_{T2} + K_{D2})Y_{II}^{2} - sX_{II}^{2} \quad (3\text{-}88)$$

3.3.5 Moments Equations for Isotactic, Atactic and Stereoblock Chains

Isotactic Chains

Isotactic chains are those that propagate and terminate at state *I,* without transformation to state *II*; therefore, all chains at state *I* and with $i = 1$ are pure isotactic chains.

The moment equations for isotactic living chains were obtained by substituting Equation (3-54) and (3-55) in Equation (3-70) and summing over *r*.

$$\frac{\mathrm{d}Y_{I,1}^{0}}{\mathrm{d}t} = (k_{i1}P_0^I + k_{iH1}P_H^I + k_{iR1}P_{Et}^I)M + k_{M1}MY_I^0 - (k_{Do}^- + K_{T1} + K_{D1} + s)Y_{I,1}^0 \tag{3-89}$$

$$\frac{\mathrm{d}Y_{I,1}^{1}}{\mathrm{d}t} = (k_{i1}P_0^I + k_{iH1}P_H^I + k_{iR1}P_{Et}^I)M + k_{p1}MY_{I,1}^0 + k_{M1}MY_I^1 - (k_{Do}^- + K_{T1} + K_{D1} + s)Y_{I,1}^1 \tag{3-90}$$

$$\frac{\mathrm{d}Y_{I,1}^{2}}{\mathrm{d}t} = (k_{i1}P_0^I + k_{iH1}P_H^I + k_{iR1}P_{Et}^I)M + k_{p1}M(2Y_{I,1}^1 + Y_{I,1}^0) + k_{M1}MY_I^2 - (k_{Do}^- + K_{T1} + K_{D1} + s)Y_{I,1}^2 \tag{3-91}$$

Similarly, moment equations for dead isotactic chains are given by the expressions:

$$\frac{\mathrm{d}X_{I,1}^{0}}{\mathrm{d}t} = (K_{T1} + K_{D1})Y_{I,1}^0 - sX_{I,1}^0 \tag{3-92}$$

$$\frac{\mathrm{d}X_{I,1}^{1}}{\mathrm{d}t} = (K_{T1} + K_{D1})Y_{I,1}^1 - sX_{I,1}^1 \tag{3-93}$$

$$\frac{\mathrm{d}X_{I,1}^{2}}{\mathrm{d}t} = (K_{T1} + K_{D1})Y_{I,1}^2 - sX_{I,1}^2 \tag{3-94}$$

The number and weight average molecular weights (M_n and M_w) are calculated using expressions similar to Equations (3-72) and (3-73). Moreover, the molar and mass fractions of isotactic chains can be calculated with the following equations:

$$\text{Purely isotactic mole \%} = \frac{X^0_{I,1} + Y^0_{I,1}}{X^0_I + Y^0_I + X^0_{II} + Y^0_{II}} \times 100 \tag{3-95}$$

$$\text{Purely isotactic mass \%} = \frac{X^1_{I,1} + Y^1_{I,1}}{X^1_I + Y^1_I + X^1_{II} + Y^1_{II}} \times 100 \tag{3-96}$$

where the moments for the whole chains, shown in the denominator of Equations (3-95) and (3-96), are calculated as indicated in Section 3.3.4.

Atactic Chains

Contrarily to the isotactic chains, the atactic chains are those that propagate and terminate at state *II* without transformation to state *I*; therefore, all chains at state *II* with $i = 1$ are purely atactic chains. By substituting Equation (3-56) and (3-57) in Equation (3-70) and summing over all *r* values, the moment equations for the atactic chains were obtained as

$$\frac{dY_{II,1}^{0}}{dt} = (k_{i2}P_0^{II} + k_{iH2}P_H^{II} + k_{iR2}P_{Et}^{II})M + k_{M2}MY_{II}^{0} - (k_{Do}^{+}Do + K_{T2} + K_{D2} + s)Y_{II,1}^{0} \quad (3\text{-}97)$$

$$\frac{dY_{II,1}^{1}}{dt} = (k_{i2}P_0^{II} + k_{iH2}P_H^{II} + k_{iR2}P_{Et}^{II})M + k_{p2}MY_{II,1}^{0} + k_{M2}MY_{II}^{1} - (k_{Do}^{+}Do + K_{T2} + K_{D2} + s)Y_{II,1}^{1} \quad (3\text{-}98)$$

$$\frac{dY_{II,1}^{2}}{dt} = (k_{i2}P_0^{II} + k_{iH2}P_H^{II} + k_{iR2}P_{Et}^{II})M + k_{p2}M(2Y_{II,1}^{1} + Y_{II,1}^{0}) + k_{M2}MY_{II}^{2} - (k_{Do}^{+}Do + K_{T2} + K_{D2} + s)Y_{II,1}^{2} \quad (3\text{-}99)$$

$$\frac{dX_{II,1}^{0}}{dt} = (K_{T2} + K_{D2})Y_{II,1}^{0} - sX_{II,1}^{0} \quad (3\text{-}100)$$

$$\frac{dX_{II,1}^{1}}{dt} = (K_{T2} + K_{D2})Y_{II,1}^{1} - sX_{II,1}^{1} \quad (3\text{-}101)$$

$$\frac{dX_{II,1}^{2}}{dt} = (K_{T2} + K_{D2})Y_{II,1}^{2} - sX_{II,1}^{2} \quad (3\text{-}102)$$

The number and weight average molecular weights (M_n and M_w) and the mole and mass percent of atactic chains in the polymer were calculated using expressions similar to Equations (3-72), (3-73), (3-95), and (3-96).

Stereoblock Chains

Moment equations for stereoblock chains are derived in a way similar to the one applied for isotactic and atactic chains. The final moment equations for stereoblock chains terminating at state *I* and with i^{th} blocks are listed below.

$$\frac{dY_{I,i}^{0}}{dt} = k_{Do}^{+} Do Y_{II,i-1}^{0} - (k_{Do}^{-} + K_{T1} + K_{D1} + s) Y_{I,i}^{0} \tag{3-103}$$

$$\frac{dY_{I,i}^{1}}{dt} = k_{p1} M Y_{I,i}^{0} + k_{Do}^{+} Do Y_{II,i-1}^{1} - (k_{Do}^{-} + K_{T1} + K_{D1} + s) Y_{I,i}^{1} \tag{3-104}$$

$$\frac{dY_{I,i}^{2}}{dt} = k_{p1} M (2Y_{I,i}^{1} + Y_{I,i}^{0}) + k_{Do}^{+} Do Y_{II,i-1}^{2} - (k_{Do}^{-} + K_{T1} + K_{D1} + s) Y_{I,i}^{2} \tag{3-105}$$

$$\frac{dX_{I,i}^{0}}{dt} = (K_{T1} + K_{D1}) Y_{I,i}^{0} - s X_{I,i}^{0} \tag{3-106}$$

$$\frac{dX_{I,i}^{1}}{dt} = (K_{T1} + K_{D1}) Y_{I,i}^{1} - s X_{I,i}^{1} \tag{3-107}$$

$$\frac{dX_{I,i}^{2}}{dt} = (K_{T1} + K_{D1}) Y_{I,i}^{2} - s X_{I,i}^{2} \tag{3-108}$$

Similarly, the moment equations for stereoblock chains terminating at state *II* and with i^{th} blocks are:

$$\frac{dY_{II,i}^{0}}{dt} = k_{Do}^{-} Y_{I,i-1}^{0} - (k_{Do}^{+} Do + K_{T2} + K_{D2} + s) Y_{I,i}^{0} \tag{3-109}$$

$$\frac{dY_{II,i}^{1}}{dt} = k_{p2} M Y_{II,i}^{0} + k_{Do}^{-} Y_{I,i-1}^{1} - (k_{Do}^{+} Do + K_{T2}^{'} + K_{D2} + s) Y_{II,i}^{1} \tag{3-110}$$

$$\frac{dY_{II,i}^{2}}{dt} = k_{p2} M (2Y_{II,i}^{1} + Y_{II,i}^{0}) + k_{Do}^{-} Y_{I,i-1}^{2} - (k_{Do}^{+} Do + K_{T2}^{'} + K_{D2} + s) Y_{II,i}^{2} \tag{3-111}$$

$$\frac{dX_{II,i}^{0}}{dt} = (K_{T2} + K_{D2}) Y_{II,i}^{0} - s X_{II,i}^{0} \tag{3-112}$$

$$\frac{\mathrm{d}X^{1}_{II,i}}{\mathrm{d}t} = (K_{T2} + K_{D2})Y^{1}_{II,i} - sX^{1}_{II,i} \tag{3-113}$$

$$\frac{\mathrm{d}X^{2}_{II,i}}{\mathrm{d}t} = (K_{T2} + K_{D2})Y^{2}_{II,i} - sX^{2}_{II,i} \tag{3-114}$$

3.3.6 Moments Equation for Chain Segments

Moment equations for chain segments were derived in a similar way, using the population balances given by Equations (3-64) to (3-69). Only their final expressions will be presented below.

The moments for the isotactic or atactic ($j = I$ or II) segments are defined as follows,

$$W_j^m = \sum_{r=1}^{\infty} r^m B_r^j \tag{3-115}$$

Isotactic Segments

$$\frac{\mathrm{d}W_I^0}{\mathrm{d}t} = k_{i1} MB_0^I + k_{M1} MB_1^I - (k_{Do}^- + K_{T1} + K_{D1} + s) W_I^0 \tag{3-116}$$

$$\frac{\mathrm{d}W_I^1}{\mathrm{d}t} = k_{i1} MB_0^I + k_{M1} MB_1^I + k_{p1} MW_I^0 - (k_{Do}^- + K_{T1} + K_{D1} + s) W_I^1 \tag{3-117}$$

$$\frac{\mathrm{d}W_I^2}{\mathrm{d}t} = k_{i1} MB_0^I + k_{M1} MB_1^I + k_{p1} M(2W_I^1 + W_I^0) - (k_{Do}^- + K_{T1} + K_{D1} + s) W_I^2 \tag{3-118}$$

Therefore, the number average molecular weight of the isotactic segments can be calculated as follows,

$$\overline{M}_n^I = mw. \frac{W_I^1}{W_I^0} \tag{3-119}$$

and the weight average molecular weight of these isotactic segments can be also calculated as follows:

$$\overline{M}_w^I = mw. \frac{W_I^2}{W_I^1} \tag{3-120}$$

Consequently the polydispersity is simply:

$$PDI_s^I = \frac{\overline{M}_w^I}{\overline{M}_n^I} \tag{3-121}$$

Atactic Segments

$$\frac{dW_{II}^0}{dt} = k_{i2} MB_0^{II} + k_{M2} MB_1^{II} - (k_{Do}^+ Do + K_{T2} + K_{D2} + s) W_{II}^0 \tag{3-122}$$

$$\frac{dW_{II}^1}{dt} = k_{i2} MB_0^{II} + k_{M2} MB_1^{II} + k_{p2} MW_{II}^0 - (k_{Do}^+ Do + K_{T2} + K_{D2} + s) W_{II}^1 \tag{3-123}$$

$$\frac{dW_{II}^2}{dt} = k_{i2} MB_0^{II} + k_{M2} MB_1^{II} + k_{p2} M(2W_{II}^1 + W_{II}^0) - (k_{Do}^+ Do + K_{T2} + K_{D2} + s) W_{II}^2 \tag{3-124}$$

The number and weight average molecular weights of the atactic segments are calculated with equations analogous to the ones used for the isotactic segments.

Chapter 4
Steady-State and Dynamic CSTR Simulations

4.1 Simulation Methodology

The differential equations derived in Chapter 3 will be used in the steady-state and dynamic simulations of propylene polymerization in this chapter.

The steady-state solution for a single-site catalyst (assuming states *I* or *II*) was derived and used to simulate the polymerization of propylene in a CSTR at different operating conditions. The effect of donor, hydrogen, and monomer concentrations on polypropylene microstructure were investigated. Moreover, the effect of changing the values of some kinetic parameters on the microstructure of polypropylene was also studied. The model was then extended to include a total of four sites types, which represent the situation more commonly encountered with heterogeneous Ziegler-Natta catalysts.

We have also simulated the dynamic behavior propylene polymerization in a CSTR with a single-site and a four-site type catalyst. Similarly to what was done for the steady-state simulations, we tested the model response to changes in reactant concentrations and kinetic parameter values.

Table 4-1 lists the concentrations of catalyst, cocatalyst, electron donor, propylene and other reagents under the reference simulation conditions. Table 4-2 lists the reference values for the reaction kinetic rate constants used in the simulations. Unless otherwise stated, these were the conditions used in all simulations.

Table 4-1: Reference polymerization conditions.

	mol/L		mol/L
C_I	0.00001	Al	0.0007
C_{II}	0.00001	I	0
M	0.20	H_2	0.004
Do	0.0007		

Table 4-2: Reference reaction rate constants (j = 1, or 2 for rate constants or $j = I$ or II for site states).

Constant	(L/mol·s)	Constant	(L/mol·s)	Constant	(s^{-1})
k_{aj}	3,000	k_{Do}^{+}	150	k_{Do}^{-}	0.01
k_{ij}	3,000	k_{Alj}	0	$k_{\beta j}$	0
k_{pj}	3,000	$k_{Al \cdot I}$	10,000	k_{dj}	0.001
k_{Hj}	110	k_{Mj}	0		
k_{dIj}	8,000				

The several rates of elementary reactions taking place during polymerization are defined with the equations

$$R_{pj} = k_{pj} M P_r^j \tag{4-1}$$

$$R_{trj} = (K_{Tj} + K_{Dj}) P_r^j \tag{4-2}$$

$$R_{tf1} = k_{Do}^{-} P_r^I \tag{4-3}$$

$$R_{tf2} = k_{Do}^{+} Do P_r^{II} \tag{4-4}$$

where R_p is the rate of propagation, R_{tr} is the overall chain transfer rate, R_{tf1} is rate of site transformation of state *I* to *II*, R_{tf2} is the rate of site transformation from state *II* to *I*, and j = 1, or 2 for rate constants or $j = I$ or *II* for site states.

4.2 Steady-State Simulation

The dynamic equations derived for a CSTR in the previous chapter can be solved analytically under steady-state conditions, as will be shown below. In order reduce the size of the resulting set of equations, we defined the following lumped-parameter constants:

$$\alpha_1 = k_{Do}^{-} + K_{D1} + s \tag{4-5}$$

$$\alpha_2 = k_{Do}^{+} Do + K_{D2} + s \tag{4-6}$$

$$K_{A1} = k_{a1} Al \tag{4-7}$$

$$K_{A2} = k_{a2} Al \tag{4-8}$$

$$\beta_1 = \frac{k_{Do}^{+} Do}{k_{Do}^{-} + K_{T1} + K_{D1} + s} \tag{4-9}$$

$$\beta_1^{'} = \frac{k_{Do}^{+} Do}{k_{Do}^{-} + K_{T1}^{'} + K_{D1} + s} \tag{4-10}$$

$$\beta_2 = \frac{k_{Do}^{-}}{k_{Do}^{+} Do + K_{T2} + K_{D2} + s} \tag{4-11}$$

$$\beta_2^{'} = \frac{k_{Do}^{-}}{k_{Do}^{+} Do + K_{T2}^{'} + K_{D2} + s} \tag{4-12}$$

$$\delta_1 = \frac{k_{p1}}{k_{Do}^{-} + K_{T1} + K_{D1} + s} \tag{4-13}$$

$$\delta_1^{'} = \frac{k_{p1}}{k_{Do}^{-} + K_{T1}^{'} + K_{D1} + s} \tag{4-14}$$

$$\delta_1^{''} = \frac{k_{M1}}{k_{Do}^{-} + K_{T1} + K_{D1} + s} \tag{4-15}$$

$$\delta_2 = \frac{k_{p2}}{k_{Do}^{+} Do + K_{T2} + K_{D2} + s} \tag{4-16}$$

$$\delta_2^{'} = \frac{k_{p2}}{k_{Do}^{+} Do + K_{T2}^{'} + K_{D2} + s} \tag{4-17}$$

$$\delta_2^{''} = \frac{k_{M2}}{k_{Do}^{+} Do + K_{T2} + K_{D2} + s} \tag{4-18}$$

$$\gamma_1 = \frac{(k_{i1} P_0^I + k_{iH1} P_H^I + k_{iR1} P_{Et}^I)}{(k_{Do}^{-} + K_{T1} + K_{D1} + s)} \tag{4-19}$$

$$\gamma_1^{'} = \frac{k_{i1} P_0^I + k_{iH1} P_H^I + k_{iR1} P_{Et}^I}{k_{Do}^{-} + K_{T1}^{'} + K_{D1} + s} \tag{4-20}$$

$$\gamma_1^{''} = \frac{k_{i1} B_0^I + k_{M1} B_1^I}{k_{Do}^{-} + K_{T1} + K_{D1} + s} \tag{4-21}$$

$$\gamma_2 = \frac{k_{i2} P_0^{II} + k_{iH2} P_H^{II} + k_{iR2} P_{Et}^{II}}{k_{Do}^{+} Do + K_{T2} + K_{D2} + s} \tag{4-22}$$

$$\gamma_2^{'} = \frac{k_{i2} P_0^{II} + k_{iH2} P_H^{II} + k_{iR2} P_{Et}^{II}}{k_{Do}^{+} Do + K_{T2}^{'} + K_{D2} + s} \tag{4-23}$$

$$\gamma_2^{''} = \frac{k_{i2} B_0^{II} + k_{M2} B_1^{II}}{k_{Do}^{+} Do + K_{T2} + K_{D2} + s} \tag{4-24}$$

4.2.1 Active Sites

The solutions of Equations (3-42) to (3-47) at steady-state (setting the left-hand derivative term to zero) are given by the following equations:

$$P_0^I = \frac{K_{A1} C_I + k_{Do}^{+} Do P_0^{II}}{k_{i1} M + \alpha_1} \tag{4-25}$$

$$P_0^{II} = \frac{K_{A2}C_I + k_{Do}^{-}P_0^I}{k_{i2}M + \alpha_2} \tag{4-26}$$

$$P_H^I = \frac{(k_{\beta 1} + k_{H1}H)Y_I^0 + k_{Do}^{+}DoP_H^{II}}{k_{iH1}M + \alpha_1} \tag{4-27}$$

$$P_H^{II} = \frac{(k_{t\beta 2} + k_{tH2}H)Y_{II}^0 + k_{Do}^{-}P_H^I}{k_{iH2}M + \alpha_2} \tag{4-28}$$

$$P_{Et}^I = \frac{k_{Al1}AlY_I^0 + k_{Do}^{+}DoP_{Et}^{II}}{k_{iR1}M + \alpha_1} \tag{4-29}$$

$$P_{Et}^{II} = \frac{k_{Al2}AlY_{II}^0 + k_{Do}^{-}P_{Et}^I}{k_{iR2}M + \alpha_2} \tag{4-30}$$

4.2.2 Moment Equations for Whole Chains

Similarly, the moment equations for the whole chains, Equations (3-77) to (3-88), have been solved at steady-state to obtain the expressions:

$$Y_I^0 = \gamma_1^{'}M + \beta_1^{'}Y_{II}^0 \tag{4-31}$$

$$Y_I^1 = \gamma_1^{'}M + \delta_1^{'}MY_I^0 + \beta_1^{'}Y_{II}^1 \tag{4-32}$$

$$Y_I^2 = \gamma_1^{'}M + \delta_1^{'}M(2Y_I^1 + Y_I^0) + \beta_1^{'}Y_{II}^2 \tag{4-33}$$

$$X_I^0 = (1/s)(K_{T1} + K_{D1})Y_I^0 \tag{4-34}$$

$$X_I^1 = (1/s)(K_{T1} + K_{D1})Y_I^1 \tag{4-35}$$

$$X_I^2 = (1/s)(K_{T1} + K_{D1})Y_I^2 \tag{4-36}$$

$$Y_{II}^0 = \gamma_2^{'} M + \beta_2^{'} Y_I^0 \tag{4-37}$$

$$Y_{II}^1 = \gamma_2^{'} M + \delta_2^{'} M Y_{II}^0 + \beta_2^{'} Y_I^1 \tag{4-38}$$

$$Y_{II}^2 = \gamma_2^{'} M + \delta_2^{'} M (2Y_{II}^1 + Y_{II}^0) + \beta_2^{'} Y_I^2 \tag{4-39}$$

$$X_{II}^0 = (1/s)(K_{T2} + K_{D2})Y_{II}^0 \tag{4-40}$$

$$X_{II}^1 = (1/s)(K_{T2} + K_{D2})Y_{II}^1 \tag{4-41}$$

$$X_{II}^2 = (1/s)(K_{T2} + K_{D2})Y_{II}^2 \tag{4-42}$$

4.2.3 Moment Equations for Isotactic, Atactic and Stereoblock Chains

Steady-state solutions for the moments of isotactic, atactic and stereoblock chains were derived in a similar manner and are listed below.

Isotactic Chains

The steady-state solution for the moments of the purely isotactic chains were obtained from Equations (3-89) to (3-94) and found as follows:

$$Y_{I,1}^0 = \gamma_1 M + \delta_1^{"} M Y_I^0 \tag{4-43}$$

$$Y_{I,1}^1 = \gamma_1 M + \delta_1 M Y_{I,1}^0 + \delta_1^{"} M Y_I^1 \tag{4-44}$$

$$Y_{I,1}^2 = \gamma_1 M + \delta_1 M (2Y_{I,1}^1 + Y_{I,1}^0) + \delta_1^{"} M Y_I^2 \tag{4-45}$$

$$X_{I,1}^{0} = (1/s)(K_{T1} + K_{D1})Y_{I,1}^{0} \tag{4-46}$$

$$X_{I,1}^{1} = (1/s)(K_{T1} + K_{D1})Y_{I,1}^{1} \tag{4-47}$$

$$X_{I,1}^{2} = (1/s)(K_{T1} + K_{D1})Y_{I,1}^{2} \tag{4-48}$$

Atactic Chains

Similarly, the steady-state solution for the moments of the purely atactic chains, derived from Equations (3-97) to (3-102), is given by the equations:

$$Y_{II,1}^{0} = \gamma_2 M + \delta_2^{"} M Y_{II}^{0} \tag{4-49}$$

$$Y_{II,1}^{1} = \gamma_2 M + \delta_2 M Y_{II,1}^{0} + \delta_2^{"} M Y_{II}^{1} \tag{4-50}$$

$$Y_{II,1}^{2} = \gamma_2 M + \delta_2 M (2Y_{II,1}^{1} + Y_{II,1}^{0}) + \delta_2^{"} M Y_{II}^{2} \tag{4-51}$$

$$X_{II,1}^{0} = (1/s)(K_{T2} + K_{D2})Y_{II,1}^{0} \tag{4-52}$$

$$X_{II,1}^{1} = (1/s)(K_{T2} + K_{D2})Y_{II,1}^{1} \tag{4-53}$$

$$X_{II,1}^{2} = (1/s)(K_{T2} + K_{D2})Y_{II,1}^{2} \tag{4-54}$$

Stereoblock Chains Terminated During the Stereospecific State

The steady-state solution for stereoblock chains that terminate during the stereoselective state of the catalyst site are obtained from Equations (3-103) to (3-108):

$$Y_{I,i}^{0} = \beta_1 Y_{II,i-1}^{0} \tag{4-55}$$

$$Y^1_{I,i} = \delta_1 M Y^0_{I,i} + \beta_1 Y^1_{II,i-1} \tag{4-56}$$

$$Y^2_{I,i} = \delta_1 M (2Y^1_{I,i} + Y^0_{I,i}) + \beta_1 Y^2_{II,i-1} \tag{4-57}$$

$$X^0_{I,i} = (1/s)(K_{T1} + K_{D1}) Y^0_{I,i} \tag{4-58}$$

$$X^1_{I,i} = (1/s)(K_{T1} + K_{D1}) Y^1_{I,i} \tag{4-59}$$

$$X^2_{I,i} = (1/s)(K_{T1} + K_{D1}) Y^2_{I,i} \tag{4-60}$$

Stereoblock Chains Terminated During the Aspecific State

Similar equations for chains terminated during the aspecific state are derived from Equations (3-109) to (3-114):

$$Y^0_{II,i} = \beta_2 Y^0_{I,i-1} \tag{4-61}$$

$$Y^1_{II,i} = \delta_2 M Y^0_{II,i} + \beta_2 Y^1_{I,i-1} \tag{4-62}$$

$$Y^2_{II,i} = \delta_2 M (2Y^1_{II,i} + Y^0_{II,i}) + \beta_2 Y^2_{I,i-1} \tag{4-63}$$

$$X^0_{II,i} = (1/s)(K_{T2} + K_{D2}) Y^0_{II,i} \tag{4-64}$$

$$X^1_{II,i} = (1/s)(K_{T2} + K_{D2}) Y^1_{II,i} \tag{4-65}$$

$$X^2_{II,i} = (1/s)(K_{T2} + K_{D2}) Y^2_{II,i} \tag{4-66}$$

4.2.4 Chain Segments

Isotactic Segments

The equations for the steady-state of the moments of the isotactic segments were solved using Equations (3-116) to (3-118) and found to be as follows:

$$W_I^0 = \gamma_1^{"} M \tag{4-67}$$

$$W_I^1 = \gamma_1^{"} M + \delta_1 M W_I^0 \tag{4-68}$$

$$W_I^2 = \gamma_1^{"} M + \delta_1 M (2W_I^1 + W_I^0) \tag{4-69}$$

Atactic Segments

Similarly, the steady-state moments for the atactic segments were derived using Equations (3-124) to (3-126):

$$W_{II}^1 = \gamma_2^{"} M \tag{4-70}$$

$$W_{II}^1 = \gamma_2^{"} M + \delta_2 M W_{II}^0 \tag{4-71}$$

$$W_{II}^1 = \gamma_2^{"} M + \delta_2 M (2W_{II}^1 + W_{II}^0) \tag{4-72}$$

4.3 Steady-State Simulations

The steady-state equations shown in Section 4.2 were solved simultaneously at different polymerization conditions. The model was first solved for one single site with two states, stereospecific (making isotactic chains or blocks) and aspecific (producing atactic chains or blocks). These simulations represent the main contribution of this thesis, since no mathematical model for active sites existing in two states has been presented in the literature, even though the concept has been analyzed qualitatively in many previous publications, as discussed in the section on literature review.

Ziegler-Natta catalysts, however, have multiple types of sites and only some are considered to go through this reversible transformation from stereospecific to aspecific state. Most of the other site types are presumed to make only isotactic polypropylene. Therefore, a four-site model, with two stereospecific sites and 2 aspecific (two-state) sites, was proposed to model the behaviour of a heterogeneous Ziegler-Natta catalyst. The number of site types was chosen arbitrarily in our simulations since we did not make use of experimental data for model validation, but the predicted trends agree well with the general behaviour of Ziegler-Natta catalysts used industrially for the production of polypropylene. The following discussion summarizes the responses to changes in donor type and concentration, catalyst activity and hydrogen concentration. All of the simulation results presented in this section are tabulated in Appendix A.

Figure 4-1 shows that, in the absence of electron donor, no stereoblock chains are made, only purely atactic or isotactic chains. This is, of course, a consequence of our choice of model parameters in Table 4-1: the concentration of active sites fed to the reactor in state I and II is the same and they have the same value for their propagation rate constants; consequently, in the absence of electron donors, no site transformation will take place and both states will make the same amount of polymer. Contrarily, when electron donor is introduced in the reactor, a significant fraction of sites on state II (aspecific) are converted to state I (isospecific), decreasing the mass fraction of atactic polypropylene to approximately 6%, with the consequent increase in the fraction of isotactic and stereoblock chains to about 87% and 7%, respectively, as illustrated in Figure 4-2. Interestingly, according to the simulations, most of the stereoblock chains are atactic-isotactic diblocks (6 %), with a very low fraction of multiblock chains (1%).

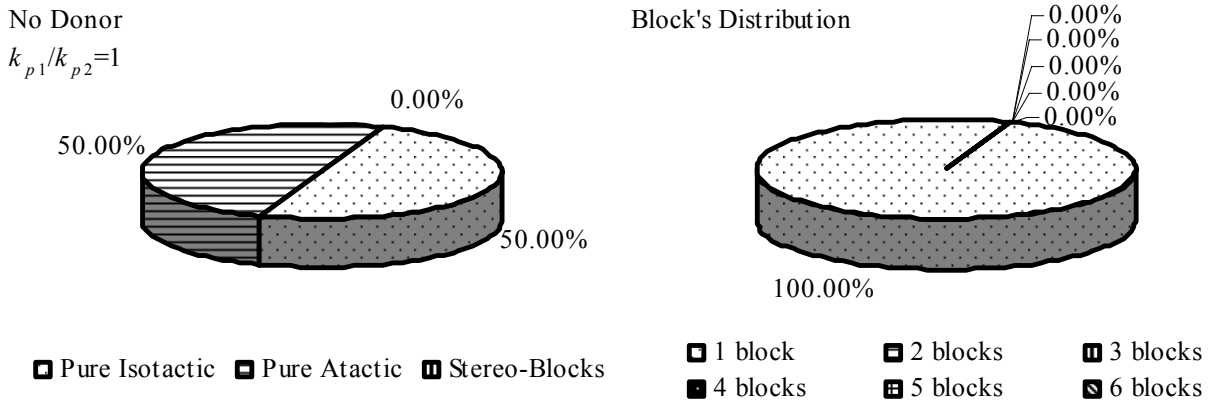

Figure 4-1: Tacticity and block distributions for propylene made with a single-site catalyst without donor at the reference polymerization conditions. (k_{p1}/k_{p2} = 1, R_{p1}/R_{tr1} =1364, R_{p2}/R_{tr2} =1364, M_n = 57,270 g/mol, M_w = 114,497 g/mol, and *PDI* = 2.00)

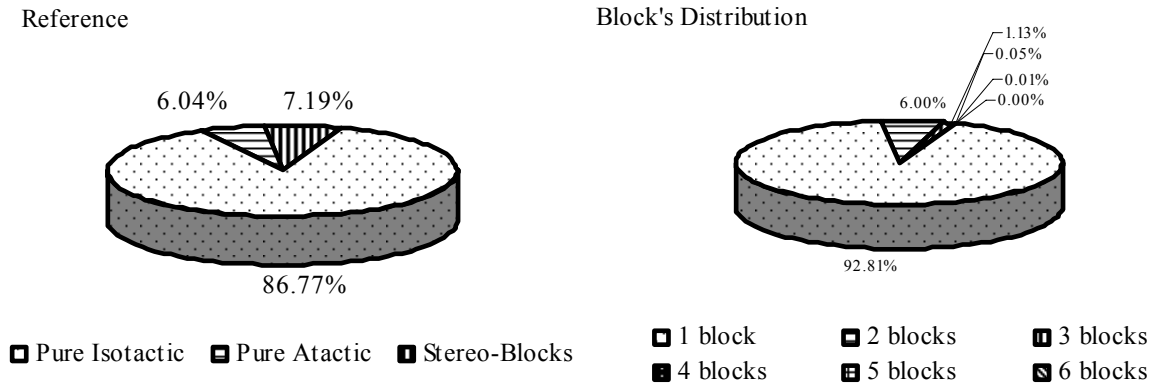

Figure 4-2: Tacticity and block distributions for propylene made with a single-site catalyst at reference polymerization conditions. (k_{p1}/k_{p2} = 1, R_{p1}/R_{tr1} =1364, R_{p2}/R_{tr2} =1364, M_n = 57,270 g/mol, M_w = 114,497 g/mol, and PDI = 2.00)

The effect of changing donor concentration is illustrated in Figures 4-3 and 4-4. When the donor concentration is reduced by half of the value used in the simulations shown in Figure 4-2 (Figure 4-3), the mass fraction of atactic polypropylene increases from 6.04% to 13.38%, as expected. Contrarily, Figure 4-4 demonstrates that if the donor concentration is doubled, the mass fraction of atactic polypropylene will be reduced to 2.26%. The mass fraction of stereoblock chains is also affected by the concentration of electron donor, but the diblock chains continue to be the dominant population among the stereoblock chains for all simulations.

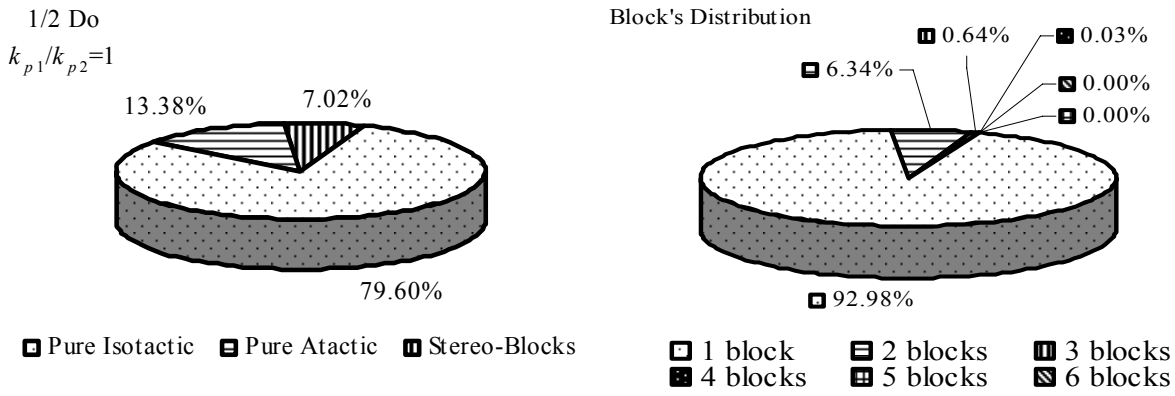

Figure 4-3: Tacticity and block distributions for propylene made with a single-site catalyst with half the reference donor concentration shown in Figure 4-2. Other polymerization conditions are the same as shown in Figure 4-1.

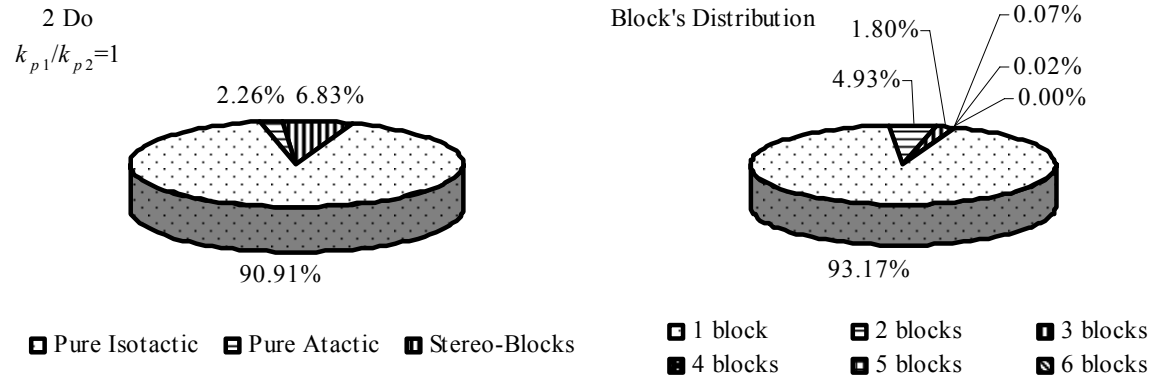

Figure 4-4: Tacticity and block distributions for propylene made with a single-site catalyst with twice the reference donor concentration shown in Figure 4-2. Other polymerization conditions are the same as shown in Figure 4-1.

Figure 4-5 shows complete weight distribution for the stereoblock chains and Table 4-7 their molecular weight averages (M_n, M_w, and *PDI*). We have also classified the chains according to the state of the site when chain growth was terminated. This distinction is immaterial for the case of diblocks, but is important for triblocks and higher odd-numbered multiblock chains, since an

isotactic-terminated chain (isotactic-atactic-isotactic-…) has a different microstructure from an atactic-terminated chain (atactic-isotactic-atactic-…) for odd-numbered multiblock chains. Table 4-7 shows that the molecular weight averages increase and the polydispersity index decreases with increasing number of blocks per chain. Both trends are expected, since longer chains will have a higher probability of experiencing site transformation events than shorter chain; the effect on *PDI* is a simple consequence of sampling an increasingly narrower polymer population: uniblock chains are those that follow Flory's statistics with *PDI* = 2, diblocks will have *PDI* = 1.5 in a similar fashion to chains made by termination by combination in free radical polymerization, and chains with three or more blocks will have even narrower MWDs, since they are being selected from a subpopulation with increasing molecular weights.

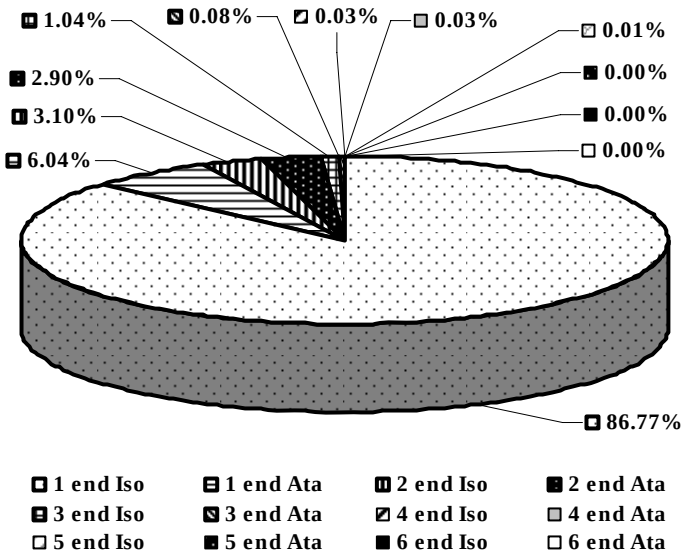

Figure 4-5: Mass fractions of stereoblock chain populations for the reference polymerization conditions shown in Table 4-1.

Table 4-3: Molecular weight averages and polydispersity for stereoblock chains made under the reference polymerization conditions.

# of blocks	End with isotactic block			End with atactic block		
I	M_n	M_w	*PDI*	M_n	M_w	*PDI*
1	56,002	111,961	2.00	46,269	92,495	2.00
2	102,229	153,807	1.50	102,229	153,806	1.50
3	158,188	211,331	1.34	148,457	198,382	1.34
4	204,417	256,005	1.25	204,415	256,003	1.25
5	260,374	312,911	1.20	250,644	301,251	1.20
6	306,604	358,196	1.17	306,601	358,193	1.17

Figure 4-6 shows the effect of changing the relative propagation rates of states *I* and *II*. The value of k_{p1}/k_{p2} has been increased to 10, as opposed to Figure 4-2 where $k_{p1}/k_{p2} = 1$. As expected, the fraction of purely atactic chains drops from approximately 6% to 0.66% as the ratio k_{p1}/k_{p2} increases, since much more polymer is made during state *I* in this case. In addition, since the two states produce polymer with different molecular weight averages, a broadening of the MWD will take place and *PDI* is higher than 2. In the previous simulations we assumed that both states produced polypropylene with the same average molecular weights.

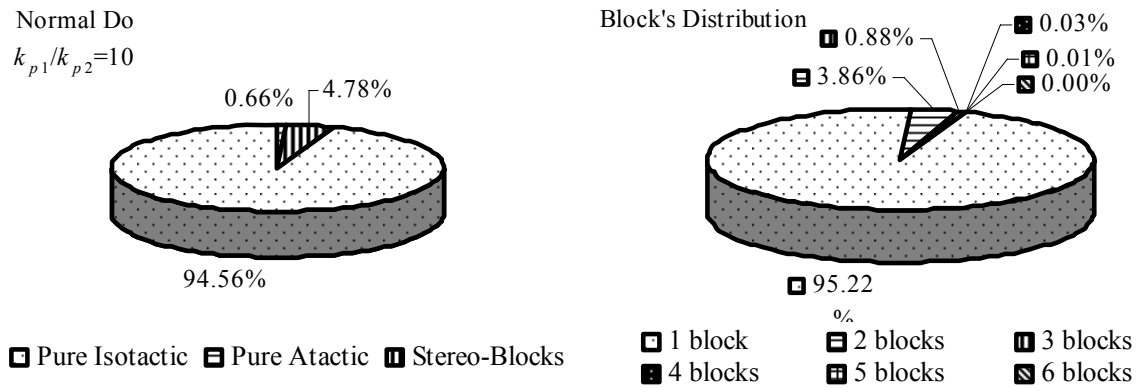

Figure 4-6: Tacticity and block distributions for propylene made with a single-site catalyst at normal donor concentration and increased k_{p1}/k_{p2} ratio (k_{p1}/k_{p2} = 10, R_{p1}/R_{tr1} =1364, R_{p2}/R_{tr2} =136, M_n = 52,600 g/mol, M_w = 111,800 g/mol, *PDI* = 2.13)

The effect of donor type has been also examined by manipulating the values of the parameter for site transformation by donor, k_{Do}^{+} and k_{Do}^{-}. Figure 4-7 and Figure 4-8 show the effect of selecting donor types with different values of site transformation rate constants. When the value of k_{Do}^{+} is doubled and k_{Do}^{-} is reduced by a factor of ½ with respect with the value listed in Table 4-2, the mass fraction of purely isotactic chain increases to 95.07 % (as compared to 86.77% for the reference case) as shown in Figure 4-7; when the value of k_{Do}^{+} is reduced by a factor of ½ and k_{Do}^{-} is doubled, on the other hand, as the mass fraction of purely isotactic chains drops to 65.84 % as presented in Figure 4-8. No significant effect is observed in the values of M_n, M_w, and *PDI*, since the propagation and termination rates are not affected by site state transformation.

The use of better donors also reduces the weight percent of stereoblock chains, since the transition from isotactic to atactic state is less likely to occur during the lifetime of a polypropylene chain.

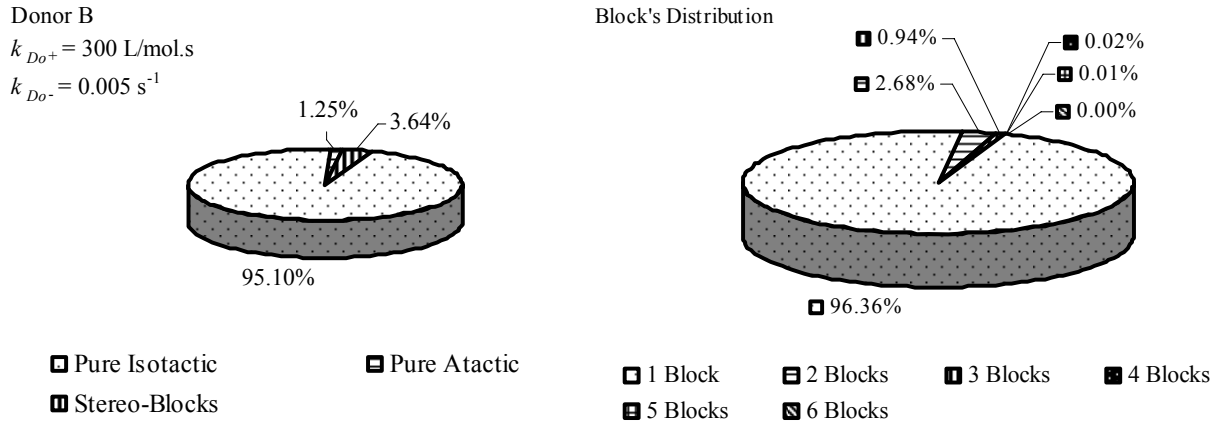

Figure 4-7: Better donor type effect at steady state reference polymerization conditions for single site. ($k_{Do}^{+}(B)/k_{Do}^{+}$(reference) = 2, $k_{Do}^{-}(B)/k_{Do}^{-}$(reference) = 0.5, k_{p1}/k_{p2} = 1, R_{p1}/R_{tr1} =*1364,* and R_{p2}/R_{tr2} =1364)

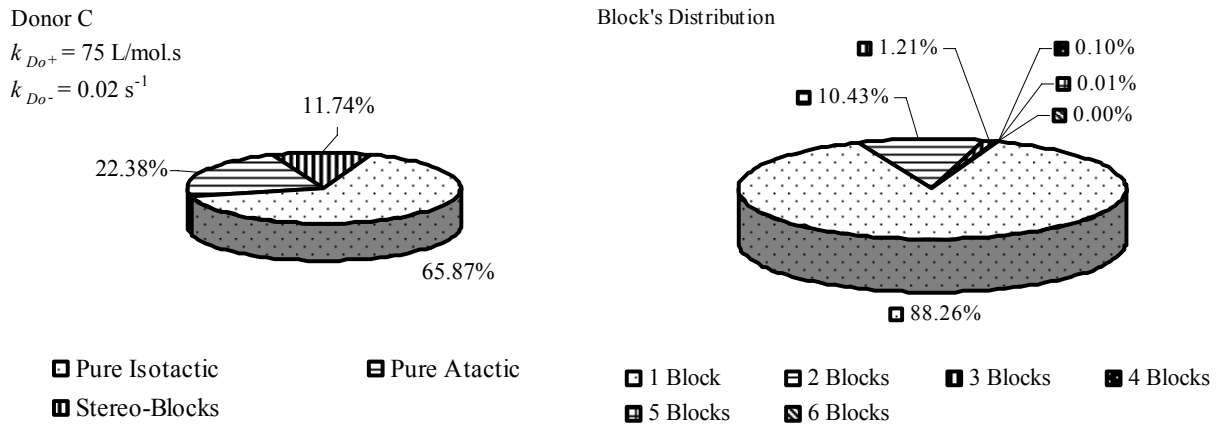

Figure 4-8: Worse donor type effect at steady state reference polymerization conditions for single site, ($k_{Do}^{+}(C)$/ k_{Do}^{+}(reference) = 0.5, k_{Do}^{-} (C)/ k_{Do}^{-}(reference) = 2, k_{p1}/k_{p2} = 1, R_{p1}/R_{tr1} =*1364,* and R_{p2}/R_{tr2} =1364)

Figure 4-9 shows how the polymer microstructure is affected when the propagation rate constant of state *I* and *II* are both doubled with respect to the reference case, maintaining the same ratio of (k_{p1}/k_{p2}), while all other model parameters remain the same. This would correspond to change the catalyst type or polymerization temperature, for instance although, in reality, all other polymerization kinetic constants would also be affected by a change of catalyst. As expected, M_n and M_w almost double when the propagation rate constant is doubled (compare catalyst C2 with C1). In contrast, catalyst C3 makes polymer with approximately half the M_n and M_w of catalyst C1, since its propagation rate constant was reduced by a factor of ½. It is interesting to notice that the tacticities do not change in all three cases, since the value of the propagation rate constant does not affect the frequency of site state transformation, as shown in Figure 4-9 and Figure 4-10. This proves that our model equations were properly derived and are consistent with the expected theoretical behavior for these catalysts.

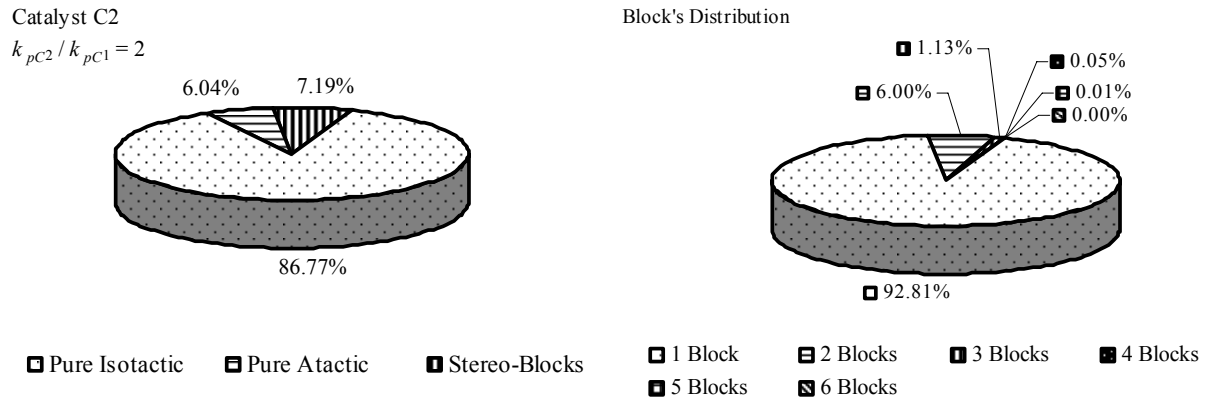

Figure 4-9: C2 catalyst type at steady state reference polymerization conditions for single site. (k_{p1}/k_{p2} = 2, $R_{p1}/R_{tr1} = R_{p2}/R_{tr2}$ = 1364, , M_n =114,497 g/mol, and M_w =228,952 g/mol)

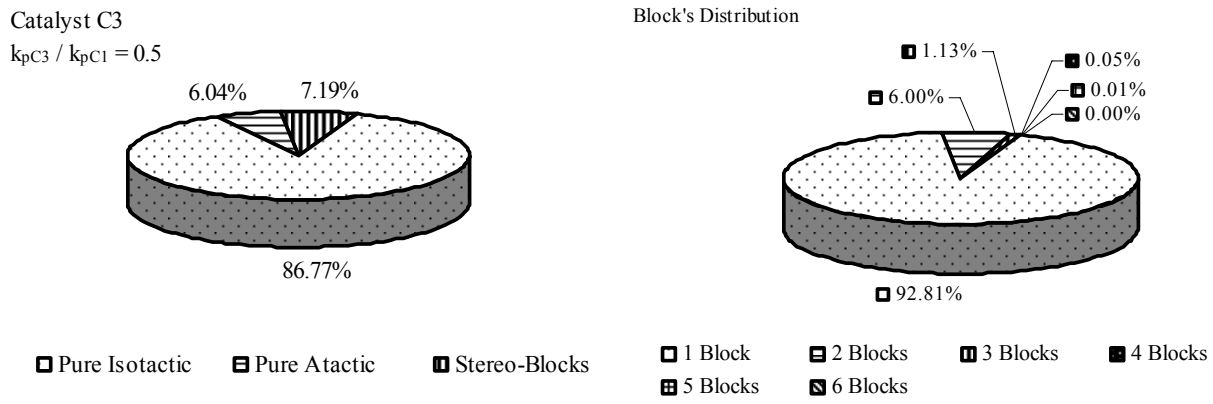

Figure 4-10: C3 catalyst type at steady state reference polymerization conditions for single site. (k_{p1}/k_{p2} = 0.5, $R_{p1}/R_{tr1} = R_{p2}/R_{tr2}$ = 1364, , M_n = 28,656 g/mol, and M_w =57,270 g/mol)

Figure 4-11 and Figure 4-12 study the effect of changing the concentration of hydrogen on polypropylene microstructure. Molecular weight naturally decreases with increasing hydrogen concentration. More interesting, changes in hydrogen concentration also have a pronounced

effect on the fraction of stereoblock chains. This may seem surprising at first, but it is easily explained: as hydrogen concentration increases, the polymer chains become (in average) shorter and, consequently, the likelihood of a change in site state taking place during the lifetime of a polymer chains decreases. Therefore, as the hydrogen concentration increases, the fraction of stereoblock chains decreases, as illustrated in Figure 4-11.

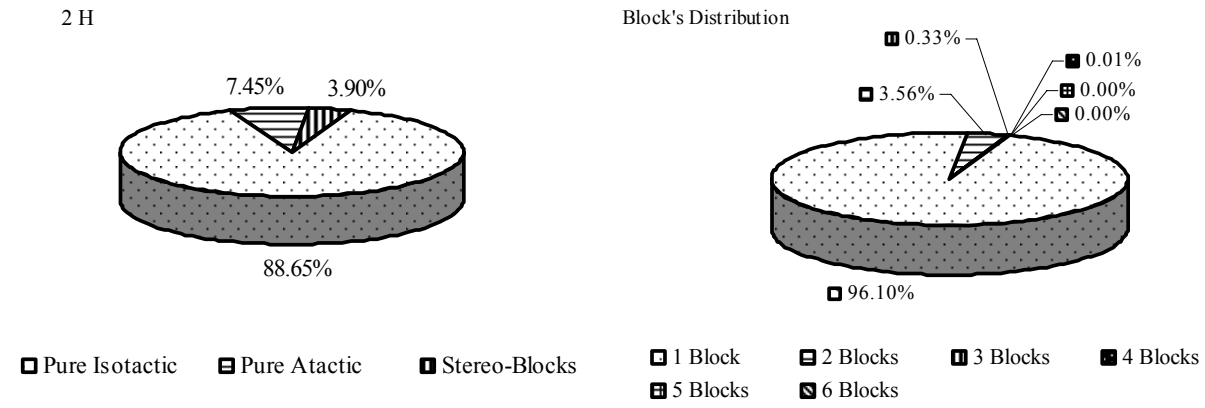

Figure 4-11: Doubling hydrogen concentration at steady state reference polymerization conditions for single site. (M_n = 28,689 g/mol, and M_w =57,336 g/mol)

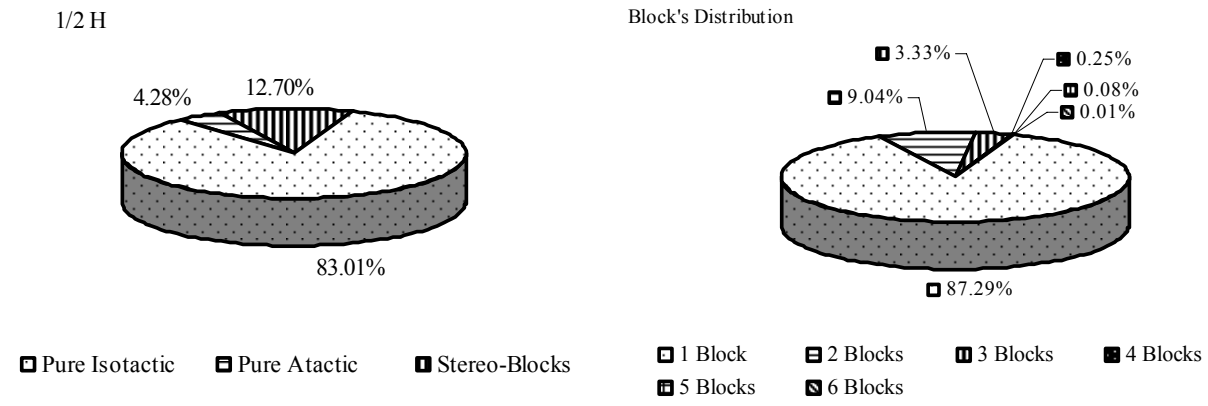

Figure 4-12: Decreasing hydrogen concentration by half at steady state reference polymerization conditions for single site. (M_n = 114,214 g/mol, and M_w =228,385 g/mol)

Due to the presence of more than one active site type in heterogenous Ziegler-Natta catalysts using industrially to polymerize propylene, the model was extended to include multiple sites. The different active sites on heterogeneous Ziegler-Natta catalysts are characterized by distinct polymerization kinetic parameters than can be estimated by MWD deconvolution (Faldi and Soares, 2001; Soares and Hamielec, 1995).

Table 4-4: Simulation results for a 4-site model

Site	Overall		1		2		3		4	
	Mole %	Mass %	Mole %	Mass %	Mole %	Mass %	Mole %	Mass %	Mole %	Mass %
Pure Isotactic	95.13%	98.22%	100.0%	100.0%	100.0%	100.0%	91.16%	93.40%	84.84%	86.47%
Pure Atactic	3.41%	0.30%	0.00%	0.00%	0.00%	0.00%	6.41%	2.84%	6.17%	0.88%
Stereoblocks	1.46%	1.48%	0.00%	0.00%	0.00%	0.00%	2.43%	3.76%	8.99%	12.64%
Block weight %:										
1 block	98.62%	97.98%	100.0%	100.0%	100.0%	100.0%	97.57%	96.24%	91.01%	87.35%
2 blocks	1.12%	1.44%	0.00%	0.00%	0.00%	0.00%	2.22%	3.24%	6.79%	7.89%
3 blocks	0.24%	0.52%	0.00%	0.00%	0.00%	0.00%	0.21%	0.50%	2.00%	4.25%
4 blocks	0.02%	0.04%	0.00%	0.00%	0.00%	0.00%	0.00%	0.01%	0.15%	0.35%
5 blocks	0.00%	0.01%	0.00%	0.00%	0.00%	0.00%	0.00%	0.00%	0.04%	0.14%
6 blocks	0.00%	0.00%	0.00%	0.00%	0.00%	0.00%	0.00%	0.00%	0.00%	0.01%
M_n (g/mol)	52,081		62,957		167,316		7,902		191,523	
M_w (g/mol)	231,513		125,890		334,595		16,013		398,055	
PDI	4.45		2.00		2.00		2.03		2.08	
k_{p1}/k_{p2}							2.50		6.67	
R_{p1}/R_{tr1}			1500		4000		194		5000	
R_{p2}/R_{tr2}			0		0		97		1071	

Table 4-4 shows the simulation results for a four-site-type catalyst model where model parameters were chosen so that the overall polymer properties are within values observed in industrial range. Sites 1 and 2 make only isotactic chains, while Sites 3 and 4 can produce isotactic, atactic and stereoblock chains because they may exist in two states, as described in our proposed mechanism above. Site 1 produces isotactic polypropylene chains with R_{p1}/R_{tr1} = 1500 (rate of propagation to rate of termination ratio). However, Site 2 makes chains with longer average molecular weight with R_{p1}/R_{tr1} = 4000. Sites 3 and 4 can suffer transformation between

stereoselective and non stereoselective states by complexation with an electron donor. Site 3 was assumed to produce around 93 wt% pure isotactic chains, with a ratio of the rate constant of propagation at stereoselective state to the rate constant of propagation of the non stereoselective state of k_{p1}/k_{p2} = 2.5 and shorter chains with R_{p1}/R_{tr1} = 194 and R_{p2}/R_{tr2} = 97. Site 4 was the least stereoselective site, producing only 86.5 wt % pure isotactic chains with k_{p1}/k_{p2} = 6.7 and higher molecular weight averages with R_{p1}/R_{tr1} = 5000 and R_{p2}/R_{tr2} = 1071. Table 4-4 shows that the model can predict the individual properties of polymer made on each site type such as molecular weight averages, polydispersity and molar and mass fractions of each population. The overall properties of the polymer produced by this 4-site catalyst were also predicted where the pure isotactic content was around 98 wt% and with M_n = 52,081 g/mol, M_w = 231,513 g/mol, and polydispersity of 4.45. These results are typical of commonly encountered industrial polypropylene resins made with heterogeneous Ziegler-Natta catalysts.

4.4 Dynamic Simulations

In order to compare the steady-state simulations of the previous section and the dynamic simulations shown in this section, the feed flow rate of catalyst was calculated from Equations (3-40) and (3-41) assuming steady-state (that is, setting the left hand derivative term to zero) as follows,

$$\hat{C}_I = (k_{a1} Al + s) C_I \tag{4-73}$$

$$\hat{C}_{II} = (k_{a2} Al + s) C_{II} \tag{4-74}$$

Similarly, the feed flow rates of all other reagents were calculated from their dynamic mass balances given below

$$\frac{\mathrm{d}M}{\mathrm{d}t} = \hat{M} - M(P_0^I k_{i1} + P_H^I k_{iH1} + P_{Et}^I k_{iR1} + P_0^{II} k_{i2} + P_H^{II} k_{iH2} + P_{Et}^{II} k_{iR2} + Y_I^0 (k_{p1} + k_{M1}) + Y_{II}^0 (k_{p2} + k_{M2}) + s) \tag{4-75}$$

$$\frac{\mathrm{d}H}{\mathrm{d}t} = \hat{H} - H(k_{H1} Y_I^0 + k_{H2} Y_{II}^0 + s) \tag{4-76}$$

$$\frac{\mathrm{d}Al}{\mathrm{d}t} = A\hat{l} - Al(k_{a1} C_I + k_{a2} C_{II} + k_{Al} I + k_{Al1} Y_I^0 + k_{Al2} Y_{II}^0 + s) \tag{4-77}$$

$$\frac{\mathrm{d}Do}{\mathrm{d}t} = D\hat{o} + k_{Do}^{-}(P_0^I + P_H^I + P_{Et}^I + Y_I^0) - Do(k_{Do}^{+}(P_0^{II} + P_H^{II} + P_{Et}^{II} + Y_{II}^0) + s) \tag{4-78}$$

By solving these equations at steady –state (as indicated below), we are able to obtain the molar flow rates for each of the reactants,

$$\hat{M} = M(P_0^I k_{i1} + P_H^I k_{iH1} + P_{Et}^I k_{iR1} + P_0^{II} k_{i2} + P_H^{II} k_{iH2} + P_{Et}^{II} k_{iR2} - Y_I^0 (k_{p1} + k_{M1}) + Y_{II}^0 (k_{p2} + k_{M2}) + s) \quad (4\text{-}79)$$

$$\hat{H} = H(k_{H1} Y_I^0 + k_{H2} Y_{II}^0 + s) \quad (4\text{-}80)$$

$$A\hat{l} = Al(k_{a1} C_I + k_{a2} C_{II} + k_{Al \cdot I} I + k_{Al1} Y_I^0 + k_{Al2} Y_{II}^0 + s) \quad (4\text{-}81)$$

$$D\hat{o} = Do(k_{Do}^+ (P_0^{II} + P_H^{II} + P_{Et}^{II} + Y_{II}^0) + s) - k_{Do}^- (P_0^I + P_H^I + P_{Et}^I + Y_I^0) \quad (4\text{-}82)$$

Since some feed rates depend on more than one reference concentration, different feed flow rates will result when concentrations are changed. For instance, the propylene flow rate calculated for the reference conditions $C_I = C_{II} = 0.00001$, $M = 0.2$, $Al = Do = 0.0007$, and $H = 0.004$ mol/L, is 19.633 mol/s. However, when the hydrogen concentration is double to $H = 0.008$ mol/L, the propylene flow rate changes to 15.9 mol/s as shown in Table 4-5.

The dynamic population balances derived in Section 3.3.4 to 3.3.6 were solved using the "ode15s" solver in MATLAB (Higham and Higham, 2005). The effect of changing the concentrations of donor, hydrogen, and propylene on polymer microstructure was studied by manipulating their feed rates as shown in Table 4-5. The input data used in the dynamic simulations is identical to those used for the steady-state simulations. All initial values of concentrations and moments were set to zero; therefore, the simulations reflect a reactor start-up

condition. Similarly to the steady-state simulations, dynamic simulations were first applied to a single-site, two–state catalyst and then extended to a four-site catalyst model.

Table 4-5: Feed flow rates for the reference conditions and for each targeted concentration.

Feed mol/s	Reference	0.5 *Do*	2 *Do*	0.5 *H*	2 *H*	0.5 *M*	2 *M*
$\hat{C}_I$	2.10×10^{-5}	2.10×10^{-5}	2.10×10^{-5}	2.10×10^{-5}	2.10×10^{-5}	2.10×10^{-5}	2.10×10^{-5}
$\hat{C}_{II}$	2.10×10^{-5}	2.10×10^{-5}	2.10×10^{-5}	2.10×10^{-5}	2.10×10^{-5}	2.10×10^{-5}	2.10×10^{-5}
$\hat{M}$	1.96×10	2.03×10	2.03×10	2.20×10	1.59×10	1.02×10	4.06×10
$\hat{H}_2$	1.44×10^{-2}	1.49×10^{-2}	1.49×10^{-2}	8.05×10^{-3}	2.33×10^{-2}	1.49×10^{-2}	1.49×10^{-2}
$\hat{Al}$	4.20×10^{-5}	4.21×10^{-5}	4.21×10^{-5}	4.21×10^{-5}	4.21×10^{-5}	4.21×10^{-5}	4.21×10^{-5}
$\hat{Do}$	1.73×10^{-5}	1.41×10^{-5}	1.92×10^{-5}	1.73×10^{-5}	1.72×10^{-5}	1.72×10^{-5}	1.72×10^{-5}

Donor concentration and type play a very important role in propylene polymerization; modeling their effects on polypropylene properties is very important during grade transitions to guarantee that the required polypropylene properties are achieve in a short grade transition time. Manipulating the electron donor concentration is the most common way of controlling polypropylene tacticity made with multiple-site Ziegler Natta catalysts. Similarly, changes in hydrogen and propylene concentrations will determine polymer molecular weight and reactor productivity during grade transitions and at the final reactor steady-state.

Figure 4-13 shows that doubling the donor concentration does not affect the value of the molecular weight averages of the polymer. On the other hand, M_n and M_w decrease when the hydrogen concentration is doubled and increase when the propylene concentration is doubled, as expected from the polymerization model adopted for these simulations. The dynamic simulations shown in Figure 4-13 capture nicely the overall reactor dynamics and the time elapsed between the grade transitions.

Figure 4-14 shows how changing the same concentrations affects the stereoregularity of the polymer. The mass fraction of isotactic chains increases from approximately 86.8 % to 90.9 % by doubling the donor concentration, while the mass fraction of atactic chains drops from 6.0 % to 2.3 % and stereoblock chains from 7.2 % to approximately 6.8 %. It is also interesting to see that, by doubling the concentration of hydrogen, the mass fraction of isotactic chains drops to 88.7 % which is still higher than the reference value 86.8 % and the mass fraction of the atactic chains increases by 1.5 % from its reference value of 6.0 %. However, the mass fraction of the stereoblock chains drops from 7.2 % to approximately 3.9 %. Moreover, by doubling the concentration of monomer, the fractions of isotactic, atactic, and stereoblock chains are not affected, because monomer concentration affects propagation rate only and does not have any effect on site transformation rate.

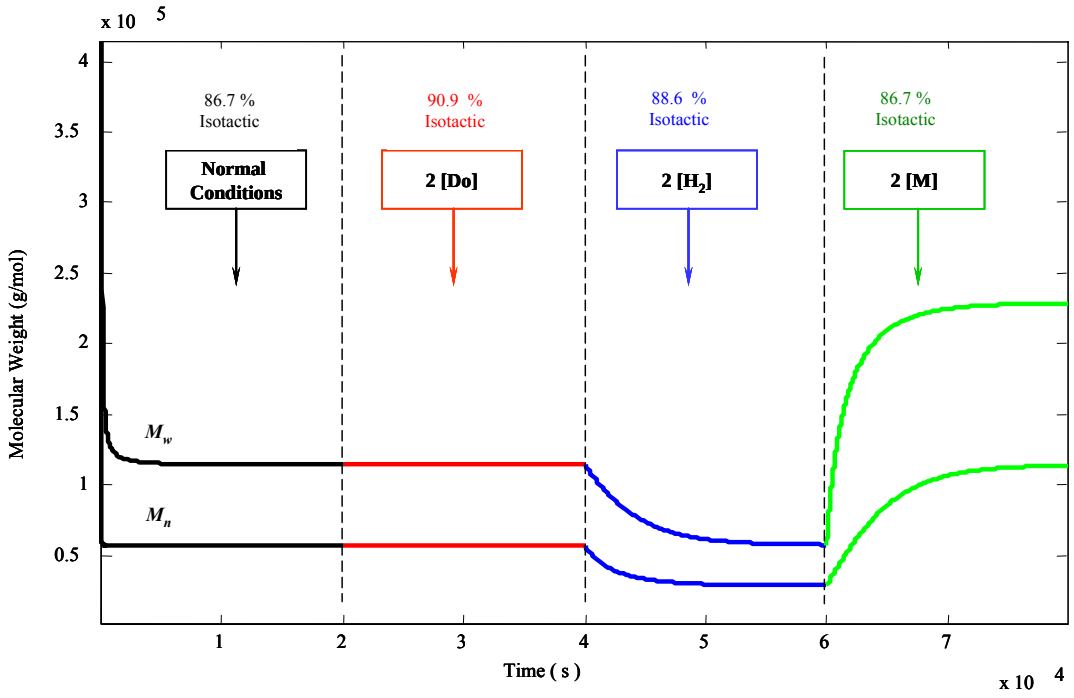

Figure 4-13: Effect of changing the concentrations of donor, hydrogen, and monomer on M_n and M_w.

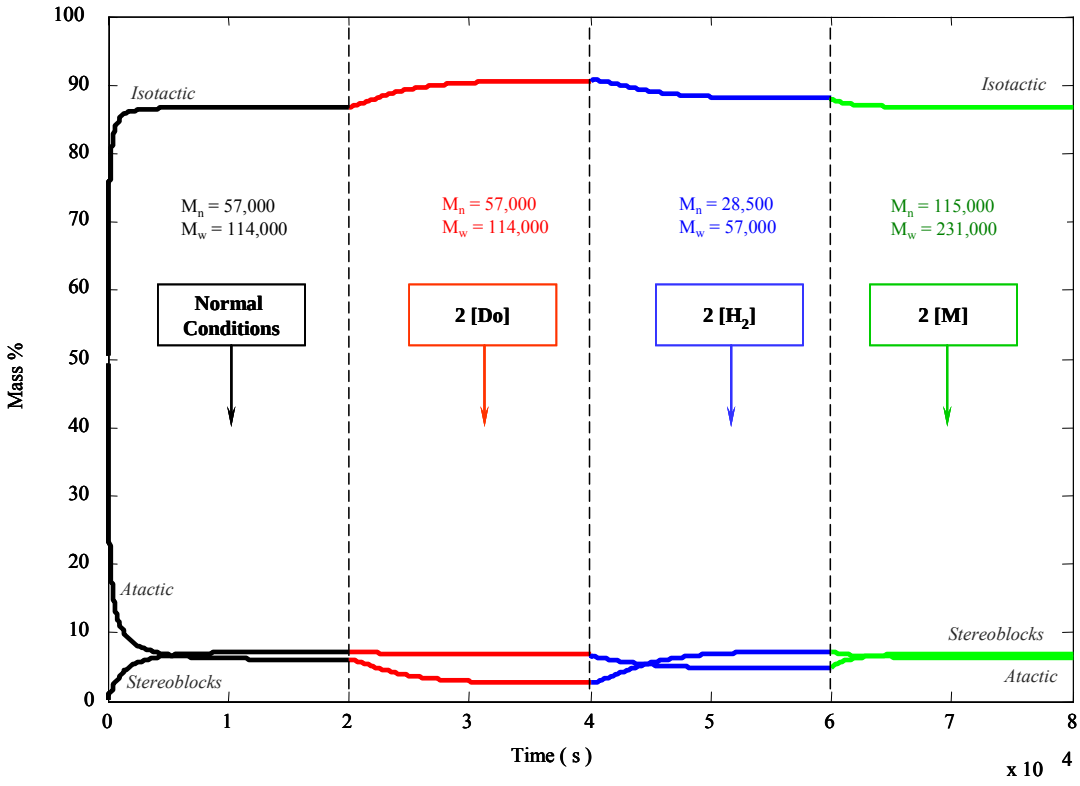

Figure 4-14: Effect of changing the concentration of donor, hydrogen, and monomer on mass fraction of isotactic, atactic and stereoblock chains.

As demonstrated with the steady-state model, the molecular weights obtained for the stereoblock chains increase with the number of blocks in the chain, while their polydispersities decrease. The same phenomenon is predicted with the dynamic model, as illustrated in Figure 4-15 and Figure 4-16.

Variation in the properties of stereoblock chains was also studied as a function of donor, hydrogen, and monomer concentrations. Figure 4-17 shows that the number average molecular

weight of chains with one to four stereoblocks increases very slightly when the concentration of electron donor is reduced. This is easy to understand, since the donor acts as a "pseudo chain transfer agent", shortening the average lengths of a stereoblock as it transforms the site from the aspecific to the stereospecific state, and vice-versa as shown in Figure 4-18. Similarly, a decrease in the concentration of the actual chain transfer agent, hydrogen, will lead to an increase in the molecular weight averages of the stereoblocks, in this case much more pronounced. Differently, a decrease in monomer concentration will lead to a drop in the average size of the stereoblocks.

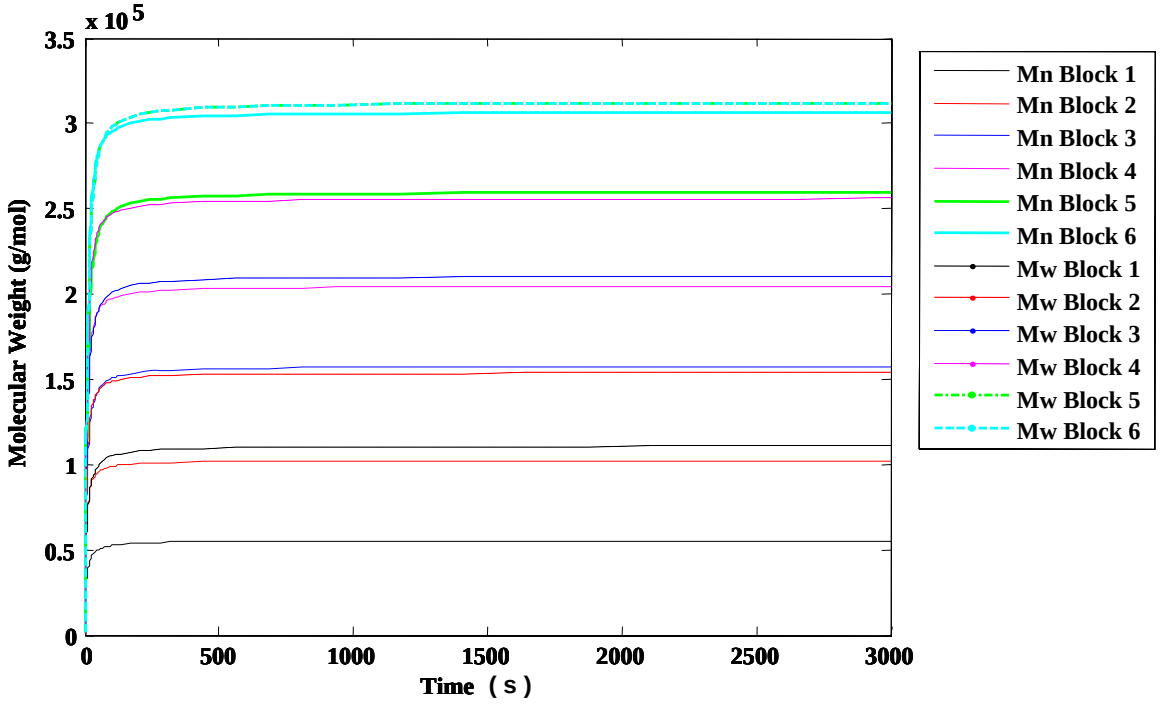

Figure 4-15: Dynamic evolution of molecular weight averages for chains with different number of stereoblocks. (One block accounts for both isotactic and atactic chains).

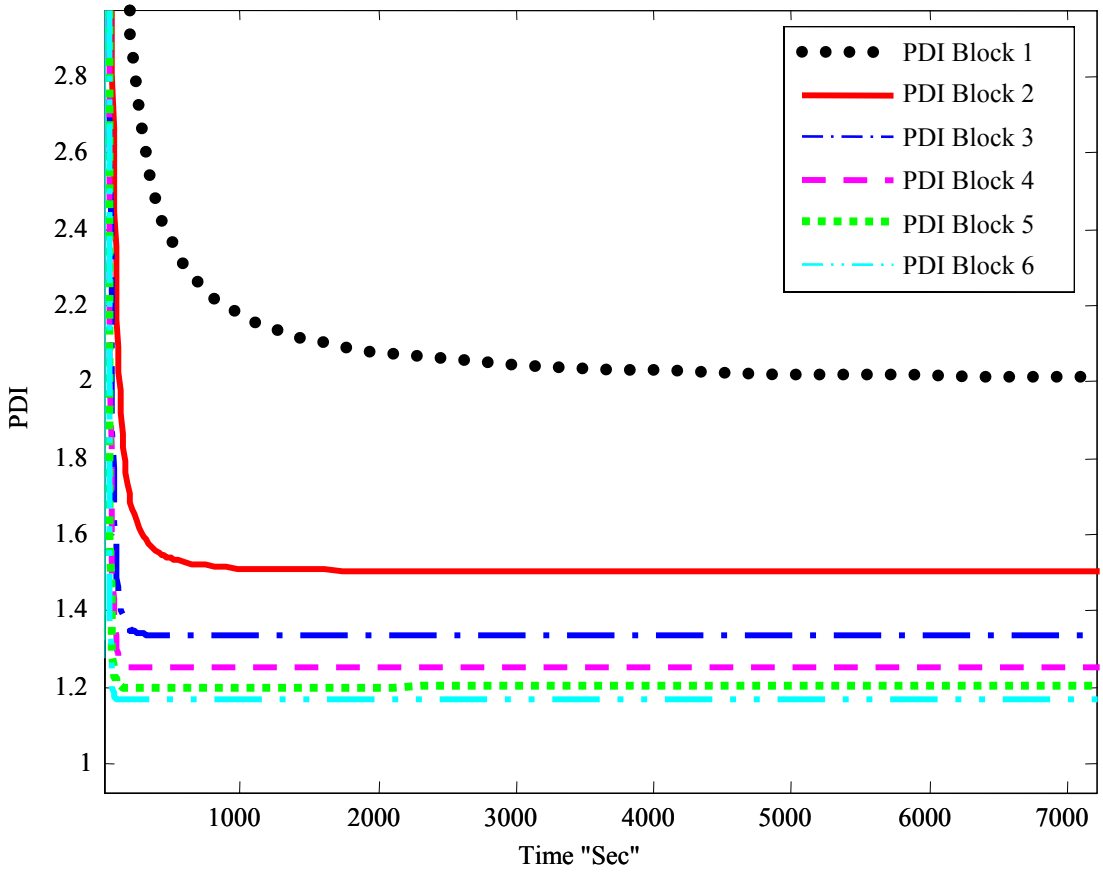

Figure 4-16: Dynamic evolution of polydispersity for chains with different numbers of stereoblocks.

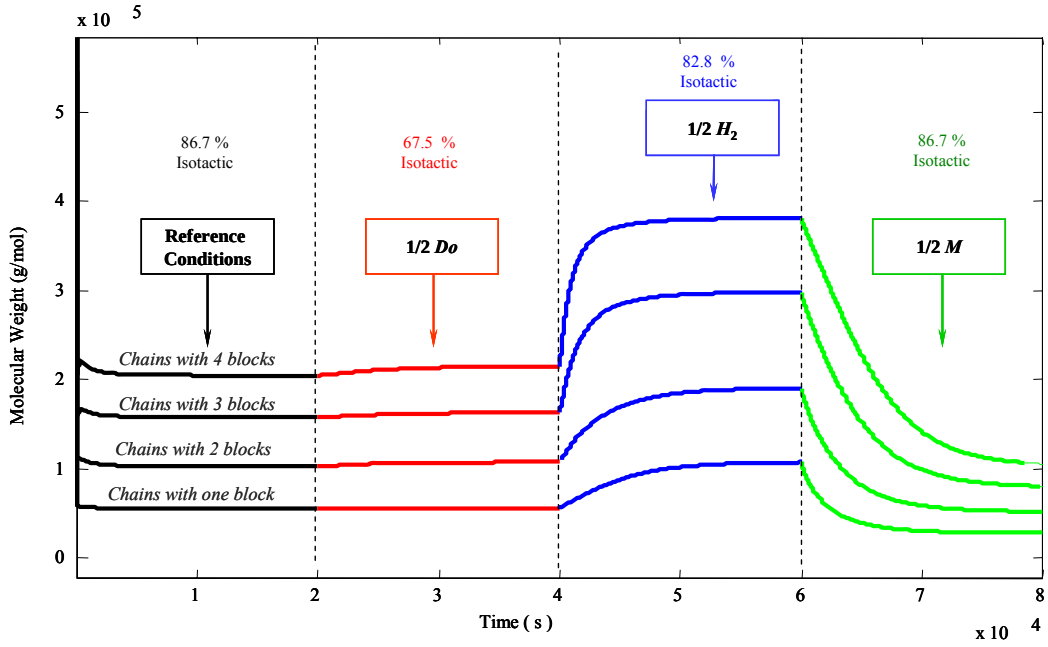

Figure 4-17: Number average molecular weights (M_n) responses to the reduction of donor, hydrogen, and monomer concentrations for chains with one to four blocks (One block accounts for both isotactic and atactic chains).

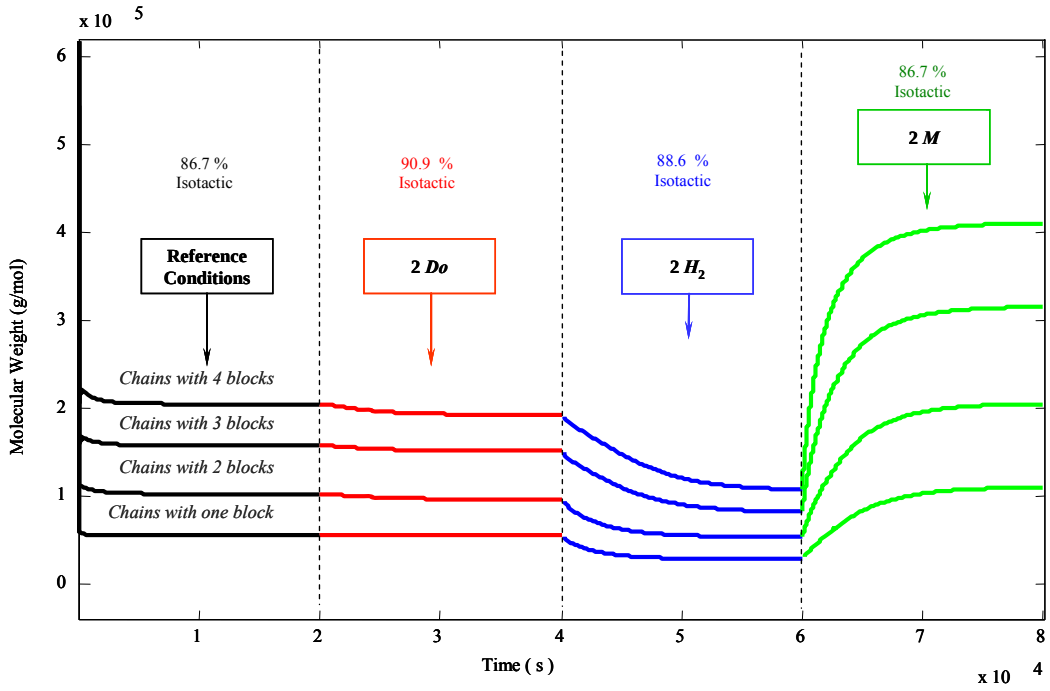

Figure 4-18: Number average molecular weights (M_n) responses to the increase of donor, hydrogen, and monomer concentrations for chains containing from one to four blocks.

4.5 Comparison between Steady-State and Dynamic Solutions

To insure the accuracy of both dynamic and steady-state simulations, we compared the steady-state results of the dynamic simulation with those obtained with the steady-state model. Tables 4-6 to 4-8 show that both simulation methods are in excellent agreement for all predicted properties. The slight differences shown in those tables are due to round off errors between the different mathematical techniques used to solve the steady-state and dynamic problems.

Table 4-6: Comparison of one-site steady-state and dynamic models: Overall properties.

Mass %	Steady State	Dynamic	Difference %
Pure Isotactic	86.73%	86.68%	-0.1%
Pure Atactic	6.07%	6.10%	0.5%
Stereo-Blocks	7.20%	7.22%	0.2%
By Block			
1 block	92.81%	92.81%	0.0 %
2 blocks	6.00%	6.00%	0.0 %
3 blocks	1.13%	1.13%	0.0 %
4 blocks	0.05%	0.05%	0.0 %
5 blocks	0.01%	0.01%	0.0 %
6 blocks	0.00%	0.00%	0.0 %
M_n (g/mol)	57,270	57,270	0.0 %
M_w (g/mol)	114,497	114,497	0.0 %
PDI	2.00	2.00	0.0 %

Table 4-7: Comparison of one-site steady-state and dynamic models: Stereoblock properties.

	Steady State			Dynamic			Difference %		
i	M_n	M_w	*PDI*	M_n	M_w	*PDI*	M_n	M_w	*PDI*
1	55,246	110,695	2.00	55,245	110,690	2.00	0.00%	0.00%	0.00%
2	102,229	153,807	1.50	102,230	153,810	1.50	0.00%	0.00%	0.00%
3	157,432	210,382	1.34	157,430	210,380	1.34	0.00%	0.00%	0.00%
4	204,416	256,004	1.25	204,420	256,010	1.25	0.00%	0.00%	0.00%
5	259,619	312,037	1.20	259,620	312,040	1.20	0.00%	0.00%	0.00%
6	306,603	358,194	1.17	306,610	358,200	1.17	0.00%	0.00%	0.00%

Table 4-8: Comparison of one-site steady-state and dynamic models: Chain segment properties

	Steady State			Dynamic			Difference %		
	M_n	M_w	*PDI*	M_n	M_w	*PDI*	M_n	M_w	*PDI*
Isotactic segments	56,008	111,939	2.00	56,002	111,960	2.00	0.01%	-0.02%	-0.03%
Atactic segments	46,274	92,507	2.00	46,271	92,500	2.00	0.01%	0.01%	0.00%
All segments	55,058	110,377	2.00	55,112	110,470	2.00	-0.01%	-0.08%	0.01%

Chapter 5

Monte Carlo Simulation

5.1 Mechanistic Approach

Monte Carlo simulation uses randomly generated numbers to select one event from a series of events based on its probability of occurrence. For our model of olefin polymerization, probabilities can be defined for propagation, termination, and transformation. Since the chains are made one-by-one, the maximum microstructural information can be obtained by Monte Carlo simulation. In olefin polymerization, several researchers have used Monte Carlo simulation to keep track of microstructural information that could not be achieved by other modeling techniques. Soares (2006) summarized Monte Carlo simulation techniques for single-site catalysts and illustrated some of its applications. Simon and Soares (2002) used a Monte Carlo model to describe the long-chain branch formation in polyethylene made with a combination of single-site catalysts. A Monte Carlo model was also used to analyze the microstructure of polyolefin thermoplastic elastomers made with two single-site catalysts (Haag *et al.*, 2003). Furthermore, Beigzadeh *et al*. (2001) simulated CRYSTAF fractionation of ethylene/1-octene copolymers made with single-site catalysts using a Monte Carlo model.

In this chapter, we used Monte Carlo techniques to develop a new model to simulate propylene polymerization taking in consideration site transformation in the presence of electron donors.

The model can predict the same properties modeled by the method of moments and, in addition, the complete MWD of the several polymer populations.

Figure 5-1 shows the algorithm developed for the one-site, two–state catalyst model. The model consists of two main loops: one for constructing the isotactic segments (growing when the site is in the isospecific state) and the other for constructing the atactic segments (when the site is in the aspecific state). In each loop, propagation, termination or state transformation events may take place. The probabilities for each event have been calculated using the values of the kinetic constants and polymerization conditions, as will be explained in Figure 5-1. The algorithm starts by generating a random number (*Rand*), uniformly distributed between zero and one, which is then used to select a reaction step. The algorithm generally starts with the site in the most probable state, the isospecific state *I*, but the choice of initial state will not affect the outcome of the simulations. This algorithm was coded using MATLAB. It takes apperoximatly 80 minutes to simulate the full molecular weight distribution for about 205,000 chains and approximately 230 minutes for the NMR prediction with around 900,000 sequences using an AMD Turion 64x2, 1.6 GHz, and 512KB L2 cache.

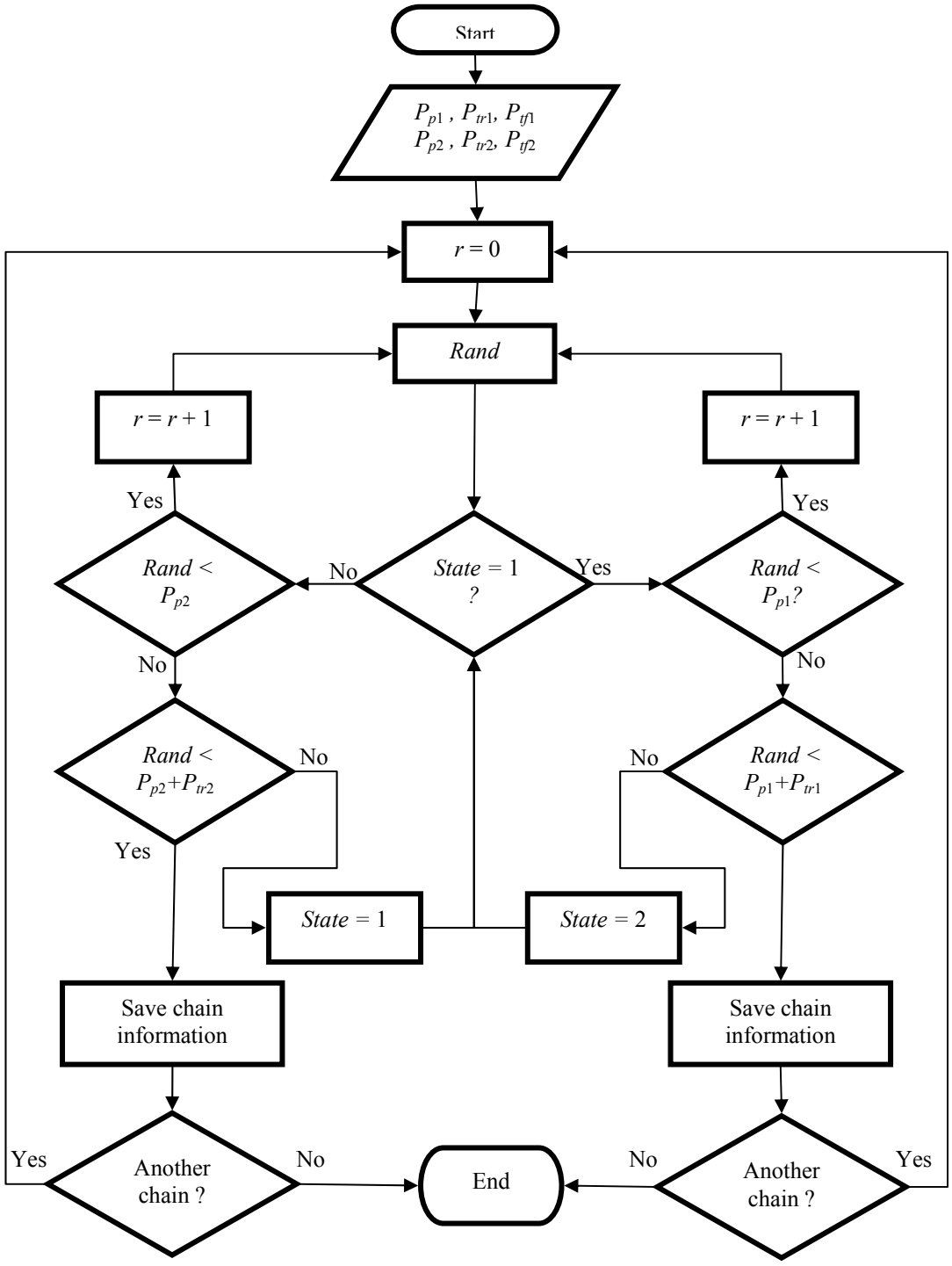

Figure 5-1: Monte Carlo simulation flowchart.

Reaction rates for propagation, termination, and site transformation are given by the equations

$$R_{pj} = k_{pj} M Y_j^0 \tag{5-1}$$

$$R_{trj} = (K_{Tj} + K_{Dj}) Y_j^0 \tag{5-2}$$

$$R_{tf1} = k_{Do}^{+} Do Y_{II}^0 \tag{5-3}$$

$$R_{tf2} = k_{Do}^{-} Y_I^0 \tag{5-4}$$

where j = 1, or 2 for reaction rates and their rate constants or $j = I$ or II for site states.

The probability for each event taking place is given by the ratio of the rate for that event divided by the sum of the rates of all events Equations (5-5) to (5-7):

$$P_{pj} = \frac{R_{pj}}{R_{pj} + R_{trj} + R_{tfj}} \tag{5-5}$$

$$P_{trj} = \frac{R_{trj}}{R_{pj} + R_{trj} + R_{tfj}} \tag{5-6}$$

$$P_{tfj} = \frac{R_{tfj}}{R_{pj} + R_{trj} + R_{tfj}} \tag{5-7}$$

where P_{pj} is the probability of propagation, P_{trj} is the probability of termination, and P_{tfj} is the probability of transformation at state j = 1 or 2.

5.2 Simulation Results

Figure 5-2 shows the full chain length distributions (CLDs) for all polymer chains, isotactic, atactic, and stereoblock chains predicted for the polymerization at the reference conditions shown in Table 4-1 and Table 4-2. The random noise observed in the CLD is characteristic of Monte Carlo simulations and can be reduced by generating more polymer chains. For the present simulation, over 205,000 polymer chains were generated. This type of detailed microstructural information can only be obtained by the complete solution of the population balances or by Monte Carlo simulation. Monte Carlo simulation is usually much easier to implement, albeit it may require considerable computational time. In the case of the reference electron donor concentration, the mass fraction of isotactic chains was approximately 87.2 %, of atactic 5.6 %, and of stereoblock 7.2 % (the area under the CLDs is proportional to the mass fraction of polymer belonging to that population). The model can also predict number and weight average molecular weights for the overall polymer (M_n= 57,212 M_w= 114,600, and PDI = 2.0.), isotactic (M_n = 56,819 , M_w = 113,620, PDI = 2.0), atactic (M_n = 45,612 , M_w = 89,699, PDI = 2.0), and stereoblock chains (M_n = 113,780 , M_w = 169,830 and PDI = 1.5). Figure 5-3, shows that the Monte Carlo and method of moments predictions for molecular weights and polydispersities agree very well with increasing number of Monte Carlo iterations (an iteration counts the number

of propagation, termination or site transformation events during the simulation) Similarly, Figure 5-4 demonstrates that tacticity predictions by both models are in good agreement, proving that both models describe the polymerization adequately.

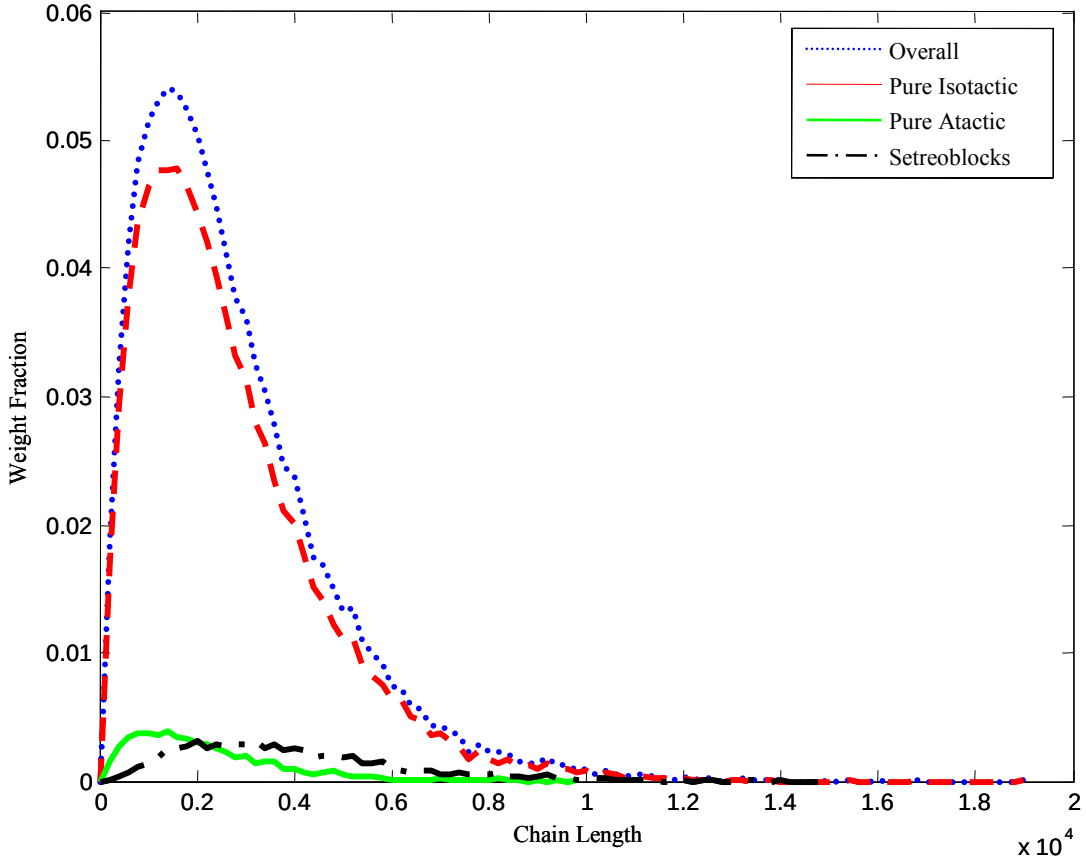

Figure 5-2: Monte Carlo simulation of the chain length distributions at reference polymerization conditions; M_n= 57,212 M_w= 114,600, *PDI* = 2.0, Isotactic = 87.2%, Atactic = 5.6%, Stereoblocks = 7.2%, and with total number of chains of 205,750.

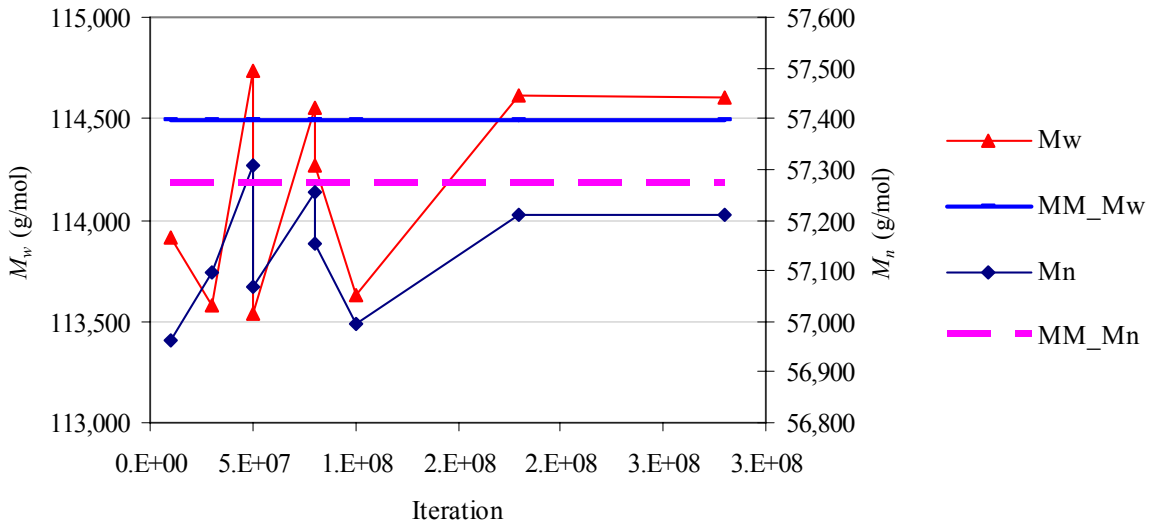

Figure 5-3: Molecular weight averages at reference polymerization conditions: Monte Carlo versus method of moments (MM).

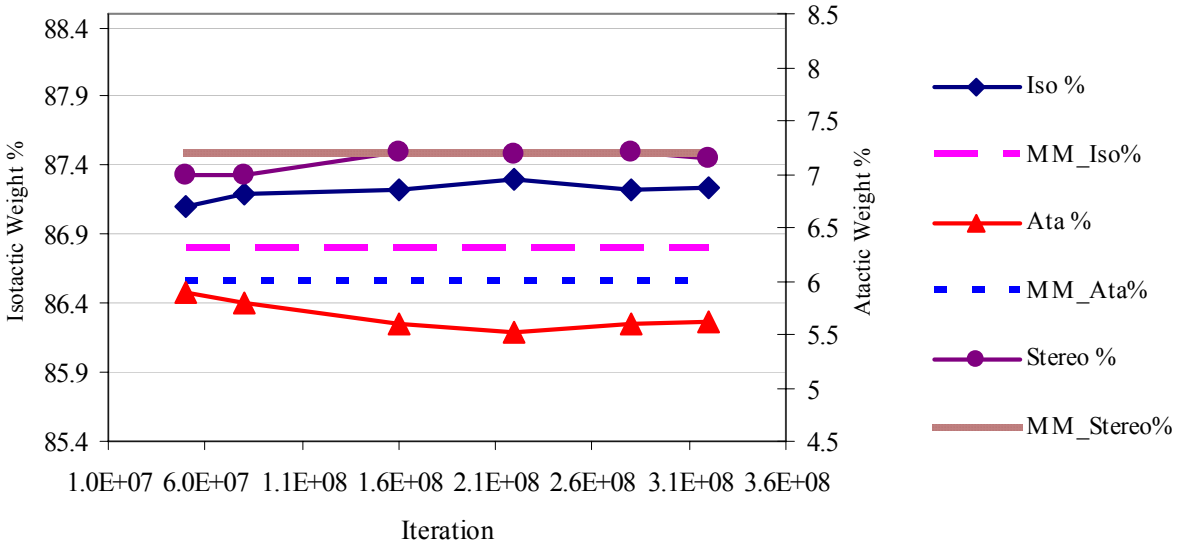

Figure 5-4: Tacticity distribution at reference polymerization conditions: Monte Carlo versus method of moments (MM); for reference polymerization conditions, refer to Table 4-1 and 4-2.

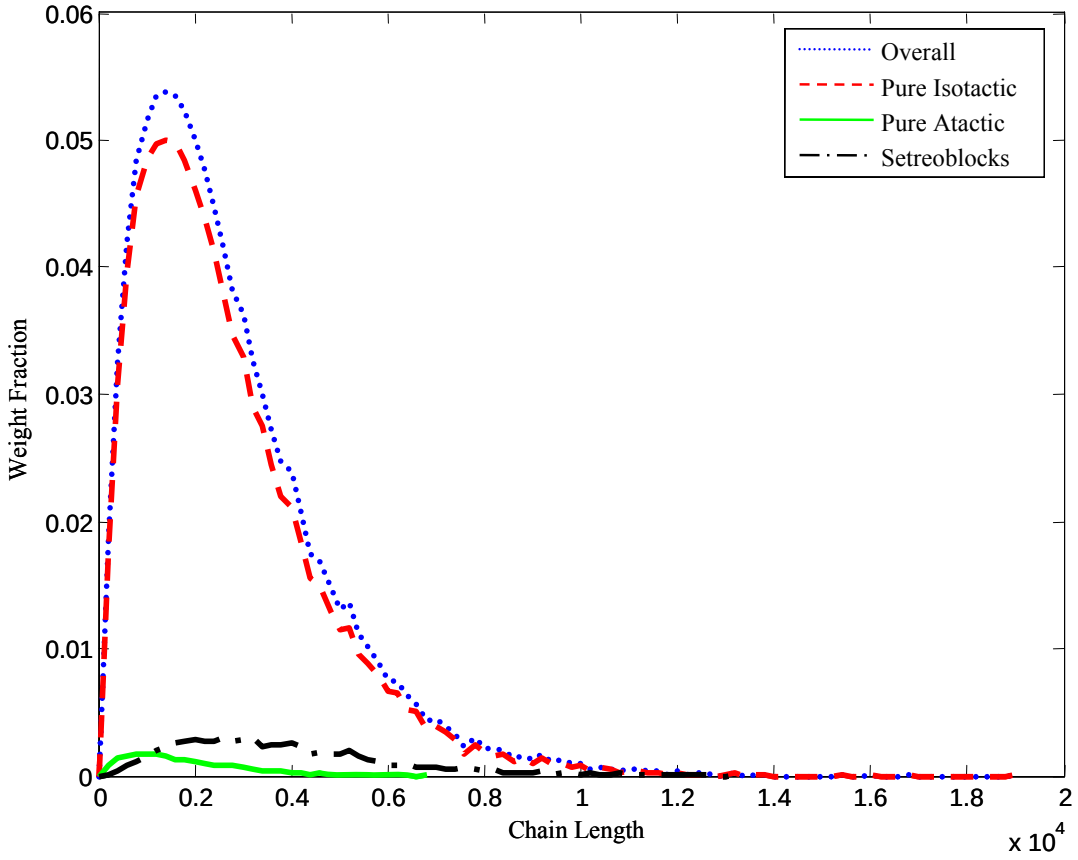

Figure 5-5: Monte Carlo simulation of the chain length distribution at 2×*Do*; M_n= ,57,106 M_w= 114,460, *PDI* = 2.0, Isotactic = 91.1%, Atactic = 2.1%, Stereoblocks = 6.8%, and with total number of chains of 205,780.

Similar CLDs are shown in Figure 5-5 for the case when the concentration of electron donor is doubled. In this case, the mass fraction of isotactic chains increased to 91.1 %, that of atactic chains decreased to 2.1 %, and the mass fraction of stereoblock chains change only slightly to 6.8 %. The predicted number and weight average molecular weights for the overall polymer (M_n = 57,106, M_w = 114,460, *PDI* = 2.0), isotactic (M_n = 55,810, M_w = 111,840, *PDI* = 2.0), atactic (M_n = 37,942, M_w = 75,625, *PDI* = 2.0), and stereoblock chains (M_n = 106, 640, M_w = 161,420,

PDI = 1.51) are also predicted easily by the Monte Carlo simulation. These results are also in excellent agreement in terms of their molecular weights with those obtained through the method of moments model shown previously in Figure 4-4.

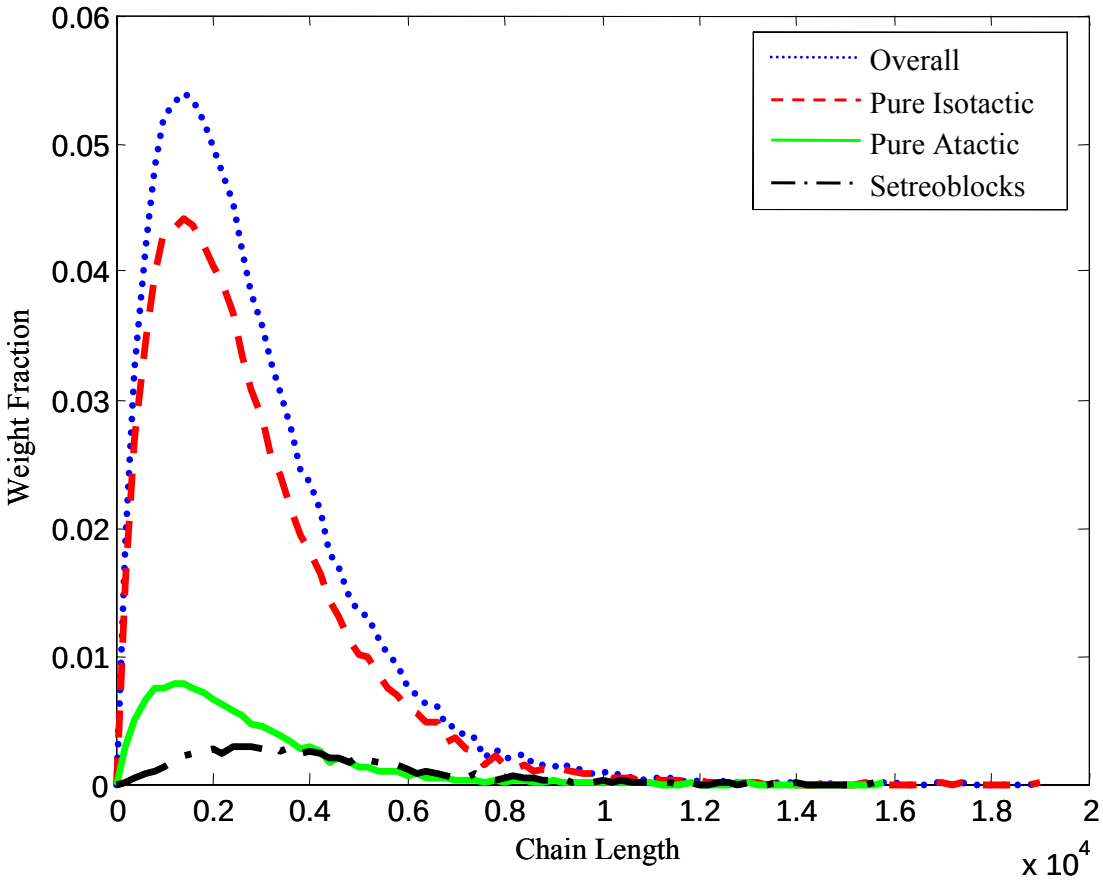

Figure 5-6: Monte Carlo simulation of the chain length distributions at ½ × *Do* ; M_n= 57,098 M_w = 114,530, *PDI* = 2.0, Isotactic = 80.1%, Atactic = 12.9%, Stereoblocks = 7.1%, and with total number of chains of 205,800.

On the other hand, Figure 5-6 shows the CLDs predicted when the donor concentration is reduced to half its reference value: the mass fraction of isotactic chains decrease to 80.1 %, while

that of atactic chains increase to 12.9 % and stereoblock chains have a slight decrease to 7.1 %. The predicted number and weight average molecular weights were for the overall polymer (M_n = 57,098 , M_w = 114,530, *PDI* = 2.0), isotactic (M_n = 55,824, M_w = 111,940, *PDI* = 2.0), atactic (M_n = 51,185, M_w = 102,248, *PDI* = 2.0), and stereoblock chains (M_n = 110,660, M_w = 165,860, *PDI* = 1.5) are predicted and agree with the results from the method of moments shown Figure 4-3.

5.3 ^{13}C NMR Simulation

One of the most common techniques for determining the degree of tacticity in polypropylene is carbon-13 nuclear magnetic resonance (^{13}C NMR). ^{13}C NMR measures the sequence distribution of meso (isotactic, *m*) and racemic (syndiotactic, *r*) placements of the methyl groups along the polymer chain. Figure 5-7 shows the two possible dyad arrangements. Triad, tetrad, pentad and higher sequences are similarly defined, as illustrated for a particular sequence in Figure 5-8.

Figure 5-7: Dyad arrangements (*m* = *meso*, *r* = *racemic*).

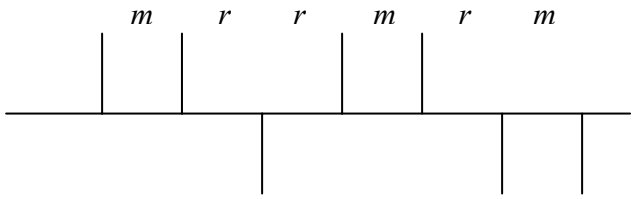

Figure 5-8: Higher *meso* and *racemic* sequence distributions.

These sequences obey the following mathematical relationships that will be used later for verification of our Monte Carlo model (Odian, 2004):

$$m + r = 1 \tag{5-8}$$

$$mm + rr + mr = 1 \tag{5-9}$$

$$m = mm + 0.5mr \tag{5-10}$$

$$r = rr + 0.5mr \tag{5-11}$$

$$mm = mmm + 0.5mmr \tag{5-12}$$

$$mr = mmr + 2rmr = mrr + 2mrm \tag{5-13}$$

$$mmmr + 2rmmr = mmrm + mmrr \tag{5-14}$$

$$mrr + 2mrrm = rrmr + rrmm \tag{5-15}$$

$$mmm = mmmm + 0.5mmmr \tag{5-16}$$

$$mmr = mmmr + 2rmmr = mmrm + mmrr \tag{5-17}$$

$$rmr = 0.5mrmr + 0.5rmrr \tag{5-18}$$

$$mrm = 0.5mrmr + 0.5mmrm \tag{5-19}$$

$$rrm = 2mrrm + mrrr = mmrr + rmrr \tag{5-20}$$

$$rrr = rrrr + 0.5mrrr \tag{5-21}$$

Sequence distributions up to the pentads were simulated using our Monte Carlo model. Each sequence was simulated individually as shown in detail in Appendix B, Tables B-1 to B-4. The model iteration was statistically checked in order to decrease the model noise as shown in Figure 5-9. The model predictions agree well with the theoretical relations defined in Equations (5-8) to (5-21), as listed in Table 5-1.

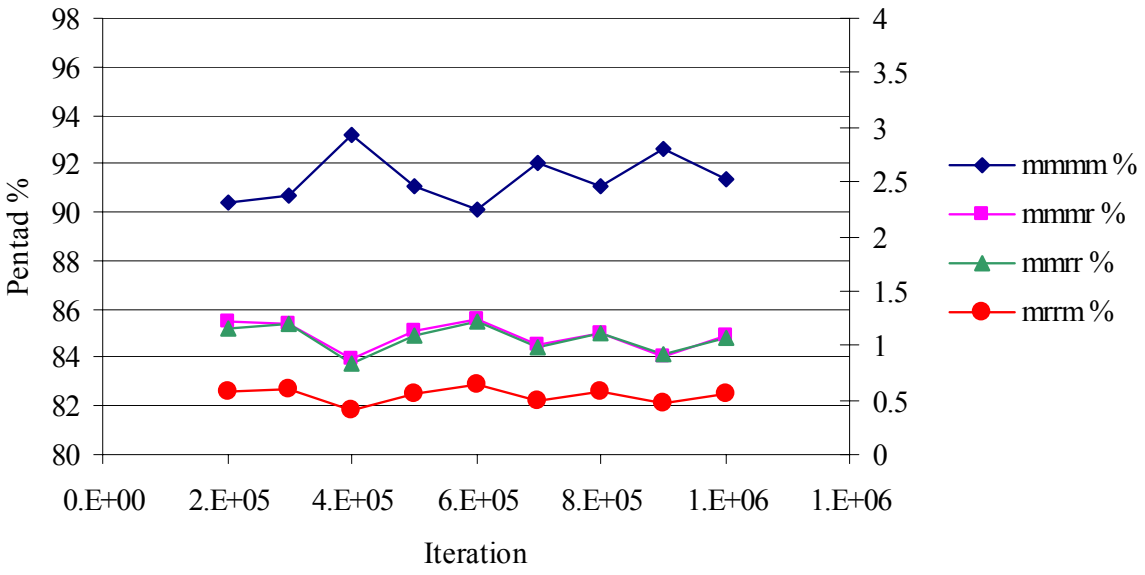

Figure 5-9: Pentad % by increasing the model iterations

Table 5-1: Model verification using Equations (5-8) to (5-21) at different donor concentrations, R.H.S and L.H.S stand for right and left hand side of the equation respectively.

	0.5 x *Do*			*Do*			2 x *Do*		
Equation #	R.H.S	L.H.S	Δ	R.H.S	L.H.S	Δ	R.H.S	L.H.S	Δ
(5-8)	100	100	0	100	100	0	100	100	0
(5-9)	100	100	0	100	100	0	100	100	0
(5-10)	94.1	94.1	0	94.7	94.7	0	96.4	96.4	0
(5-11)	5.9	5.9	0	5.3	5.3	0	3.6	3.6	0
(5-12)	91.1	92.5	1.4	92.1	93.3	0.8	94.6	95.5	0.9
(5-13)	6	6	0	5.3	5.3	0	3.6	3.6	0
(5-14)	2.9	3.7	0.8	2.6	3.3	0.7	1.8	2.2	0.4
(5-15)	4.5	2.9	-1.6	4	2.6	-1.4	2.7	1.8	-0.9
(5-16)	91	89	-2	92	90.2	-1.8	94.6	93.3	-1.3
(5-17)	3	3	0	2.7	3	0.3	1.8	2	0.2
(5-18)	1.5	1.5	0	1.3	1.3	0	0.9	0.9	0
(5-19)	1.5	1.5	0	0.8	1.3	0.5	0.9	0.9	0
(5-20)	3	2.9	-0.1	2.7	2.6	-0.1	1.8	1.8	0
(5-21)	1.5	1.5	0	1.3	1.3	0	0.9	0.9	0
Total Difference (%)			5.9			6			3.7
Number of Deviations			5			7			5

Figure 5-10 to 5-10 illustrate the effect of varying the donor concentration on the dyad, triad, tetrad and pentad sequences of polypropylene. As expected, increasing donor concentration will increase the fraction of *m* placements at the expense of *r* sequences.

Table 5-2: Full Monte Carlo simulation analysis; see also Figure 5-2, Figure 5-5, and Figure 5-6.

	½ x *Do*	*Do*	2 x *Do*
Isotactic mass %	80.1 %	87.2 %	91.1 %
Atactic mass %	12.9 %	5.6 %	2.1 %
Stereoblock mass %	7.1 %	7.2 %	6.8 %

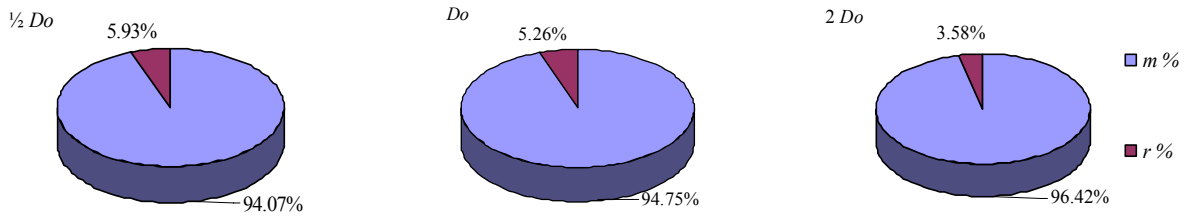

Figure 5-10: Dyad sequence distribution.

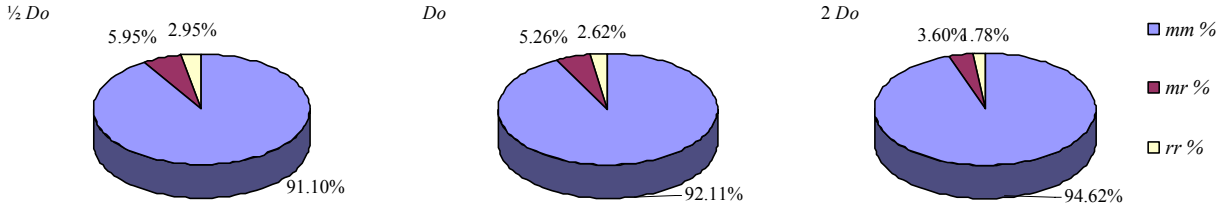

Figure 5-11: Triad sequence distribution.

The values of the pentad sequence distribution shown in Figure 5-13 can also be used to back calculate the values of the tetrad, triad, and dyad sequences using Equations (5-8) to (5-21).

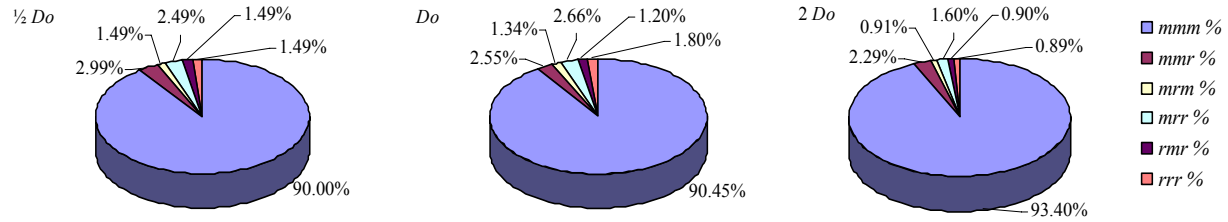

Figure 5-12: Tetrad sequence distribution.

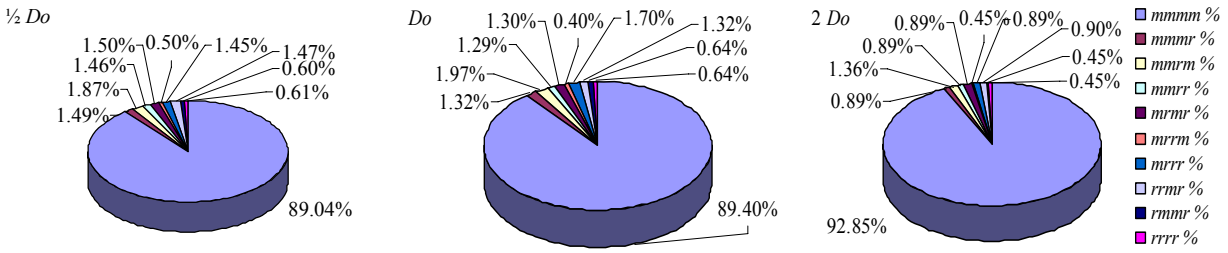

Figure 5-13: Pentad sequence distribution.

Chapter 6

Conclusion and Future Work

Variations in stereoregularity can be described by assigning two different states to each active site: P_0^I is a stereospecific state that produces isotactic polymer and P_0^{II} is a aspecific state that produces atactic polymer. The aspecific state can be converted to the stereospecific state by reaction with an electron donor. Most of the commercial heterogeneous Ziegler -Natta catalysts for propylene polymerization have several active site types with varying stereoregular control characteristics that can be affected by the addition of electron donors. Polypropylene chains can be atactic, isotactic, or have an atactic-isotactic stereoblock structure. The stereoblock structure will be produced if the chain starts growing while the site is at the aspecific state and than reacts with an electron donor molecule and in converted to the stereospecific state before chain termination (or vice-versa). Our model is the first to describe qualitative this state transformation step during propylene polymerization.

We used the model to show how the several polypropylene chain populations were affected by changing the concentration of hydrogen, electron donor, and propylene in the reactor, for both steady-state and dynamic simulations.

As expected, molecular weight averages decrease with increasing hydrogen concentration but, more interestingly, hydrogen concentration also affects the fractions of each polypropylene

population. Increasing hydrogen concentration favors the formation of atactic or isotactic chains because it reduces the average lifetime of the polymer chain and decreases the probability of a change in state taking place as the chain grows, forming a stereoblock chain.

Moreover, the model shows the effect of the electron donor concentration on polypropylene tacticity. In our simulations, the weight percent of isotactic chains decreases by approximately 6.4% when the donor concentration was reduced by half of its original value. To the best of our knowledge, this is the first time a mathematical model was developed to describe this effect.

In addition, our model gives a very detailed description of the polypropylene populations. The polydispersity of the purely atactic or isotactic chains is equal to 2.0, but the *PDI* decreases as the number of stereoblocks increases due to the statistical averaging of the chain lengths. The molecular weight averages increase with increasing number of blocks, as expected. The model is also capable to predict the mole and mass fraction of each polymer species in the mixture.

Typical heterogeneous Zigler-Natta catalysts used for propylene polymerization have two or more site types. These catalysts can be modeled with the same approach described above, provided that each site type is described with a different set of polymerization kinetic parameters. Therefore, both steady-state and dynamic simulations for a 4-site type catalyst were carried out where sites type 1 and 2 make only isotactic chains and sites type 3 and 4 alternate between aspecific and stereospecific states. The polydispersity of chains made on each site type is still equal to 2.0, but the overall polydispersity of the polymer was 4.45. Moreover, illustration

of how varying the donor concentration affects the mass fraction of atactic and isotactic chains in the reactor was reported. Finally, the time evolution of molecular weight averages of polymer made in each site type of a 4-site type catalyst was depicted.

The model using the method of moments can follow molecular weight averages, but not the complete molecular weight distribution. Monte Carlo simulation was used to predict the complete MWD and tacticity sequence length distribution.

In the next step of model development, we will extend this Monte Carlo method to describe in addition to the stereoregularity, the regioregularity and to use it further to predict polypropylene fractionation with temperature rising elution fractionation (TREF). Moreover, the ^{13}C NMR spectra plot will be also simulated.

The model will be extended to account to determine the catalyst sites type distribution in term of stereospecific and non stereospecific ones. This is will be done through the deconvolution of the overall site state distribution. The model will be used as tool to estimate some kinetic parameters including the reaction rate constants of the transformation by donor for some catalyst/donor systems. By estimating the kinetic parameter of the individual donors, it would be possible to predict any combination of these donors in order to have some features of each donor such as high activity, high stereoselectivity, high regioregularity, reactor self extinguishing and any other product or process feature.

References

Arlman, E. J. and Cossee, P. J., *J. Catal.*, **3**, 99 (1964).

Arlman, E. J., *J. Catal.*, **5**, 178 (1966).

Barino L., Scordamaglia R., *Macromol. Theory Simul*. **7**, 407 (1998).

Beigzadeh D., Soares J. B. P., Duever T. A., *J. Appl. Polym. Sci.* **80**, 2200 (2001).

Boucheron B., *Eue. Polym. J.,* **11**, 131 (1975).

Busico V., Corradini P., De Martino L., Proto A., Savino V., Albizzati E., *Makromol. Chem.* **186**, 1279 (1985).

Busico V., Cipullo R., Corradini P., *Makromol. Chem. Rapid Commun,* **13**, 15 (1992).

Busico V., Cipullo R., Corradini P., De Biasio R., *Macromol. Chem. Phys*. **196**, 491 (1995).

Busico V., Cipullo R., Monaco G., Talarico G., Chadwick J.C., Segre A.L., Sudmeijer O., *Macromolecules* **32**, 4173 (1999).

Chadwick J.C., Meedema A., Sudeijer O., *Macromol. Chem. Phys.* **195**, 167 (1994).

Chadwick J.C., van Kessel G.M.M., Sudmeijer O., *Macromol. Chem. Phys.* **196**, 1431 (1995).

Chadwick J.C., Morini G., Albizzati E., Balbontin G., Mingozzi I., Cristofori A., Sudmeijer O., van Kessel G.M.M., *Macromol. Chem. Phys.* **197**, 2501 (1996).

Chadwick J.C., Heere J., Sudmeijer O., *Macromol. Chem. Phys.* **201**, 1846 (2000).

Chadwick J.C., Morini G., Balbontin G., Camurati I., Heere J.J.R., Mingozzi I., Testoni F., *Macromol. Chem. Phys.* **202**, 1995 (2001).

Faldi A., Soares J. B. P., *Polymer* **42**, 3057 (2004).

Guastalla G., Giannini U., *Makromol. Chem. Rapid Commun.,* **4**, 519 (1983).

Higham D., Higham N., "MATLAB Guide", 2nd edition (2005).

Kakugo M., Miyatake T., Naito Y., Mizunuma K., *Macromolecules*, **21**, 314 (1988).

Kissin, Y.V.; Mink, R. I.; Nowlin, T.E. *J. Pol. Sci. A*: *Pol. Chem*, 4255 (1999).

Kissin Y.V., Rishina L. A., *J. Pol. Sci. A*: *Pol. Chem* .,**40**, 1353 (2002).

Kissin Y.V., Rishina L. A., Vizen E.I., *J. Pol. Sci. A*: *Pol. Chem.,* **40**, 1899 (2002).

Morini G., Albizzati E., Balbontin G., Mingozzi I., Sacchi M. C., Forlini F., Toritto I., *Macromolecules* **29**, 5770 (1996).

Natta G., *Adv. Catal.*, **11**, 1 (1959).

Odian G. "Principles of Polymerization", 4th edition (2004).

Rishina L., Vizen E., Sosnovskaya L., Dyachkovsky F., *Eur. Polym. J.*, **30**, 1309 (1994).

Shaffer W.K., Harmon Ray W., *J. Appl. Polym. Sci.* **65**, 1053 (1997).

Simon L. C., Soares J. B. P., *Macromol. Theory Simul*. **11**, 222 (2002).

Soares J. B. P., Hanielec A. E. *Polymer* **36**, 2257 (1995).

Soares J. B. P., *Chem. Eng. Sci.* **56**, 4131 (2001).

Soares J. B. P., *The Catalyst Group* **XV No. 3**, (December 2006) .

Soga K., Sino T., *Polym. Bull.*, **8**, 261 (1982).

Appendix A

Steady-State Simulation Results

Appendix A

Table A- 1: Steady-state solution for one-site catalyst at reference simulation conditions; f_D: a factor multiplied by the donor concentration, $k_{p1}/k_{p2} = 1$, $R_{P1}/R_{T1} = 1364$, $R_{P2}/R_{T2} = 1364$

f_D	0.00		1.00		2.00		0.50	
	Mole %	Mass %	Mole %	Mass %	Mole %	Mass %	Mole %	Mass %
Pure Isotactic	50.00	50.00	88.74	86.77	92.97	90.91	81.40	79.60
Pure Atactic	50.00	50.00	7.47	6.04	3.34	2.26	14.97	13.38
Stereoblocks	0.00	0.00	3.79	7.19	3.7	6.83	3.63	7.02
Block weight %:								
1 block	100.00	100.00	96.21	92.81	96.30	93.17	96.37	92.98
2 blocks	0.00	0.00	3.36	6.00	2.98	4.93	3.39	6.34
3 blocks	0.00	0.00	0.41	1.13	0.69	1.80	0.23	0.64
4 blocks	0.00	0.00	0.01	0.05	0.02	0.07	0.01	0.03
5 blocks	0.00	0.00	0.00	0.01	0.00	0.02	0.00	0.00
6 blocks	0.00	0.00	0.00	0.00	0.00	0.00	0.00	0.00
M_n (g/mol)	57,264		57,270		57,270		57,270	
M_w (g/mol)	114,511		114,497		114,497		114,497	
PDI	2.00		2.00		2.00		2.00	

See Figure 4-1 to Figure 4-4 for the graphical representation of these results.

Table A- 2: Blocks properties of the steady-state solution for one-site catalyst at reference simulation conditions: (k_{p1}/k_{p2} = 1, R_{P1}/R_{T1} =1364, R_{P2}/R_{T2} =1364)

	End Iso			End Ata			End Iso	End Ata	End Iso	End Ata
I	M_n	M_w	*PDI*	M_n	M_w	*PDI*	Mole %	Mole %	Mass %	Mass %
1	55,989	111,935	2.00	46,261	92,480	2.00	88.70%	7.51%	86.73%	6.07%
2	102,208	153,775	1.50	102,207	153,774	1.50	1.75%	1.62%	3.12%	2.90%
3	158,154	211,285	1.34	148,427	198,341	1.34	0.38%	0.03%	1.04%	0.08%
4	204,374	255,951	1.25	204,372	255,949	1.25	0.01%	0.01%	0.03%	0.02%
5	260,319	312,844	1.20	250,592	301,189	1.20	0.00%	0.00%	0.01%	0.00%
6	306,539	358,120	1.17	306,537	358,118	1.17	0.00%	0.00%	0.00%	0.00%

See Figure 4-5 for the graphical representation of these results.

Table A- 3: Steady state solution for one low stereo-specific site at reference conditions (f_D: a factor multiplied by the donor concentration)

f_D	1.00		2.00		1.00		2.00	
	k_{p1}/k_{p2} = 1, R_{P1}/R_{T1} =1364 , R_{P2}/R_{T2} =1364				k_{p1}/k_{p2} = 10, R_{P1}/R_{T1} =1364 , R_{P2}/R_{T2} =136			
	Mole %	Mass %	Mole %	Mass %	Mole %	Mass %	Mole %	Mass %
Pure Isotactic	88.74	86.77	92.97	90.91	88.81	94.56	93.01	95.03
Pure Atactic	7.47	6.04	3.34	2.26	7.42	0.66	3.31	0.24
Stereoblocks	3.79	7.19	3.79	6.83	3.78	4.78	3.68	4.74
Block weight %:								
1 block	96.21	92.81	96.30	93. 17	96.22	95.22	96.32	95.26
2 blocks	3.36	6.00	2.98	4.93	3.35	3.86	2.97	3.24
3 blocks	0.41	1.13	0.69	1.8	0.41	0.88	0.69	1.43
4 blocks	0.01	0.05	0.02	0.07	0.01	0.03	0.02	0.05
5 blocks	0.00	0.01	0.00	0.02	0.00	0.01	0.00	0.02
6 blocks	0.00	0.00	0.00	0.00	0.00	0.00	0.00	0.00
M_n (g/mol)	57,270		57,270		52,593		54,813	
M_w (g/mol)	114,497		114,497		111,832		114,595	
PDI	2.00		2.00		2.13		2.05	

See Figure 4-2, Figure 4-4, and Figure 4-6 for the graphical representation of these results.

Table A- 4: Steady state solution results for high stereo-specific catalyst with two different donors (k_{p1}/k_{p2} = 1, R_{P1}/R_{T1} =1364 , R_{P2}/R_{T2} =1364)

	Donor	Reference (A)	B	C
k_{Donor}^{+}/k_{A}^{+}		1	2	0.5
k_{Donor}^{-}/k_{A}^{-}		1	0.5	2
Pure Isotactic	Mole %	88.74	96.18	68.85
	Mass %	86.77	95.10	65.87
Pure Atactic	Mole %	7.47	1.85	25.05
	Mass %	6.04	1.25	22.38
Stereoblocks	Mole %	3.79	1.97	6.10
	Mass %	7.19	3.64	11.74
M_n (g/mol)		57,270	57,270	57,270
M_w (g/mol)		114,497	114,497	114,497
PDI		2.00	2.00	2.00
Block weight %:				
	1 block	92.81	96.36	88.26
	2 blocks	6.00	2.68	10.43
	3 blocks	1.13	0.94	1.21
	4 blocks	0.05	0.02	0.10
	5 blocks	0.01	0.01	0.01
	6 blocks	0.00	0.00	0.00

See Figure 4-2, Figure 4-7, and Figure 4-8 for the graphical representation of these results.

Table A- 5: Steady state solution results using different catalysts (k_{p1}/k_{p2} = 1, R_{P1}/R_{T1} =1364 , R_{P2}/R_{T2} =1364)

Catalyst		*C*1	*C*2	*C*3
kp/kp_{C1}		1	2	0.5
Pure Isotactic	Mole %	88.74	88.74	88.74
	Mass %	86.77	86.77	86.77
Pure Atactic	Mole %	7.47	7.47	7.47
	Mass %	6.04	6.04	6.04
Stereoblocks	Mole %	3.79	3.79	3.79
	Mass %	7.19	7.19	7.19
M_n (g/mol)		57,270	114,497	28,656
M_w (g/mol)		114,497	228,952	57,270
PDI		2.00	2.00	2.00
Block weight %:				
	1 block	92.81	92.81	92.81
	2 blocks	6.00	6.00	6.00
	3 blocks	1.13	1.13	1.13
	4 blocks	0.05	0.05	0.05
	5 blocks	0.01	0.01	0.01
	6 blocks	0.00	0.00	0.00

See Figure 4-2, Figure 4-9, and Figure 4-10 for the graphical representation of these results.

Table A- 6: Steady state solution results at other two different H_2 (k_{p1}/k_{p2} = 1)

		H_2 R_{P1}/R_{T1} =1364 , R_{P2}/R_{T2} =1364	2 x H_2 R_{P1}/R_{T1} =682 R_{P2}/R_{T2} =682	½ x H_2 R_{P1}/R_{T1} =2727 R_{P2}/R_{T2} =2727
Pure Isotactic	Mole %	88.74	89.65	86.76
	Mass %	86.77	88.65	83.01
Pure Atactic	Mole %	7.47	8.34	6.32
	Mass %	6.04	7.45	4.28
Stereoblocks	Mole %	3.79	2.01	6.92
	Mass %	7.19	3.90	12.70
M_n (g/mol)		57,270	28,689	114,214
M_w (g/mol)		114,497	57,336	228,385
PDI		2.00	2.00	2.00
Block weight %:				
	1 block	92.81	96.10	87.29
	2 blocks	6.00	3.56	9.04
	3 blocks	1.13	0.33	3.33
	4 blocks	0.05	0.01	0.25
	5 blocks	0.01	0.00	0.08
	6 blocks	0.00	0.00	0.01

See Figure 4-2, Figure 4-11, and Figure 4-12 for the graphical representation of these results.

Appendix B

^{13}C NMR Simulation Tables

Table B- 1: Dyad sequence distribution.

	½ x *Do*	*Do*	2 x *Do*
M %	94.07 %	94.75 %	96.42 %
r %	5.93 %	5.26 %	3.58 %
Pure Isotactic mass %	87.84 %	89.55 %	91.78 %
Pure Atactic mass %	9.84 %	6.26 %	3.86 %
Stereoblocks mass %	2.32 %	4.19 %	4.36 %

See Figure 5-10 for the graphical representation of these results.

Table B- 2: Triad sequence distribution.

	½ x *Do*	*Do*	2 x *Do*
mm %	91.10 %	92.11 %	94.62 %
mr %	5.95 %	5.26 %	3.60 %
Rr %	2.95 %	2.62 %	1.78 %
Pure Isotactic mass %	87.84 %	89.55 %	91.78 %
Pure Atactic mass %	9.84 %	6.26 %	3.86 %
Stereoblocks mass %	2.32 %	4.19 %	4.36 %

See Figure 5-11 for the graphical representation of these results.

Table B- 3: Tetrad sequence distribution.

	½ x *Do*	*Do*	2 x *Do*
mmm %	90.00 %	90.45 %	93.40 %
mmr %	2.99 %	2.55 %	2.29 %
mrm %	1.49 %	1.34 %	0.91 %
mrr %	2.49 %	2.66 %	1.6 %
rmr	1.49 %	1.20 %	0.90 %
rrr %	1.49 %	1.80 %	0.89 %
Pure Isotactic mass %	87.84 %	89.55 %	91.78 %
Pure Atactic mass %	9.84 %	6.26 %	3.86 %
Stereoblocks mass %	2.32 %	4.19 %	4.36 %

See Figure 5-12 for the graphical representation of these results.

Table B- 4: Pentad sequence distribution.

	½ x *Do*	*Do*	2 x *Do*
mmmm %	89.04 %	89.40 %	92.85 %
mmmr %	1.49 %	1.32 %	0.89 %
mmrm %	1.87 %	1.97 %	1.36 %
mmrr %	1.46 %	1.29 %	0.89 %
mrmr %	1.50 %	1.30 %	0.89 %
mrrm %	0.50 %	0.40 %	0.45 %
mrrr %	1.45 %	1.70 %	0.89 %
rrmr %	1.47 %	1.32 %	0.90 %
rmmr %	0.60 %	0.64 %	0.45 %
rrrr %	0.61 %	0.64 %	0.45 %
Pure Isotactic mass %	87.84 %	89.55 %	91.78 %
Pure Atactic mass %	9.84 %	6.26 %	3.86 %
Stereoblocks mass %	2.32 %	4.19 %	4.36 %

See Figure 5-13 for the graphical representation of these results.